A MOLECULAR THERMODYNAMIC MODEL FOR SURFACTANT AGGREGATE FORMATION

By

MICHEL J. BOURANI

A DISSERTATION PRESENTED TO THE GRADUATE SCHOOL OF
THE UNIVERSITY OF FLORIDA
IN PARTIAL FULFILLMENT OF THE REQUIREMENTS FOR THE
DEGREE OF DOCTOR OF PHILOSOPHY

UNIVERSITY OF FLORIDA

1984

To

Peace on Earth

ACKNOWLEDGMENTS

I would like to express my sincere gratitude and thanks to Dr. John O'Connell for his enthusiastic guidance and encouragement during the course of this research. Working with him has been a truly valuable and enjoyable experience.

I also would like to thank Drs. D.O. Shah, K.W. Fahien, T.E. Hogen Esch, and F.A. Vilallonga for serving on my supervisory committee.

I thank my colleagues in the Department of Chemical Engineering for providing an enjoyable environment in which I could pursue my research, and Mrs. Jeanne Ojeda for her excellent technical typing.

Finally, I wish to express my thanks to the consortium of oil and chemical companies and Westvaco for their support of this research.

TABLE OF CONTENTS

		Page
ACKNOWLEDGMENTS		iii
LIST OF TABLES		vi
LIST OF FIGURES		viii
KEY TO SYMBOLS		x
ABSTRACT		xiii
CHAPTER I	INTRODUCTION	1
CHAPTER II	THERMODYNAMIC PROPERTY CHANGES OF AGGREGATION	4
	2.1 Observations on Aggregating Systems	4
	2.2 Thermodynamic Framework	11
	2.3 Experimental Measurements and Thermodynamic Properties	15
CHAPTER III	A THERMODYNAMIC PROCESS FOR AGGREGATE FORMATION	18
	3.1 Concept and Development of a Multistep Process	18
	3.2 Solvent Cavity Models for Gaseous and Organic Solubility	22
	3.3 Equations of State for Nonspherical Molecules	27
	3.4 Electrostatic Interactions and Counterion Binding	30
	3.5 Thermodynamic and Material Constraints on Aggregate Formation	33
CHAPTER IV	A SPECIFIC MODEL FOR THE THERMODYNAMIC PROPERTIES OF AGGREGATE FORMATION	47
	4.1 Model Formulation	47
	4.2 Solubility of Organic Monomers as Input Data (Steps 1 and 2)	51
	4.3 Equation of State for Monomer Compression	56
	4.4 Micelle Cavity Properties	59
	4.5 Micelle Surface Properties	63
	4.6 Total Free Energy Change Upon Micellization	76
	4.7 Model Parameters	79
CHAPTER V	CORRELATION AND PREDICTION OF AGGREGATE PROPERTIES	81
	5.1 Nonionic Systems	81

5.2 Ionic Systems 103

CHAPTER VI SUMMARY AND CONCLUSIONS 139

APPENDIX A NUMERICAL SOLUTION OF THE POISSON-BOLTZMANN EQUATION 144

APPENDIX B PROPERTIES OF DISTRIBUTED SURFACTANTS IN MIXED MICELLES 153
B.1 Discrete Distribution of Surfactants 153
B.2 Continuous Distribution of Surfactants 160

REFERENCES 167

BIOGRAPHICAL SKETCH 176

LIST OF TABLES

Table		Page
4.1	Correlation of Normal Paraffin Solubilities in Water	54
4.2	Comparison of Estimated and Experimental Enthalpies of Solution of n-Pentane and n-Hexane in Water	55
4.3	Characteristic Volumes for Rigid Body Equation of State	58
5.1	Data Collected on Polyoxyethylenated Surfactants $C_xH_{2x+1}(OC_2H_4)_6OH$ in Aqueous Solutions	82
5.2	Parameter Values for $C_xH_{2x+1}(OC_2H_4)_6OH$ Surfactant Systems in Aqueous Solutions	83
5.3	Parameter Values for $C_{12}H_{25}(OC_2H_4)_6OH$ Surfactant System for Different Nonspherical Aggregate Shapes	91
5.4	Data Collected, Parameter Values and Predicted $\bar{N}$ for Alkyltrimethylammonium Bromide Systems in Aqueous Solutions	104
5.5	Electrostatic Interaction Parameters for the Systems in Table 5.4	105
5.6	Data Collected on Sodium Alkyl Sulfate Systems ($C_xH_{2x+1}SO_4^-Na^+$) in Aqueous Solutions	115
5.7	Experimental and Predicted $\bar{N}$ for Sodium Dodecyl Sulfate Aggregates as a Function of NaCl Concentration	117
5.8	Parameter Values for Sodium Alkyl Sulfate Systems in Aqueous Solutions	120
5.9	Electrostatic Interaction Parameters for the Systems in Table 5.8	121
5.10	Predicted $\bar{N}$ and Average Free Energy Change	122
5.11	Model Parameters for $C_{12}SO_4^-Na^+$ at Different Concentrations	126
5.12	CMC and Parameter Values for $C_{12}TAB$ in Hydrazine	135

LIST OF FIGURES

Figure		Page
3.1	Thermodynamic Process for Micelle Formation	20
3.2	Standard Entropy Change Upon Micelle Formation in Aqueous Solutions at Low Temperatures	36
3.3	Standard State Enthalpy Change Upon Micelle Formation in Aqueous Solutions at Low Temperatures	37
3.4	Standard State Gibbs Energy Change Upon Micelle Formation in Aqueous Solutions at Low Temperatures	38
3.5	Standard State Entropy Change Upon Micelle Formation in Aqueous Solutions at High Temperatures	39
3.6	Standard State Enthalpy Change Upon Micelle Formation in Aqueous Solutions at High Temperatures	40
3.7	Standard State Gibbs Energy Change Upon Micelle Formation in Aqueous Solutions at High Temperatures	41
3.8	Standard State Entropy Change Upon Micelle Formation in Nonaqueous Solutions at all Temperatures	43
3.9	Standard State Enthalpy Change Upon Micelle Formation in Nonaqueous Solutions at all Temperatures	44
3.10	Standard State Gibbs Energy Change Upon Micelle Formation in Nonaqueous Solutions at all Temperatures	45
4.1	Electrostatic Free Energy Change With Aggregate Size	71
4.2	Electrostatic Free Energy Change with Counterion Binding	71
4.3	Electrostatic Free Energy Change with Surfactant and/or Salt Concentration	72
4.4	Electrostatic Free Energy Change with Chain Length	72
4.5	Counterion Binding Change with Aggregate Size	75
5.1	Free Energy Change Upon Micelle Formation of C_xH_{2x+1} - $(OC_2H_4)_6OH$ in Aqueous Solutions	87

5.2 Aggregate Population Density of $C_xH_{2x+1}(OC_2H_4)_6OH$ at 298 K 89

5.3 Aggregate Population Density of $C_8H_{17}(OC_2H_4)_6OH$ at Different Temperatures 90

5.4 Free Energy Change of $C_{12}H_{25}(OC_2H_4)_6OH$ Micelle Formation for Different Nonspherical Shapes 92

5.5 Aggregate Population Density of $C_{12}H_{25}(OC_2H_4)_6OH$ for Different Nonspherical Shapes 92

5.6 Enthalpy Change Upon Aggregation of $C_{12}H_{25}(OC_2H_4)_6OH$ .. 95

5.7 Enthalpy Change Upon Aggregation of $C_xH_{2x+1}(OC_2H_4)_6OH$ at 298 K 96

5.8 Free Energy Change Dependence on Surfactant Concentration ($C_{12}H_{25}(OC_2H_4)_6OH$ at 298 K) 100

5.9 Aggregate Population Density of $C_{12}H_{25}(OC_2H_4)_6OH$ at Different Concentrations (T = 298°K) 101

5.10 Average Free Energy Change with Surfactant Concentration ($C_{12}H_{25}(OC_2H_4)_6OH$ at 298 K) 102

5.11 Mean Aggregate Size Dependence on Surfactant Concentration ($C_{12}H_{25}(OC_2H_4)_6OH$ at 298 K) 102

5.12 Free Energy Change Upon Micelle Formation of $C_xH_{2x+1}N^+(CH_3)_3\ Br^-$ in Aqueous Solutions 108

5.13 Average Free Energy Change Upon Micelle Formation of $C_xH_{2x+1}N^+(CH_3)_3\ Br^-$ 109

5.14 Aggregate Population Density of $C_xH_{2x+1}N^+(CH_3)_3\ Br^-$ at 298 K 110

5.15 Aggregate Population Density of $C_{14}H_{29}N^+(CH_3)_3\ Br^-$ at Different Temperatures 111

5.16 Enthalpy Change Upon Aggregation of $C_{14}H_{29}N^+(CH_3)_3\ Br^-$ 112

5.17 Temperature Effect on the Enthalpy Change ($C_{14}H_{29}N^+(CH_3)_3\ Br^-$) 112

5.18 Chain Length Effect on the Enthalpy Change (C_xTAB at 298 K) 113

5.19 Free Energy Change Upon $C_{12}SO_4^-\ Na^+$ Aggregate Formation as a Function of Salt Concentration 123

5.20 Aggregate Population Density of $C_{12}SO_4^-Na^+$ as a Function of Salt Concentration ... 123

5.21 Enthalpy Change Upon $C_{12}SO_4^-Na^+$ Aggregation with no Added Salt ... 124

5.22 Free Energy Change Dependence on $C_{12}SO_4^-Na^+$ Concentration ... 127

5.23 Aggregate Distribution of $C_{12}SO_4^-Na^+$ at Different Concentrations ... 128

5.24 Mean Aggregate Size Dependence on Surfactant Concentration ($C_{12}SO_4^-Na^+$ at 298 K) ... 129

5.25 Sphere-to-Rod Transition in C_xTAB as a Function of Chain Length ... 131

5.26 Free Energy Change Upon $C_{12}TAB$ Aggregate Formation in N_2H_4 and H_2O ... 136

5.27 Aggregate Population Density of $C_{12}TAB$ in N_2H_4 and H_2O 136

5.28 Enthalpy Change Upon $C_{12}TAB$ Aggregate Formation in N_2H_4 and H_2O ... 137

KEY TO SYMBOLS

a = Geometrical factor

C = Concentration

CMC = Critical Micelle Concentration

f = Geometrical ratio

G = Gibbs free energy

G(r) = Probability density

H = Enthalpy

K = Boltzmann constant

N = Aggregate size

P = Pressure

P(r) = Probability

R = Gas constant

r = Separation distance

S = Entropy

T = Temperature

V = Volume

W(r) = Work of cavity formation

X = Mole fraction

x = Dimensionless distance

y = Dimensionless electrostatic potential

Greek Letters

α = Nonsphericity factor

β = Fraction of counterion bound

γ = Surface tension

γ_o = Planar surface tension

β = Curvature dependence parameter for surface tension

Δ = Denotes a property change

ε = Dielectric constant

κ = Inverse Debye length

μ = Chemical potential

ρ = Density

σ = Surface charge density or surface area

ϕ = Fugacity coefficient

Ψ = Mean electrostatic potential

Subscripts

o = Total solution property

1 = Monomer property

2 = Solvent property except for ρ_2 which a micelle property

avg = Average

c = Counterion property

comp = Compression

el = Electrostatic

M = Micelle property

mc = Monomer cavity

ms = Monomer surface

N = N-mer aggregate property

O = Oblate

P = Prolate

r = Cavity property

S = Spherocylinder

σ = Surface property

Σ = Total surfactant property

Superscripts

o = Standard state property

* = Characteristic property

g = Gas

l = Liquid

O = Oblate

P = Prolate

S = Spherocylinder

vap = Vaporization

Overline

$\bar{}$ = Denotes partial molar or average property

Underline

$\underline{}$ = Denotes molar property

Abstract of Dissertation Presented to the Graduate School
of the University of Florida in Partial Fulfillment of the Requirements
for the Degree of Doctor of Philosophy

A MOLECULAR THERMODYNAMIC MODEL FOR SURFACTANT AGGREGATE FORMATION

By

Michel J Hourani

August, 1984

Chairman: Dr. John P. O Connell
Major Department. Chemical Engineering

A molecular thermodynamic process has been developed to model the properties of aggregation. It provides a conceptual and calculational framework for the thermodynamic properties of aggregate formation, the mean and distribution of aggregate sizes and shapes and the degree of counterion binding in ionic systems. Included are changes in intermolecular interactions upon aggregation, restriction of surfactant head groups to the micelle surface, effects of excluded volume from destroying monomer cavities and creating micelle cavities in the solvent, changes in entropy for concentrating the surfactant from the solution density to the aggregate density and binding of counterions in ionic solutions

The mass-action law of reaction equilibrium thermodynamics is used. The standard state thermodynamic property changes upon aggregation are calculated for each step in the process These steps

are related to molecular phenomena with similar physical behavior and modeled the monomer-solvent interactions and solvent cavity formation are related to the solubility of organic substances in the solvent, the micelle-solvent interactions and cavity properties are connected to monomer-solvent properties by only geometrical considerations, an equation of state for rigid nonspherical molecules is used for monomer and counterion compression, and the Poisson-Boltzmann theory is used to account for the surface electrostatic interactions and salt effects on ionic aggregates. This procedure leads to expressions for the free energy change upon aggregation which, with the material constraint on the overall surfactant concentration in the solution, describes all aspects of aggregate formation

The only experimental measurements the model uses are a single mean aggregate size for a given family of surfactants and the CMC to determine values for its parameters. The monomer cavity contribution, based on organic solubility, is universal. The nonsphericity factor associated with the entropy changes for concentrating the surfactant is assumed independent of temperature so only one parameter remains to be found from CMC measurements. The model then predicts aggregate and thermodynamic properties for a given surfactant-solvent system. Comparisons of these properties with data for ionics and nonionics including varying temperature, salt and surfactant concentrations and with solvent media are excellent. Micellization occurs only at a particular balance between solvophobic and solvophilic interactions.

CHAPTER I
INTRODUCTION

Much interest has been devoted to the association of amphiphilic molecules in aqueous and nonaqueous media. These solutions have assumed importance in practical situations such as enhanced oil recovery, organic solubilization and detergency. The objective of this investigation is the development of a molecular thermodynamic analysis that describes the molecular effects and mechanisms in micelle formation. The development considers micellization as a reversible formation of aggregates to which equilibrium thermodynamic formulations can be applied. A multistep thermodynamic process is developed for amphiphile association which provides a conceptual and calculational framework for the thermodynamic properties of micelle formation, the mean and distribution of aggregate sizes and shapes and the degree of counterion binding in ionic systems.

The solution thermodynamic property changes upon aggregate formation and their dependence on the variables of state, temperature, pressure and species concentration are discussed in chapter II. The discussion points out the difference of micelle formation in different solvents, or what is called the "Solvophobic Effect" (Sinanoglu, 1980) and (Ben-Naim, 1974), molecular conformations in the aggregates (Dill and Flory, 1981) and size distributions (Ruckenstein and Nagarajan, 1975) and (Tanford, 1974). Available models for the thermodynamic

formalism of micellization are then reviewed. Finally, experimental measurements and their connections with thermodynamics are discussed. Those measurements include critical micelle concentration (CMC) at different temperatures and pressures, calorimetry, light scattering and ion-selective electrode voltages.

A multistep process has been developed for the molecular effects and mechanisms involved in micelle formation which provides a calculational framework for these systems. It is presented in chapter III. The process includes all of the significant effects such as changes in intermolecular interactions upon aggregation, restriction of surfactant head groups to the micelle surface, excluded volume effects associated with destroying and creating the appropriate size cavities in the solvent, entropy changes upon surfactant compression from solution density to micellar density and counterion binding in ionic systems. A qualitative analysis for all of the thermodynamic property changes upon aggregate formation is presented for each of these steps as a function of aggregate size. This leads to a discussion of the thermodynamic or free energy constraint on micelle size formation and its relation to the material balance constraint.

A quantitative model for the thermodynamic properties of aggregate formation is presented in chapter IV. The development of the model is based upon considering micelle formation as an isothermal reaction equilibrium process where exact thermodynamic relations are available for standard state thermodynamic properties. Each step in the process is related to similar molecular phenomena and is modelled accordingly: monomer-solvent interactions and solvent cavity formation are related

to gaseous and organic solubility, micelle-solvent interactions and cavity properties are related to monomer-solvent properties by geometrical considerations, an equation of state for non-spherical molecules is used for monomer and counterion compression, the Poisson-Boltzmann theory was used to account for the surface electrostatic interactions in ionic aggregates and salt effects. The experimental information needed to determine the model parameters and the calculational technique to obtain aggregate properties are described.

Chapter V shows the use of the model to correlate and predict aggregate properties such as free energies and enthalpies of formation and the aggregate size distribution. Also, presented are the property dependence on temperature, salt and surfactant concentrations and on the chemical constitution of the system (chain length of the surfactant tail and the nature of its head group, the ions and the solvent involved).

Chapter VI provides a summary of all of the significant conclusions of this analysis and its uniqueness compared to other approaches. Extensions of this model to multicomponent aggregate systems are suggested.

CHAPTER II
THERMODYNAMIC PROPERTY CHANGES OF AGGREGATION

2.1 Observations on Aggregating Systems

The fundamental characteristic of monomers that form aggregates in liquid solvents is their amphiphilicity, i.e., the presence in the same molecule of one or more polar parts usually called head groups and a nonpolar part usually a hydrocarbon chain or tail. The head group can be ionic (anionic, cationic or zwitterionic) or nonionic. The ionic monomers have associated counterions and their properties depend on the particular counterion (Doughty, 1983) and change when salts are added. All amphiphilic molecules tend to associate in such a way that the nonpolar part is partially or completely removed from contact of the polar solvent while the polar groups remain wetted by the solvent.

Because the onset of aggregation can appear over small ranges of concentration there are relatively abrupt changes in the solution properties. Many properties of surfactant solutions (surface tension, electrical conductivity, refractive index, viscosity), if plotted against the concentration, change at a different rate above and below a relatively small range of concentrations (Mosan et al., 1982). Below that range, virtually no aggregates appear to be formed, while above it, the concentration of monomeric species changes relatively little with added surfactant. Virtually all additional surfactant forms aggregates. The loci of such a property above and below that range can

be extrapolated until they intersect at the concentration known as the Critical Micelle Concentration (CMC). Hall and Pethica (1970) defined the CMC as the concentration at which the change of monomer and micelle concentrations with the overall concentration is equal to 0.5, which is derived from the formulation of Phillips (1955):

$$\lim_{C \to CMC} \left. \frac{\partial (C_1 + C_M)}{\partial C} \right|_{T,P} = 0.5 \qquad (2.1)$$

Many CMC values have been obtained experimentally. Examination of the data reported by Mukerjee and Mysels (1971), Sugihara and Mukerjee (1981), Evans and Wightman (1982), Evans et al. (1982, 1983a, 1984), Lianos and Zana (1980, 1981, 1982, 1983), Omuta et al. (1968), Ueno et al. (1977), Hamann (1978), Donbrow and Jan (1963), Ray and Nemethy (1971) and Singh et al. (1980) shows the effects of solvent structure, temperature, pressure and added salt on the CMC of ionic and nonionic amphiphiles.

The driving forces associated with micelle formation are several. They vary in magnitude for different systems but not in kind. The thermodynamic property changes are directly related to the balance of these forces and in order to discuss that relationship, the thermodynamic formulation for such systems needs to be developed. Section 2.2 discusses the different thermodynamic models or formulations for micelle formation and will not be repeated here. Instead, a brief description of the relation between the thermodynamic properties and the experimental solution properties is made.

The standard free energy of micellization, ΔG°_{M}, at constant temperature and pressure is approximately related to the

CMC property by the following equation (Corkill et al., 1964):

$$\Delta G_M^o = RT \ln CMC \qquad (2.2)$$

The standard enthalpy change can then be obtained by using the Gibbs-Helmholtz equation:

$$\Delta H_M^o = \frac{\partial(\Delta G_M^o/T)}{\partial(1/T)}\bigg|_p = - RT^2 \frac{d(\ln CMC)}{dT} \qquad (2.3)$$

The standard entropy change can then be obtained

$$\Delta S_M^o = \frac{\Delta H_M^o - \Delta G_M^o}{T} \qquad (2.4)$$

From the examination of the CMC measurements and their temperature dependence in aqueous solutions, it can be observed that the entropy change upon micellization is large and positive at room temperature and becomes negative with increasing temperature. The enthalpy change is generally small at room temperature and can be either positive or negative. It becomes large and negative with increasing temperature. These changes in thermodynamic properties with temperature are due to the variations of the forces associated with micelle formation. These involve both the energetic effects of solvent-monomer and monomer-monomer interactions and the entropic effects of coalescence of volume excluded to the solvent when micelles are formed from the monomers and of collection of the surfactants and counterions into the micelles. At room temperature, the large positive entropy change indicates that the major molecular factors are due to changes in solvent structure and solvent conformation rather than to intermolecular potential energy changes. This entropy change accompanies the removal of water from

around the hydrocarbon chain and the increase in volume available for the small water molecules. This factor is called the "Solvophobic Effect" and is described by Ben-Naim (1974) and Sinanoglu (1980). The solvophobic effect becomes weaker with increasing temperature and the energetic effects, associated with the hydrocarbon chain condensation and the decrease in water-hydrocarbon surface interaction, lead to a large negative enthalpy change at higher temperatures.

Aggregating systems are not limited to aqueous media. Amphiphilic molecules associate in nonaqueous media of relatively high polarity such as hydrazine, glycerol and ethylammonium nitrate. Compared to aqueous solutions, solvophobic interactions of surfactants in nonaqueous media appear to be weaker. CMC measurements in nonaqueous solutions show that the enthalpy and entropy changes upon micelle formation are strikingly different than the same property changes in aqueous solutions. While the entropy change is large and positive in aqueous media at room temperature, it is large and negative in nonaqueous media at all temperatures. This entropy decrease reflects the association and ordering accompanying the transfer of surfactant ions and counterions into the micelle structure, dominating the weak solvophobic effect of a nonaqueous solvent. The formation of micelles in these media appears then to be entirely a result of a favorable enthalpy change. The entropy and enthalpy changes in nonaqueous media at any temperature are then similar to those observed in aqueous media at high temperatures because water becomes a more normal fluid at these conditions. The free energy is, however, similar in both systems and that means that they appear to be equally lipophobic.

Another aspect of aggregating systems is the conformation of the surfactant in micelles. The organization of the hydrocarbon chains in the micellar interior is constrained by the geometry of the micelle, the space-filling requirements of the chain segments or intramolecular structure, and the continuity and flexibility of the chains. Three different models have been used to describe the micelle configuration - the radial chain model, the oil droplet model and the interphase model. In the radial chain model, the chains are all-trans and directed radially inward. Chain termini are located in the single layer at the center of the micellar core, leading to an extremely high density. The oil droplet model assumes the chains to be fully disordered as in an amorphous alkane liquid. In this perfectly disordered model, all the chain segments have equal probability of occurring in any layer of the core while the highest probability is actually in the outermost layer. This model does not take into account intramolecular steric constraints and chain flexibility. The interphase model is a lattice based model where the core is divided into layers and equally sized cells. These cells are filled with chain segments according to a statistical analysis developed by Dill and Flory (1981) and it leads to a uniformly dense micellar interior. This model has been generally adopted here because it carefully considers all the molecular constraints imposed on the surfactant molecules.

The oil droplet and the interphase models suggest that solvent/hydrocarbon contact occurs at the surface of the micelle and there is no solvent penetration into the micellar core, while the radial chain model allows for such penetration to occur.

Extensive experimental observations have been made to determine the water/surfactant interface at different conditions. Studies such as Small Angle Neutron Scattering (Bendedouch et al., 1983), (Hayter and Penfold, 1981) and (Hayter and Zemb, 1982), Nuclear Magnetic Resonance and Proton Relaxation (Nilsson et al., (Cabane, 1981), Laser-Excited Raman Scattering (Kalyanasundaram and Thomas, 1976), Partial Molar Volume and Isentropic Partial Molar Compressibility (Brun et al., 1978) imply that the micellar core does not contain any significant concentrations of water. Other measurements that use sensitive probes of micellar environments such as Optical Rotary Dispersion (Menger and Boyer, 1980) are interpreted in an opposite way. From these probe measurements, however, it cannot be concluded that water penetrates the core. The major assumption is that the probe molecules are completely buried within the hydrophobic cores. Rather, it is likely that the probe molecules reside at the hydrocarbon core interface adjacent to external water and thus "see" water. The assertion that water penetration into the core is negligible does not imply that the fraction of hydrocarbon in contact with water is small. On the contrary, a large fraction of the surface of the hydrocarbon cores of small micelles is unprotected by head groups leading to significant contacting. It is important to note that the contacting, on a monomer basis, decreases as the size of the micelle increases due to its dependence on the surface area of that micelle.

Micelle shape and its dependance on size are related to the molecular conformations and the density assumed for the micellar interior. The oil droplet and the interphase models lead to a uniform

density micellar interior that is constant and independent of the micelle size. As the micelle grows spherically, it reaches a point where at least one surfactant chain has the all-trans configuration. Beyond that size, a transition from spherical to nonspherical shape must occur in order for the density to stay constant and uniform. Tanford (1972) and Mukerjee et al. (1983) discussed that transition and the thermodynamic property changes associated with the nonspherical micelles. In chapter V, the shape of nonspherical micelles will be discussed along with its effect on the thermodynamic properties.

Finally, the aggregate population density is important. The size distribution of the aggregates varies with the surfactant constitution and concentration, as well as with added salts and temperature. Surfactant solutions that have a sharp break point at the CMC tend to be close to monodisperse. However, in most systems, the solution properties change rapidly, but continuously, with surfactant concentration in the region close to the CMC. Because of that continuity, aggregates are found at all surfactant concentrations, though at low concentrations, the number of aggregates and their average size are small. The first attempt to make a connection between population variations and the CMC was by Ruckenstein and Nagarajan (1975) who defined the CMC as the concentration at which an inflection point occurs in the micelle size distribution as surfactant is added. Below that concentration, the distribution is monotonically decreasing while above it the distribution exhibits a maximum and a minimum. Ben-Naim and Stillinger (1980) criticized that definition of the CMC noting that the CMC can be far above the concentration at which the

size distribution changes from monotonically decreasing to nonmonotonic. Hall and Pethica's interpretation of the CMC (Equation 2.1) is equivalent to this one, this will be discussed and shown in chapter V.

2.2 Thermodynamic Framework

The thermodynamics of micelle formation has been treated by three approaches. The mass-action approach assumes stepwise reaction equilibrium of aggregates of various sizes while the phase-separation equilibrium approach regards micelles as a distinct phase in equilibrium with the surfactant monomer/solvent solution. The latter does not allow for a size distribution. The third approach is based on the thermodynamics of small systems of Hill (1963-64) and was developed by Hall and Pethica (1970) for micelle formation in nonionic systems. It also allows for a distribution of sizes through a single thermodynamic variable.

In the mass-action approach, micellar aggregates of size N, surfactant molecules, M, and counterions, C, are in association-dissociation equilibrium, at fixed temperature, pressure and overall concentration of components

$$N\,M_1^- + N_c\,C^+ \;=\; M_N^{N-} + N_c{}^+ \qquad (2.5)$$

Here the charges are assumed to be unity with a countercation, but this can be varied with no substantial change in the final expressions. The chemical potentials of the monomer, counterions and micelles can be

written in terms of their standard state potentials and their activities:

$$\begin{aligned} \mu_1 &= \mu_1^o + RT \ln a_1 \\ \mu_c &= \mu_c^o + RT \ln a_c \\ \mu_M &= \mu_M^o + RT \ln a_M \end{aligned} \tag{2.6}$$

The charged species chemical potentials have been written even though they do not rigorously exist (Perry et al., 1981).
At reaction equilibrium,

$$\mu_M = N \mu_1 + N_c \mu_c \tag{2.7}$$

giving

$$\mu_M^o + RT \ln a_M = N \mu_1^o + N RT \ln a_1 + N_c \mu_c^o + N_c RT \ln a_c \tag{2.8}$$

Note that this equation defines the number, N_c, of adsorbed counterions since all others not adsorbed must be unaffected by the reaction.
At the CMC, the solution is dilute in both surfactant monomers and micelles and, therefore, ideal solution with a Henry's Law reference state can be assumed and the monomer and micelle activities are replaced by their respective concentrations. Equation (2.8) can then be written as

$$\mu_M^o + RT \ln C_M = N \mu_1^o + N RT \ln C_1 + N_c \mu_c^o + N_c RT \ln C_c \tag{2.9}$$

From equation (2.9), the standard state thermodynamic property changes upon formation of an N-mer are explicitly related to the monomer, micelle and counterion concentrations and temperature. Equation (2.9) is valid for all values of N. The standard state properties are

functions only of temperature and pressure, the effect of pressure will be neglected in the present treatment.

The pseudo-phase approach, where a micelle is regarded as a separate phase, proceeds from the phase equilibrium relation:

$$\mu_{i,M} = \mu_{i,1} \qquad \text{(Species 1)} \qquad (2.10)$$

giving

$$\mu^{o}_{i,M} + RT \ln a_{i,M} = \mu^{o}_{i,1} + RT \ln a_{i,1} \qquad (2.11)$$

Again assuming ideality

$$\mu^{o}_{i,M} + RT \ln C_{i,M} = \mu^{o}_{i,1} + RT \ln C_{i,1} \qquad (2.12)$$

which is different from equation (2.9) because it does not depend on N and the counterion is not explicitly separated. Rather, for ionic micelles, the separate micellar phase includes the ionic double layer and, therefore, the species 1 in equation (2.12) involves the charged surfactant and the counterion bound to the surface of the micelle.

If the values of N and N_c are fixed in equation (2.9), it becomes equivalent to (2.12). To allow for variations in N, Hall and Pethica (1970) proposed an alternative based on the thermodynamics of small systems relevant to micellization. An ensemble of n fixed small systems of c nonionic components, open to all components, was defined and the total free energy was written as

$$d G_T = - S_T \, dT + V_T \, dP + \sum_{i=1}^{c} \mu_{i,1} \, d N_{i,1} + \sum_{i=1}^{c} \mu_{i,M} \, d N_{i,m} + \varepsilon \, dM \qquad (2.13)$$

where

$$\left.\frac{\partial G_T}{\partial M}\right|_{T,P,N_{i,1},N_{i,M}}$$

The quantity ε is strictly formal since its general modelling is not known.

From this fundamental equation, Hall and Pethica proceeded with equilibrium relations to obtain the standard state thermodynamic properties and the final results are

$$-\frac{\Delta H_M^o}{RT} = T\left.\frac{\partial \ln X_1}{\partial T}\right|_P - \frac{T}{\bar{N}}\left.\frac{\partial \ln X_M}{\partial T}\right|_P \qquad (2.14)$$

$$\frac{\Delta V_M^o}{RT} = \left.\frac{\partial \ln X_1}{\partial P}\right|_T - \frac{1}{\bar{N}}\left.\frac{\partial \ln X_M}{\partial P}\right|_T \qquad (2.15)$$

where $\bar{N}$ is the number average aggregate size, a function of T and P. Equations (2.14) and (2.15) are equivalent to those obtained from the mass-action treatment as will be shown in chapter IV.

The phase-separation approach is defective because a phase, by definition, is homogeneous and uniform throughout its extent. Further in the case of ionic micelles, counterions are distributed in an electrical double layer outside the micelle surface and are not found in the core of the aggregates. Also, micellar aggregates are highly distributed in size and, in most systems, there are many more small aggregates than very large ones and their dimensions cannot be accepted as a separate phase. On the other hand, the mass-action and

small-system approaches do not have these deficiencies and their formulations are equally applicable to all aggregate sizes.

2.3 Experimental Measurements and Thermodynamic Properties

Extensive experimental measurements on surfactant solutions have been collected and the connections between these quantitative observations and the thermodynamics of aggregate formation need to be made for applications to micellar systems.

As it was discussed earlier, the CMC and its dependence on the chemical and physical constitutions of the system is a very important measurement. All three formulations (Equations 2.9, 2.12 and 2.13) plus equation (2.1) yield the direct relation between the species concentrations at the CMC and the standard state thermodynamic properties. Except for (2.12) those equations are appropriate for any aggregate size and, therefore, the standard state free energy change upon N-mer formation and the equilibrium size distribution are related to the CMC.

The mean is the most important description of a distribution. In the case of micelle formation, the number average aggregate size, $\overline{N}$, which depends on the state and constituents can be measured and values are reported in the literature for several surfactant molecules. Light scattering (Missel et al., 1980, Mayashi and Ikeda, 1980; Zemb et al., 1983; Evans et al., 1983b) and Membrane Osmometry (Birdi et al., 1980 and Birdi, 1982) are the typical experiments. Besides using values to determine model parameters, the aggregate mean is a reflection of the

size and, thus, the balance of the force fields of the monomers and solvent. For example, an increase in the solvophobic forces or a decrease in the electrostatic interactions tends to increase the aggregate size and, therefore, its mean.

Another thermodynamic quantity of interest is the heat effect associated with micelle formation. Calorimetric measurements are available (Birdi, 1983, Desnoyers et al., 1983; Mazer and Olofsson, 1982). Also, from the temperature derivative of the free energy (Gibbs-Helmholtz equation), the standard state enthalpy of aggregate formation can be obtained and compared to the experimental results:

$$\Delta H^{o}\Big|_{T,P,N} = \frac{\partial(\Delta G^{o}/T)}{\partial(1/T)}\Big|_{P,N} \tag{2.16}$$

$$d\left[\frac{\Delta G^{o}}{T}\right]_{P,N} = \frac{\partial(\Delta G^{o}/T)}{\partial(1/T)}\Big|_{P,N} d(1/T) + \frac{\partial(\Delta G^{o}/T)}{\partial M_{N}}\Big|_{T,P,M_{N'\neq N}} dM_{N} \tag{2.17}$$

$$\Delta H^{o}\Big|_{T,P,N} = \frac{\partial(\Delta G^{o}/T)}{\partial(1/T)}\Big|_{P,N} + \frac{\partial(\Delta G^{o}/T)}{\partial M_{N}}\Big|_{T,P,M_{N'\neq N}} \frac{\partial M_{N}}{\partial(1/T)}\Big|_{P,N} \tag{2.18}$$

Equation (2.18) shows that standard state enthalpy change depends on how the standard free energy and the aggregate size distribution change with temperature. It is written at a constant aggregate size and, therefore, the enthalpy change for each size can be obtained. The relative contributions of the first and second terms depend on the size. Chapter V will show the use of equation (2.18) for several surfactant solutions and its comparison with experimental measurements.

Micelle interior density is one more property that needs to be addressed because of its geometrical and physical constraints on the thermodynamic properties. The oil droplet model where the chains are

fully disordered as in an amorphous alkane liquid is usually adopted. The micelle density would then be obtained from n-alkane liquid density at the same chain length. As it was discussed earlier, the molecular conformations in surfactant micelles are constrained by the intermolecular structure and the intermolecular forces and a perfect disorder configuration as in liquid n-alkane is not the best representation. Equation (2.15) shows that if the CMC pressure dependence is measured, volume changes upon micellization can be determined and the micelle density can be better estimated. Tanaka et al. (1974) and Brun et al (1978) have done such measurements that showed small differences between monomer and aggregate densities, micelle densities are just larger than n-alkane densities at the same chain length and primarily because of the solvophobic forces and inhomogeneouties of these aggregates.

Finally, an experimental observation limited to ionic surfactant solutions is free ion electrode measurements. The results are related to the fraction of counterions adsorbed at the micellar surface. Equation (2.9) shows that, for the free energy change to be computed, the free counterion concentration in the solution is needed. Stigter (1964), Kale et al. (1980), Zana (1980) and Ryu et al. (1983) reported some results on these measurements. By minimizing the free energy of a model with respect to fraction bound counterions in the terms associated with the electrostatic interactions at the surface, this fraction can be determined. Such a calculational scheme will be discussed in chapter IV.

CHAPTER III
A THERMODYNAMIC PROCESS FOR AGGREGATE FORMATION

3.1 Concept and Development of a Multistep Process

Aggregate formation is a result of a balance between "favorable" and "unfavorable" forces. The favorable forces arising from hydrocarbon chain condensation, minimization of solvent-hydrocarbon contact area and coalescence of volume excluded to the solvent lead to a negative free energy change. The unfavorable forces, on the other hand, arise from collecting the surfactants and counterions into the aggregates and the electrostatic and/or steric repulsions between surfactant head groups at the surface lead to a positive free energy change. To develop a theory that describes the properties of aggregate (including micelle) formation all of these effects need to be separately considered.

Thermodynamic property changes between two equilibrium states are independent of the path followed between these states. This concept can be used to determine the property changes between monomers and aggregates. An optimum path between these states would include the various effects discussed above. Our procedure is the creation of a path where steps are relevant to one type of force. That technique leads to a multistep process providing a conceptual and calculational framework for the overall thermodynamic property changes of interest.

Ionic surfactant solutions contain three species that are involved in the process of forming micelles: the charged monomers, the counterions and the solvent. Nonionic surfactants have only two species: surfactants and solvent. The state of each species can be addressed separately during that process, leading to path with independent parallel branches. Such a process is illustrated in figure 3.1.

The initial step of the process involves removal of the monomers and the appropriate fraction of counterions from their cavities in the solution. The thermodynamic property changes associated with this step are due to the elimination of the intermolecular interactions between the solvent and the amphiphile. The state of the monomers and the counterions after this step is chosen to be gaseous state at the same species density (which is generally quite low). The major reason for this choice is that the thermodynamic property changes of that step can be related to gaseous and organic solubility which can be found from experimental information. The details of this procedure will be discussed in chapter IV.

The second step in the process involves collapsing the monomer and counterion cavities. The coalescence of the volume excluded to the solvent and restructuring of the solvent molecule arrangements around these cavities give large contributions to all the thermodynamic properties. Solvent cavity models will be discussed in section 3.2.

Steps 3 and 4 are involved with the configurational change of the monomers and the counterions upon aggregate formation. The dispersed

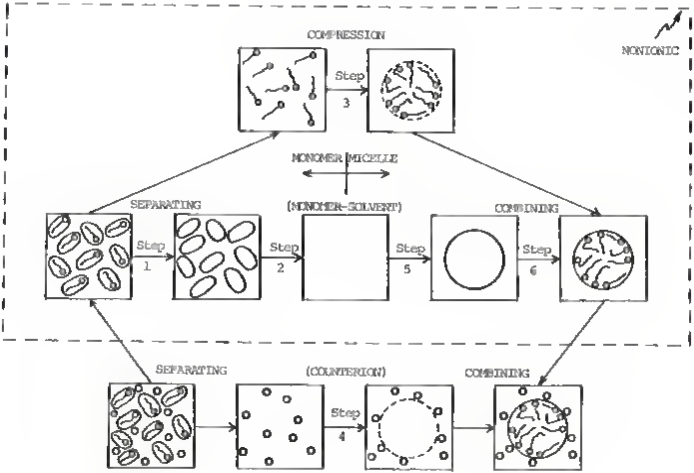

Figure 3.1 Thermodynamic Process for Micelle Formation

monomers are compressed to the aggregate density with the restriction that their head groups and bound counterions are located at the surface. Appreciable entropy decrease occurs due to all of these processes. The enthalpy will have a favorable contribution due to the hydrocarbon chain condensation and an unfavorable contribution due to head group electrostatic and/or steric repulsion. Details of the expressions for these steps will be discussed in sections 3.3 and 3.4.

Step 5 involves the creation of an N-mer cavity which partially reverses step 2. On a monomer basis, the magnitude of the changes in step 5 is smaller than those of step 2 because of their dependence on the area and curvature of the cavities. However, rather than use data, as for step 2, the property changes for step 5 are modelled with two parameters.

The final step of this thermodynamic process for aggregate formation involves placement of the compressed monomers in the cavity with the electrical double layer effects in the bound counterions around it. The properties for this step are computed similarly to those of step 1. On a monomer basis the enthalpy and entropy changes are smaller for step 6 than for step 1 because the solvent-monomer contact decreases upon aggregation.

As previously noted, this process includes all of the molecular phenomena and effects associated with surfactant aggregate formation. Further discussion and calculations involving all of the steps are included in the rest of this chapter and chapter IV.

3.2 Solvent Cavity Models for Gaseous and Organic Solubility

The intent of this section is to provide a brief survey of different models available in the literature concerning the thermodynamic property changes upon creation of a solute sized cavity in a solvent. Particular emphasis will be given to the scaled-particle theory (Reiss et al., 1959 and Tully-Smith and Reiss, 1970) and its application to aqueous solutions (Pierotti, 1965; Stillinger, 1973; Lucas and Bury, 1976; and Crovetto et al., 1982) and to the cluster or cavity model developed by Sinanoglu (1981).

The scaled-particle theory of classical fluids offers a framework which examines the relationship between molecular structure and thermodynamic properties. Its application to molecular solute properties in aqueous solutions has been disappointing however and probably because of the strong, three-dimensional interactions that exist in water. The theoretical formulation will be presented here to discuss its major features and limitations.

One of the key quantities in the scaled-particle theory is W(r), the amount of reversible, isothermal work necessary to create in a rigid body fluid of interest a spherical cavity of diameter (a) whose interior is devoid of molecular centers. The probability P(r) that a randomly chosen position in the pure solvent lies outside of all such exclusion spheres is equal to the volume fraction not within them. This probability can in turn be related to W(r):

$$P(r) = \exp\left(-W(r)/RT\right) \qquad (3.1)$$

The probability density that the spherical shell outside the cavity contains a particle center is $4\pi r^2 \rho G(r)$ where $\rho G(r)$ measures the concentration of molecular centers just outside the sphere.

From the canonical (T,V,N) ensemble, relationships between W(r), P(r) and G(r) can be derived (Stillinger, 1973). Exact results exist for these quantities in the limit of very small and very large rs. For rigid spheres in the region of $r < a/2$, the relations are

$$\begin{aligned} P(r) &= 1 - \frac{4\pi}{3}\rho r^3 \\ W(r)/KT &= -\ln\left[1 - \frac{4\pi}{3}\rho r^3\right] \\ G(r) &= \left[1 - \frac{4\pi}{3}\rho r^3\right]^{-1} \end{aligned} \tag{3.2}$$

For large r, W(r) is related to the thermodynamic properties dominated by work against the external pressure P and against the surface tension of the cavity-solvent interface. Thus, for r approaching infinity,

$$W(r) = \frac{4\pi}{3}\rho r^3 + 4\pi\gamma_\infty r^2 - 16\pi(\gamma_\infty\delta)r + O(1) \tag{3.3}$$

where γ_∞ is the surface tension in the planar interface limit and δ provides the leading term in the curvature dependence of the surface tension γ (Buff, 1951)

$$\gamma = \gamma_\infty[1 - 2\delta/r] \tag{3.4}$$

Pierotti (1963) and others adopted the procedure of bridging these two limiting results with a smooth function of r in order to determine the thermodynamic property changes upon creation of any size cavity of

radius r in a hard-sphere fluid of diameter a. The comparison of the calculated liquid-vapor interfacial tension from Pierotti model with experimental values (Stillinger, 1973) shows that the interpolation technique between the microscopic and macroscopic region was not appropriate.

Stillinger (1973) developed a revised G(r) for water using the experimental liquid-vapor interfacial tension and the radial distribution function as input data. Although this modification appears to be an appropriate extension of the Pierotti concepts, it yields results for gas solubility which are not significantly improved over Pierotti results. In fact, while the values of W(r) and its derivative with respect to r at r = a/2 are matched between the two expressions, the second derivatives are of opposite sign (Brugman, 1979).

Brugman (1979) presented a different approach to the scaled-particle theory by using a reference solute for the formation of very small cavities. Then the work required to form a larger solute cavity from the reference cavity was expressed in terms of a model for γ_{∞} and δ. The thermodynamic properties of creating the reference cavity were obtained by difference between the experimental free energy of solution and the interaction between the solvent and the solute. An inordinary large magnitude was found for the value and temperature variation of δ, the curvature dependence of the surface tension. Brugman concluded that the use of the surface tension of pure water is probably inappropriate for calculations involving a cavity in a solvent or against a wall. Tully-Smith and Reiss (1970) imply the same idea.

Sinanoglu (1981) presented a different approach from the scaled-particle theory to calculate the thermodynamic properties of cavity formation. The model relates microsurface properties to macrosurface properties. The microvalues and their dependence on the ratio of the cavity size to the average solvent molecular size were determined for common polar and nonpolar solvents.

The analysis starts from relating the planar surface free energy, G_c, to that of an empty cavity surface free energy.

$$G_c = \sigma \gamma \qquad \text{(Planar)} \qquad (3.5)$$

$$G_c = K_g \sigma \gamma \qquad \text{(Concave)} \qquad (3.6)$$

where σ is the surface area of the cavity and γ is the bulk planar surface tension of the solvent, K_g is the correction factor between microscopic and macroscopic properties. It depends on the cavity size, R_A, relative to the solvent molecule size, R_1:

$$K_g = K_g(R_A/R_1) \qquad (3.7)$$

The enthalpy and entropy changes upon creating thet cavity can be obtained from the Gibbs-Helmholtz equation (2.3 and 2.4) leading to

$$H_c = K_g \sigma \gamma \left[1 + \frac{\partial \ln K_g}{\partial \ln T} - \frac{\partial \ln \gamma}{\partial \ln T} - \frac{\partial \ln \sigma}{\partial \ln T} \right]_P \qquad (3.8)$$

$$S_c = - \sigma \gamma \left[\frac{\partial K_g}{\partial T} \right]_P + K_g \left[\frac{\partial \ln \gamma}{\partial T} + \frac{\partial \ln \sigma}{\partial T} \right]_P \qquad (3.9)$$

For very large cavities K_g approaches 1 and the planar surface properties will be appropriate.

Finally, $K_g(R_A/R_1)$ was related to $K_g(1)$ in the limit of $R_A = R_1$ where $K_g(1)$ was evaluated from the properties of pure solvents:

$$K_g(R_A/R_1) = 1 + \frac{\sigma_1}{\sigma_A}\left[K_g(1) - 1\right] \qquad (3.10)$$

$$K_g(1) = \frac{1}{\sigma_1 Y}\left[\Delta G^o_{vap} + RT \ln \frac{RT}{v_1}\right] \qquad (3.11)$$

The fundamental difference between this model and the scaled-particle theory is that the thermodynamic properties are related to the surface area of the cavity in the former while they are related to the curvature of the cavity in the latter. We have performed some calculations using Sinanoglu model to check its adequacy and predictive ability of the thermodynamic properties. Unfortunately changes of the entropy and enthalpy properties with temperature are of opposite sign to experiment In the Sinanoglu formulation, the dependence of the surface tension on temperature overwhelms that of the correction factor K_g. Even though the Sinanoglu model appears to be appropriate and simple, this conclusion means that it cannot be used for our objectives.

Along with the scaled particle theory and the analysis of Sinanoglu, several microscopic theories based on statistical mechanics (Neff and McQuarrie, 1973; Chan et al., 1978; Pratt and Chandler, 1977, 1980; Pratt et al., 1980) have been developed to describe the arrangement of aqueous and other solvent molecules around a cavity containing a nonpolar molecule and the solute-solvent interactions. The general objective of these theories is to give both

structure and thermodynamic properties of gas solubility in liquids. Also, molecular dynamics (Marchesi, 1983) and Monte Carlo (Jonsson, 1981) simulations of liquid water between two rigid walls have been performed to study the ordering of water molecules in the vicinity of the walls.

All of these theories show the difficulties encountered in correlating the properties of bulk water and aqueous solutions of apolar solutes. Statistical mechanical theories of aqueous systems usually involve complicated models requiring approximations that obscure the essential physics. A more pragmatic approach to the aqueous solutions of interest here is to input the known solution thermodynamic properties of molecules and model only the properties of the aggregates. Such an approach will then build in the unique features of water (or any other solvent for that matter). However, its capacity to provide an understanding for the properties of solvophobic solutions at a molecular level will be limited.

In chapter IV the details of this approach will be given and applied in our model by using the aqueous hydrocarbon solubility data as input information.

3.3 Equations of State for Nonspherical Molecules

The step associated with the compression of dispersed monomers and counterions in the solution has energetic and entropic effects. The energetic interactions involve hydrocarbon chain condensation and head group repulsion. These properties will be discussed in the next

section The entropic effect is due to the density increase from the dispersed monomer density to the density of the aggregate. A thermodynamic formulation for such an entropy change is as follows:

$$\Delta \underline{S} = \int_{\rho_1}^{\rho_2} \left.\frac{\partial \underline{S}}{\partial \rho}\right|_T d\rho \qquad (3.12)$$

where ρ_1 is the dispersed monomer density

and ρ_2 is the micella interior density

From Maxwell relations we know that

$$\left.\frac{\partial \underline{S}}{\partial \underline{V}}\right|_T = \left.\frac{\partial \underline{P}}{\partial T}\right|_{\underline{V}} \qquad \text{where } \underline{V} = \frac{1}{\rho} \qquad (3.13)$$

Substituting (3.13) in (3.12)

$$\Delta \underline{S} = - \int_{\rho_1}^{\rho_2} \left.\frac{\partial \underline{P}}{\partial T}\right|_{\underline{V}} \frac{d\rho}{\rho^2} \qquad (3.14)$$

From equation (3.14) we conclude that if an equation of state is used we can calculate the entropy change upon compression. As an approximation, we use a rigid body equation. Such equations of state will be discussed next.

The scaled-particle theory formulated for simple fluids by Reiss et al. (1959) yielded the first reasonably accurate equation of state of hard spheres. Other versions were given by the Percus-Yevick theory based on the pressure and compressibility equations (Reed and Gubbins, 1973). Carnahan-Starling (1969) improved the accuracy by combining the two forms. An extension of these theories to nonspherical hard convex bodies was first given by Gibbons (1969,1970). The nonspherical

equivalent to the Carnahan-Starling equation was first given by Boublik (1975)

$$\frac{P}{\rho RT} = \frac{1}{1-v} + \frac{r \cdot s}{\rho (1-v)^2} + \frac{Q\, S^2 (3-v)}{9\, \rho (1-v)^3} \qquad (3.15)$$

where $\rho = \sum_i \rho_i$ (ρ_i is the number density of i in the mixture)

$v = \sum_i \rho_i V_i^*$ (V_i^* is a characteristic volume of i)

$r = \sum_i \rho_i R_i^*$ (R_i^* is a characteristic radius of curvature of i)

$S = \sum_i \rho_i S_i^*$ (S_i^* is a characteristic surface area of i)

$Q = \sum_i \rho_i R_i^{*2}$

In the case of a one-component system, equation (3.15) reduces to the form

$$\frac{P}{\rho RT} = \frac{1 + (3\alpha - 2)y + (3\alpha^2 - 3\alpha + 1)y^2 - \alpha^2 y^3}{(1-y)^3} \qquad (3.16)$$

where

$$\alpha = R \cdot S/3V \; ; \qquad y = \rho V^*$$

Equation (3.16) was used to evaluate the compressibility factors of prolate spherocylinders (Boublik, 1975) and was found to be in good agreement with reported data up to a packing fractions y = 0.48

The entropy change upon compression is obtained by substituting equation (3.16) in (3.14). Equation (3.16) is chosed because we are dealing with single component surfactant aggregate

$$-\frac{\Delta S}{R} = \frac{}{(1-\rho_2\underline{v}^*)^2}\left\{\frac{(\rho_2\underline{v}^*)^2}{2} + \alpha^2 - \frac{1}{2}\right\}$$

$$-\frac{1}{(1-\rho_1\underline{v}^*)^2}\left\{\frac{(\rho_1\underline{v}^*)^2}{2} + \alpha^2 - \frac{1}{2}\right\}$$

$$+\frac{1}{(1-\rho_2\underline{v}^*)^2}\{2(\rho_2\underline{v}^*) - \alpha^2 + 3\alpha - 1\} \qquad (3.19)$$

$$-\frac{1}{(1-\rho_1\underline{v}^*)}\{2(\rho_1\underline{v}^*) - \alpha^2 + 3\alpha - 1\}$$

$$-\ln\left\{\frac{(1-\rho_2\underline{v}^*)^{1-\alpha^2}\cdot(\rho_1\underline{v}^*)}{(1-\rho_1\underline{v}^*)^{1-\alpha^2}\cdot(\rho_2\underline{v}^*)}\right\}$$

Equation (3.19) is used in our model. Note that the values calculated from equation (3.19) do not allow for preferential orientations of the chains as in a micelle nor for the differences of chain conformations between monomers and aggregates. Limitations of this will be discussed in chapter IV.

3.4 Electrostatic Interactions and Counterion Binding

Aggregates consisting of ionic amphiphiles will carry, in general, a high net charge at their surfaces because the head groups are restricted to that region. Thus their physicochemical properties will be strongly affected by electrostatic interactions. These interactions are directly related to the fraction of counterions bound to the aggregate. This fraction is mainly determined by the surface charge density which is, in turn, related to aggregate size. The ion binding in such systems can be observed directly by thermodynamic experiments

Work by Mukerjee (1969) and Stigter (1974a and b, 1975a and b) showed the effects of charged aggregates on the properties of micelle formation. These effects were evaluated on the basis of the classical theory of Gouy-Chapman of the electrical double layer around charged surfaces. This theory postulates a uniform, continuous, interfacial surface charge which is neutralized by a diffuse, ionic layer of point charges in the solution. That is, the space charge was assumed to have a distribution which obeys the Poisson-Boltzmann equation. It also regards the solvent as a dielectric continuum so the whole aggregate is like the "primitive" model of electrolytes. This model provides a good quantitative description of the behavior of ionic colloidal systems (Mitchell and Nunham, 1983). Carnie and Chan (1980) modified the Gouy-Chapman picture to include solvent structure effects though their surface potential relation derived for nonpolar surfaces is very complex.

Simulations such as Monte Carlo and molecular dynamics can be done to investigate how well these theories describe an electrolyte solution. Jonsson et al. (1980), and Lunse et al. (1982), have found that the results from Poisson-Boltzmann equation agree quite well with these simulations for a lamellar liquid crystal and for spherically symmetric systems. This is true despite the large local ion concentration close to the charged surface of an aggregate. The Poisson-Boltzmann equation for an electrolyte solution is

$$\nabla^2\psi = -\frac{4\pi}{\epsilon} \sum_i z_i e N_{oi} \exp(-z_i e\psi/KT) \qquad (3.20)$$

It is derived by assuming that the potential of mean force for the ionic species i is $z_i e\psi$ where e is the unit charge, ψ is the mean electrostatic potential and N_{oi} is the concentration of species i at zero potential. Supposing that the aggregate is a sphere of radius R and that the solvent contains a 1:1 electrolyte, equation (3.20) reduces to

$$\frac{d^2\psi}{dr^2} + \frac{2}{r}\frac{d\psi}{dr} = \frac{8\pi N_o e}{\varepsilon} \sinh\left(\frac{e\psi}{KT}\right) \tag{3.21}$$

The boundary conditions satisfied by the potential $\psi = \psi(r)$ are

$$\begin{aligned} \frac{d\psi}{dr} &= -\frac{4\pi\sigma}{\varepsilon} && \text{at } r = R \\ \frac{d\psi}{dr} &= 0 && \text{at } r \to \infty \end{aligned} \tag{3.22}$$

where σ is the surface charge density.

We can introduce dimensionless variables through the substitutions

$$\begin{aligned} y &= e\psi/KT \; ; \qquad x = \kappa r \\ \kappa^2 &= \frac{8\pi N_o e^2}{\varepsilon KT} \end{aligned} \tag{3.23}$$

where κ is the inverse Debye length.

Equations (3.21) and (3.22) become

$$\frac{d^2y}{dx^2} + \frac{2}{x}\frac{dy}{dx} = \sinh y \tag{3.24}$$

$$\left(\frac{dy}{dx}\right)_{x=\kappa r} = -\frac{4\pi\sigma e}{\varepsilon\kappa KT} = -S$$

$$\left(\frac{dy}{dx}\right)_{x=\infty} = 0 \tag{3.25}$$

The electrostatic free energy can be evaluated from

$$\Delta G^{o}_{el} = \int_{0}^{\sigma} \psi_o \, d\sigma \qquad (3.26)$$

where ψ_o is the potential at the charged surface

Using dimensionless variables, equation (3.26) will be

$$\Delta G^{o}_{el} = \left(\frac{KT}{e}\right)^2 \frac{\varepsilon\kappa}{4\pi} \cdot A_M \cdot \int_{0}^{s} y_o \, ds \qquad (3.27)$$

where A_M is the surface area per charge

No analytical solution to equation (3.24) has been found except for the case of Debye-Huckel linearization for small potentials. Loeb et al (1961) tabulated numerical solutions to the above nonlinear equation for some systems. Mitchell and Ninham (1983) derived an approximate solution to it in the limit of large sphere surfaces though this is not appropriate for small sizes (R<16A)

We have developed an algorithm for equation (3.24) and solved it numerically as a function of aggregate size and fraction of counterions bound to the surface. The computation technique and the results obtained from that program will be presented and discussed in chapter IV.

3.5 Thermodynamic and Material Constraints on Aggregate Formation

For the thermodynamic process in figure 3.1, the energetic and the entropic effects associated with each step and their relative contributions can be related to the overall free energy change upon aggregate formation. This analysis leads to a qualitative description of the thermodynamic properties and their effects on aggregate size.

The micelle thermodynamic properties will be given on a monomer basis, i e, they are the properties of forming an N-mer divided by N.

The effects associated with step 1 are due to the elimination of the intermolecular interactions between the solvent and the monomers and counterions. The model that will be presented in chapter IV makes the assumption that the counterions and the monomer head groups undergo no change in interaction with water upon aggregation mainly because the bound counterions and the head groups are assumed to be still surrounded by solvent molecules. The elimination of interactions between the solvent and the monomer tail will, however, contribute a positive enthalpy change which is identical for both ionic and nonionic surfactant systems. Since the density and configuration of the monomers and counterions are maintained constant and the solvent structure around the cavities is retained, there is essentially no change in their entropy.

In the second step, the thermodynamic properties for the counterion and the head group cavities will, again, be assumed unchanged upon aggregation for the same reason given earlier. The experimental solution properties show that there are significant entropy and enthalpy contributions associated with the amphiphile tail cavity, and they are highly temperature dependent. At low temperatures, the entropy change in aqueous solutions is large and positive while the enthalpy change is close to zero. At high temperatures, the enthalpy change is large and negative while the entropy change is small. Step 2 is similarly modelled for ionic and nonionic amphiphiles as can be seen from figure 3.1.

The monomer and counterion compression steps involve a large and negative entropy change due to the density increase, two enthalpy contributions that have opposite signs: a negative contribution due to the chain condensation, and a positive one due to the electrostatic and/or steric repulsions between head groups. The entropy decrease for ionic amphiphiles is greater than that of nonionic amphiphiles because it involves both the monomers and counterions (Steps 3 and 4) for the former while it involves the monomers only (Step 3) for the latter. The negative enthalpy contribution is identical for both systems while the positive contribution is greater in ionic than nonionic systems due to the electrostatic interactions. Steric repulsions are the only forces involved between nonionic head groups.

The aggregate thermodynamic properties associated with step 5 and 6 are similar in form to the monomer properties of steps 2 and 1, respectively. They do, however, have opposite signs because the processes are reversed. The aggregate property changes also decrease as the size increases because they are determined on a monomer basis.

The relative enthalpy and entropy contributions from each step of the process can now be plotted as a function of aggregate size for both ionic and nonionic systems (Figures 3.2, 3.3, 3.5 and 3.6) so that the overall Gibbs energy change upon micellization (Figures 3.4 and 3.7) can be determined from the equation:

$$\frac{\Delta G_M^o}{RT} = \frac{\Delta H_M^o}{RT} - \frac{\Delta S_M^o}{R} \qquad (3.28)$$

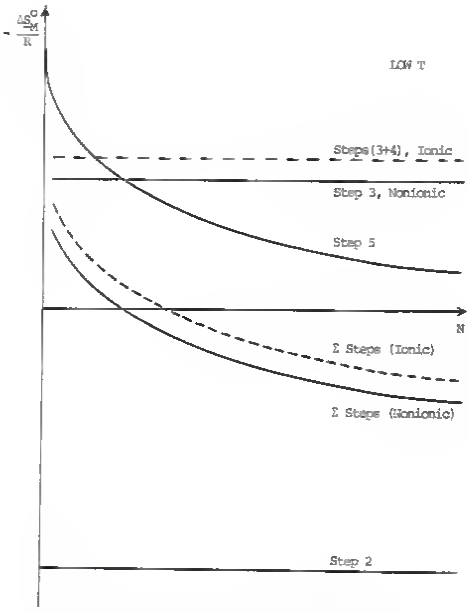

Figure 3.2 Standard State Entropy Change Upon Micelle Formation in Aqueous Solutions at Low Temperatures

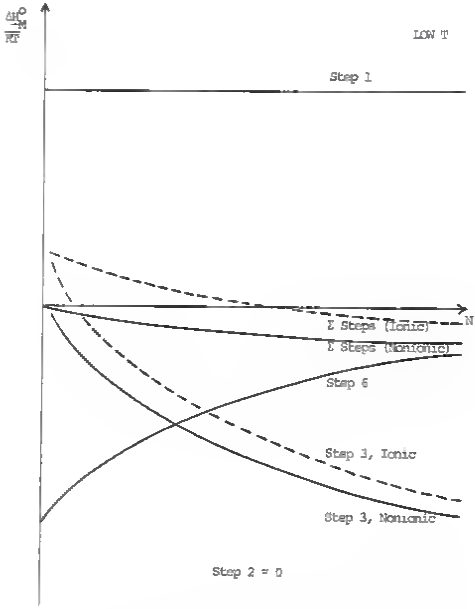

Figure 3.3 Standard State Enthalpy Change Upon Micelle Formation in Aqueous Solutions at Low Temperatures

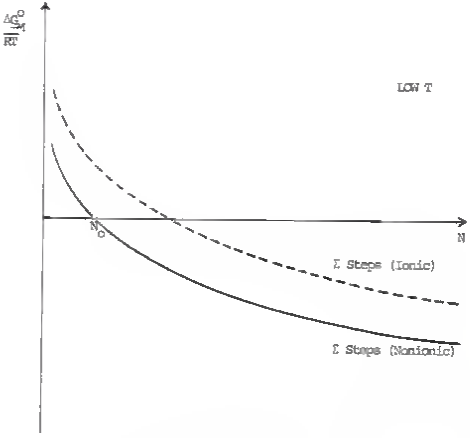

Figure 3.4 Standard State Gibbs Energy Change Upon Micelle Formation in Aqueous Solutions at Low Temperatures

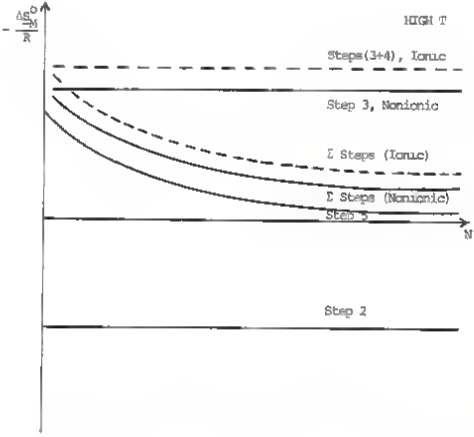

Figure 3.5 Standard State Entropy Change Upon Micelle Formation in Aqueous Solutions at High Temperatures

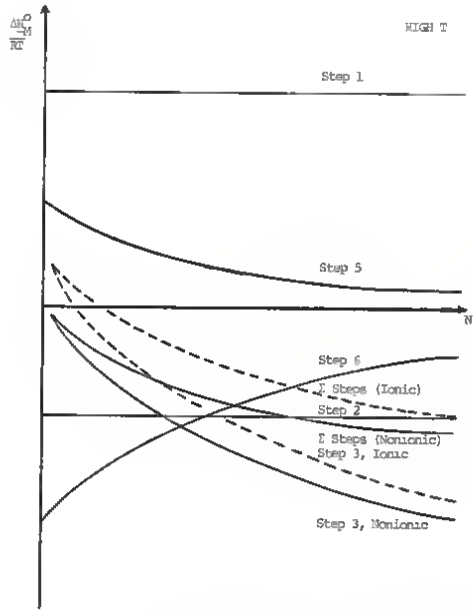

Figure 3.6 Standard State Enthalpy Change Upon Micelle Formation in Aqueous Solutions at High Temperatures

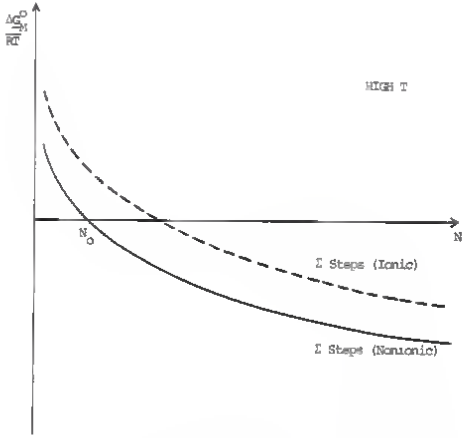

Figure 3.7 Standard State Gibbs Energy Change Upon Micelle Formation in Aqueous Solutions at High Temperatures

By comparing figures 3.2 and 3.3 to 3.5 and 3.6, one can conclude that aqueous aggregate formation is an entropy driven process at low temperatures while it is an enthalpy driven process at high temperatures. This transition in the thermodynamic properties is mainly due to the temperature dependence of step 2. This dependence is different in nonaqueous solutions (Figures 3.8, 3.9 and 3.10) where aggregate formation is an enthalpy driven process at all temperatures. The effect on the overall free energy change is, however, negligible (Figures 3.4, 3.7 and 3.10) and that is due to the compensation between the enthalpy and entropy changes. Note that the free energy change for ionic systems is larger than for nonionic systems and that is because of the larger entropy and enthalpy contributions of step 3 for ionic systems as it was discussed earlier.

Figures 3.4, 3.7 and 3.10 show the thermodynamic constraints on aggregate size. Small aggregates ($N<N_o$) which have an overall positive Gibbs energy change are thermodynamically unfavorable, while large aggregates ($N>N_o$) with a negative Gibbs energy change are thermodynamically favorable.

The free energy change decays asymptotically to a negative value as N approaches infinity. From a strictly thermodynamic point of view, aggregates of infinite size are most favored. These infinitely sized aggregates, however, would require an infinite amphiphile concentration in the solution. Since in the region of interest close to the CMC, the amphiphile concentration is small, these large aggregates cannot actually be formed. This material balance constraint can be formulated in the following form

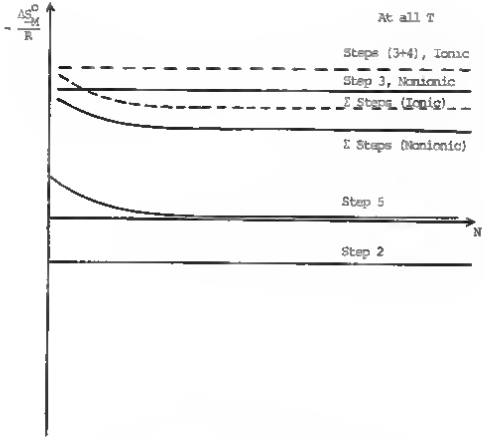

Figure 3.8 Standard State Entropy Change Upon Micelle Formation in Nonaqueous Solutions at all Temperatures

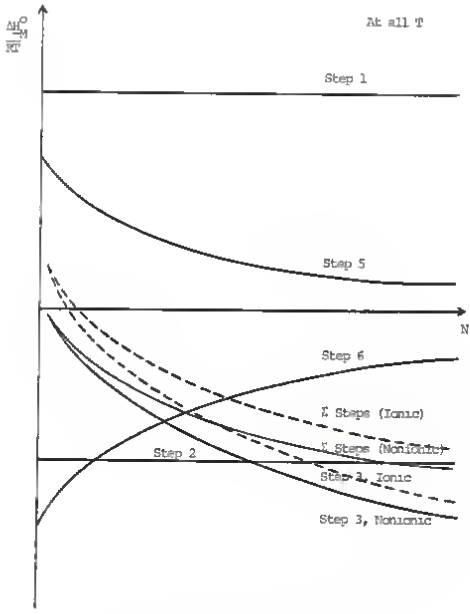

Figure 3.9 Standard State Enthalpy Change Upon Micelle Formation in Nonaqueous Solutions at all Temperatures

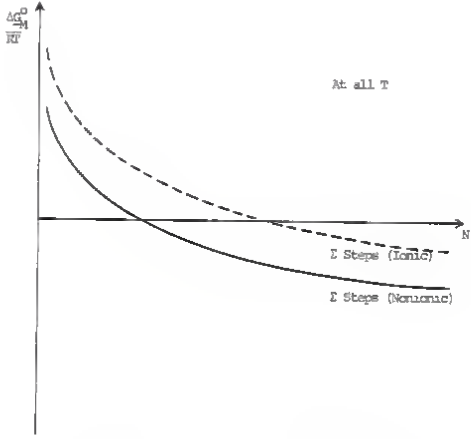

Figure 3.10 Standard State Gibbs Energy Change Upon Micelle Formation in Nonaqueous Solutions at all Temperatures

$$C_t = \sum_{N=1}^{\infty} C_N \qquad (3.29)$$

where C_t is the total amphiphile concentration

and C_N is the amphiphile concentration of an N-mer

The use of equation (3.29) and its interaction with the thermodynamic formulation for aggregate formation will be shown and discussed in chapter IV.

CHAPTER IV

A SPECIFIC MODEL FOR THE THERMODYNAMIC PROPERTIES OF AGGREGATE FORMATION

4.1 Model Formulation

The equilibrium between monomers and aggregates in amphiphilic solutions will be regarded behaving in accord with the Mass-Action Law described in chapter II. This law allows us to describe the thermodynamic relations and properties for any aggregate size. This, in turn, allows us to find the properties and population density of each possible aggregate in the solution.

The analysis considers aggregates of size N, surfactant molecules, M, and counterions, C, are in a reaction equilibrium at fixed temperature, pressure and overall concentration of components:

$$N\,M_1^{-} + N_c\,C^{+} = M_N^{N-} + N_c^{+} \qquad (4.1)$$

where N_c is the number of bound counterions to an N-mer aggregate. Here the surfactant is assumed to be anionic with unit charge, but the formulation can be easily adapted to surfactants and ions of any other charge including zero (nonionics).

Following the derivations and assumptions made in chapter II (Equations 2.6 to 2.9), the monomer, micelle and counterion concentrations C_1, C_N, and C_c, respectively are related to the standard state thermodynamic properties upon formation of an N-mer

$$\mu_M^o + RT \ln C_M = N \mu_1^o + NRT \ln C_1 + N_c \mu_c^o + N_o RT \ln C_c \qquad (4.2)$$

An N-mer aggregate concentration can be related to the surfactant incorporated into that aggregate. This is especially useful when the material balance constraint (section 3.5) is imposed on the aggregate distribution.

Define

$$C_N = N C_M \qquad (4.3)$$

where C_N is the concentration of surfactant in the N-mers

Substituting equation (4.3) in (4.2) and solving for the micelle concentration we obtain

$$C_M = \frac{C_N}{N} = \exp\left\{N\left\{\frac{(\mu_1^o + \beta\mu_c^o - \mu_N^o)}{RT} + \ln C_1 + \beta \ln C_c\right\}\right\} \qquad (4.4)$$

where $\beta = \frac{N_c}{N}$, the fraction of counterion bound and

$$\mu_N^o = \frac{\mu_M^o}{N} \qquad (4.5)$$

where μ_N^o is the standard state chemical potential of the surfactant in the N-mer.

Figures 3.4, 3.7, 3.10 were plotted on that basis where

$$\frac{\Delta\mu_M^o}{NRT} \equiv \frac{\Delta G_M^o}{RT} = \frac{\mu_N^o - (\mu_1^o + \beta\mu_c^o)}{RT} \qquad (4.6)$$

For the aggregate size distribution, the species mole fraction is preferred to the species concentration. Equation (4.4) can then be written in terms of mole fractions X_N

$$\frac{X_N}{N} = \exp\left\{N\left[\frac{(\mu_1^o + \beta\mu_c^o - \mu_N^o)}{RT} + \ln X_1 + \beta \ln X_c + \ln C_o \frac{(N + \beta N - 1)}{N}\right]\right\} \qquad (4.7)$$

where C_o is the total solution concentration of surfactant and solvent Equation (4.7) is appropriate for any ionic surfactant solution. In the case of nonionic surfactant (β=0), the reaction equilibrium becomes

$$N\,M_1 = M_N \tag{4.8}$$

and equation (4.7) reduces to

$$\frac{X_N}{N} = \exp\left\{N\left\{\frac{(\mu_1^o - \mu_N^o)}{RT} + \ln X_1 + \ln C_o \frac{(N-1)}{N}\right\}\right\} \tag{4.9}$$

The free energy change, $\Delta G_M^o = \mu_N^o - (\mu_1^o + \beta\mu_c^o)$, is found by modeling the property changes of the proposed thermodynamic process (Figure 3.1), as will be discussed in the following sections. This overall change can be divided into three main parts associated with the sections of the process

$$\frac{\Delta G_M^o}{RT} = -\left.\frac{\Delta G^o}{RT}\right|_{Monomers} - \left.\frac{\Delta S^o}{R}\right|_{comp} + \left.\frac{\Delta G^o}{RT}\right|_{Micelles} \tag{4.10}$$

where $\left.\frac{\Delta G^o}{RT}\right|_{Monomers}$ is the free energy change associated with putting the monomers into the solvent from the ideal gas

$\left.\frac{\Delta G^o}{RT}\right|_{Micelle}$ is the free energy change associated with putting the micelles into the solvent

$-\left.\frac{\Delta S^o}{R}\right|_{comp}$ is the entropy change associated with steps 3 and 4.

Note that the enthelpy contribution of the compression step is included in $\left.\frac{\Delta G^o}{RT}\right|_{Micelle}$ and that is why the entropy term, $-\left.\frac{\Delta S^o}{R}\right|_{comp}$, is not a free energy change.

Each of the monomer and micelle free energy changes has contributions from surface interactions and cavities. Equation (4.10) can then be written as

$$\frac{\Delta G_M^o}{RT} = -\left.\frac{\Delta G^o}{RT}\right|_{\substack{\text{Monomer}\\\text{Cavity}}} - \left.\frac{\Delta G^o}{RT}\right|_{\substack{\text{Monomer}\\\text{Surface}}} - \left.\frac{\Delta S^o}{R}\right|_{\text{comp}} + \left.\frac{\Delta G^o}{RT}\right|_{\substack{\text{Micelle}\\\text{Cavity}}} + \left.\frac{\Delta G^o}{RT}\right|_{\substack{\text{Micelle}\\\text{Surface}}} \qquad (4.11)$$

Models of the first two terms are described in section 4.2, while these of the third, fourth and fifth terms are given in sections 4.3, 4.4 and 4.5, respectively.

Material Balance

The population density distribution of aggregates can be obtained from equation 4.7 once the free energy change upon aggregation is determined. However, this distribution is constrained by the material balance described in section 3.5:

$$X_t = \sum_{N=1}^{\infty} X_N = X_1 + \sum_{N=2}^{\infty} X_N \qquad (4.12)$$

Since the summation in equation (4.12) extends up to infinity, it can be approximated by an integral

$$X_t = X_1 + \int_{N=2}^{N=\infty} X_N \, dN \qquad (4.13)$$

As was noted in chapter II there is a transition from spherical to nonspherical shape of a micelle when at least one surfactant chain has the all-trans configuration. Since the thermodynamic properties depend on the geometry of a micelle, the dependence of $\frac{\Delta G_M^o}{RT}$ and, therefore, X_N, on N is expected to change at that point. The integral over X_N in

equation (4.13) must then be divided into two separate integrals, one for each micellar shape

$$X_t \sim X_1 + \int_{N=2}^{N_{spherical}} X_N\Big|_{spherical} dN + \int_{N_{spherical+1}}^{N=\infty} X_N\Big|_{nonspherical} dN \qquad (4.14)$$

Mean Aggregate Size

The number average mean aggregate size, $\bar{N}$, defined in chapter II can now be formulated once $\left(\frac{X_N}{N}\right)$ or the aggregate size distribution is determined

$$\bar{N} = \frac{\int_{N=2}^{N=\infty} N\left(\frac{X_N}{N}\right) dN}{\int_{N=2}^{N=\infty} \left(\frac{X_N}{N}\right) dN} \qquad (4.15)$$

Splitting $\left(\frac{X_N}{N}\right)$ over spherical and nonspherical regions, $\bar{N}$ becomes

$$\bar{N} = \frac{\int_{N=2}^{N_{sph}} N\left(\frac{X_N}{N}\right)_{Sph} dN + \int_{N_{sph}}^{\infty} N\left(\frac{X_N}{N}\right)_{Nonsph} dN}{\int_{N=2}^{N_{sph}} \left(\frac{X_N}{N}\right)_{Sph} dN + \int_{N_{sph+1}}^{\infty} \left(\frac{X_N}{N}\right)_{Nonsph} dN} \qquad (4.16)$$

The use of equations (4.14) and (4.16) in our model will be described in section (4.7).

4-2 Solubility of Organic Monomers as Input Data (Steps 1 and 2)

The first two steps in the thermodynamic process of figure 3.1 are equivalent to the reverse of the solution process for gas solubility used by Pierotti (1965). That process consisted of the creation of a solute-sized cavity in a solvent and introduction of an interacting

solute molecule into that cavity, the opposite of our steps. As a result, we can use experimental solubility data in these two steps. This procedure eliminates modeling each step separately. As discussed in section 3.2 there are problems with cavity models to correlate solution properties, especially for molecular solutes in aqueous solutions. In this section the thermodynamic properties of solution and their relation to experimental solubility are derived.

For equilibrium between the gas and the liquid phases, the chemical potentials or the partial Gibbs energies of the gas (Species 1) in each phase are equal.

$$\bar{G}_1^g = \bar{G}_1^\ell \tag{4.17}$$

This equation can be written in terms of the standard state properties as

$$\underline{G}_1^{o,g} + RT \ln a_1^g = \underline{G}_1^{o,\ell} + RT \ln a_1^\ell \tag{4.18}$$

where the activity $a_1 = \frac{f_1}{f_1^o}$ and f is the fugacity.
The standard state of the gas in the gaseous phase at any fixed temperature is defined as that in which the gas has a fugacity of unit pressure. For the gas in the liquid phase, the standard state at that temperature is taken to be the hypothetical state found by extrapolation of the line representing Henry's Law on an f_1 vs x_1 graph to unit mole fraction for the dissolved gas solute. The fugacity in this standard state is Henry's constant, H. Equation (4.18) becomes

$$\underline{G}_1^{o,g} + RT \ln \frac{f_1^g}{1\text{atm}} = \underline{G}_1^{o,\ell} + RT \ln \frac{f_1^\ell}{H} \tag{4.19}$$

If the pure gas phase is assumed ideal at one atmospheric pressure, $\frac{f_1^g}{1atm}$ is unity:

$$\frac{f_1^g}{1atm} = \frac{y_1^g \phi_1^g P}{1atm} \simeq 1 \qquad (4.20)$$

where ϕ_1^g is the fugacity coefficient which is unity for an ideal gas. The dissolved gas has a very small mole fraction in the solution. For such a dilute solution we can approximate $\frac{f_1^\ell}{H}$ by

$$\frac{f_1^\ell}{H} \simeq X_1 \gamma_1^* = X_1 \qquad (4.21)$$

where γ_1^* is the activity coefficient in the unsymmetric convention which is unity at very low mole fraction.

Substituting (4.20) and (4.21) in (4.19) we can express the standard solution free energy change in terms of the gas solubility X_1:

$$-\Delta \underline{G}^o\Big|_{\text{Monomer}} = -\underline{G}_1^{o,\ell} + \underline{G}_1^{o,g} \simeq RT \ln X_1 \qquad (4.22)$$

The other standard state thermodynamic properties of solution can be obtained from the appropriate temperature derivatives:

$$\Delta \underline{H}^o = \frac{\partial(\Delta \underline{G}^o/T)}{\partial(1/T)}\bigg|_P ; \qquad \Delta \underline{S}^o = \frac{\Delta \underline{H}^o - \Delta \underline{G}^o}{T} = -\frac{\partial \Delta \underline{G}^o}{\partial T}\bigg|_P \qquad (4.23)$$

The equation used to correlate the gas mole fraction, X_1, as a function of temperature is that of Wilhelm et al. (1977)

$$-\ln X_1 = \frac{\Delta \underline{G}^o}{RT} = A + \frac{B}{T} + C \ln T + DT \qquad (4.24)$$

where A, B, C and D are constants.

Table 4.1
Correlation of Normal Paraffin Solubilities in Water

Solute	Solvent	T (°K)	Parameters for Equations (4.24), (4.25)			
			A	B	C	D
Methane	Water	273-353	183.786	-9112.582	-25.040	1.43(-04)
Ethane	Water	273-353	268.441	-13369.40	-37.556	2.30(-03)
Propane	Water	273-353	397.818	-18105.10	-58.513	2.29(-02)
n-Butane	Water	273-353	403.810	-18768.00	-59.111	2.23(-02)
n-Pentane*	Water	273-353		-20434.50	-63.383	2.21(-02)
n-Hexane*	Water	273-353		-22101.00	-67.657	2.19(-02)

* Extrapolated from short chain molecules

Methane and Ethane Parameters are obtained from Wilhelm et al. (1977)

Table 4.2
Comparison of Estimated and Experimental Enthalpies of Solution of n-Pentane and n-Hexane in Water

	T (°K)	$\frac{\Delta H^{\circ}}{RT}$ calc	$\frac{\Delta H^{\circ}}{RT}$ exp [a]
n-Pentane	288	- 13.93	- 13.67 0.1
	298	- 11.77	- 11.58 0.1
n-Hexane	288	- 15.39	- 15.01 0.1
	298	- 13.03	- 12.69 0.1

a : Data of Gill et al. (1976)

Collected Solubility Data

	Solute	T (°K)	x_1	Reference
Water				
	n-Pentane	273	1.6(-05)	McAuliffe (1966) &
		298	1.2(-05)	Polak and Lu (1973)
	n-Hexane	273	3.5(-06)	"
		298	2.6(-06)	"
	n-Heptane	273	7.9(-07)	"
		298	6.1(-07)	"
	n-Octane	273	2.1(-07)	"
		298	1.3(-07)	"
	n-Decane	298	2.5(-09)	Franks (1966) & Sutton and Calder(1974)
	n-Dodecane	298	4.0(-10)	"
	n-Tetradecane	298	2.0(-10)	"
	n-Hexadecane	298	0.7(-10)	"
Hydrazine				
	Helium	298	5.2(-06)	Chang et al. (1966)
	Nitrogen	298	7.2(-06)	"
	Argon	298	1.2(-05)	"
Ethyl Ammonium Nitrate				
	Krepton	298	2.9(-04)	Evans et al. (1981)
	Methane	298	2.1(-04)	"
	Ethane	298	7.4(-04)	"

From equation (4.23) the enthalpy and entropy of solution can be related to the coefficients of equation (4.24).

$$\frac{\Delta \bar{H}^{o}}{RT} = \frac{B}{T} - C - DT \qquad (4.25a)$$

$$-\frac{\Delta \bar{S}^{o}}{R} = A + C(1+\ln T) + 2DT \qquad (4.25b)$$

The solubility in water of long chain hydrocarbons is given at only one temperature (25° C). Its temperature dependence for these long chain molecules can be extrapolated from the short-chain molecules (Ethane, Propane and n-Butane). The enthalpy of solution obtained for n-Pentane and n-Hexane compared very well with the calorimetric measurements of Gill et al. (1976) as it can be seen in table 4.2. Also in table 4.2 the collected solubility data are given.

Equation (4.22) will be used in our model to compute the first two terms of equation (4.11) and the calculational technique will be described in section 4.7.

4.3 Equation of State for Monomer Compression

This section describes the entropy changes associated with the compression of dispersed monomers and counterions to make the aggregate. These changes can be modeled using the rigid-body equation of state of Boublik (Equation 3.16). The entropy change is given by equation (3.19). The four quantities in that equation are the densities, ρ_1 and ρ_2, the nonsphericity factor, α, and the characteristic volume, $\underline{V}^{*}$.

The dispersed monomer and counterion density, ρ_1, is given by the overall surfactant concentration added to the solution. For a 1:1 surfactant molecule,

$$\rho_1\Big|_{\text{Monomer}} = \rho_1\Big|_{\text{Counterion}} = C_t \qquad (4.26)$$

This can easily be adjusted for changes in charge.

The density, ρ_2, corresponds to the interior density of the aggregate. This density is approximately that of the n-alkane liquid of the same chain length. The inverse of this density, V_m, in such a hydrocarbon core is used by Tanford (1973) and Israelachvili et al. (1976):

$$V_m = (27.4 + 26.9\ N_c)\ \text{Å}^3 \qquad (4.27)$$

where N_c is the carbon number.

While it would be necessary to consider the constraints on the molecular conformations in surfactant micelles, Tanaka et al. (1974) and Brun et al. (1978) show that the pressure dependence of the CMC leads to ρ_2 values slightly larger than expression (4.27). However, the difference has negligible effect on the entropy change in equation (3.19) and it is more convenient since it is valid for all chain lengths while the experimental data are limited to only few substances and contain the head group effects as well.

The nonsphericity factor is a geometric parameter that depends on the shape and the size of the surfactant in the gaseous state. It is given by

$$\alpha = \frac{\text{Radius of Curvature} * \text{Surface Area}}{3 * \text{Volume}} \qquad (4.28)$$

Table 4.3
Characteristic Volumes for Rigid Body Equation of State

Carbon Number	V^* cc/g
12	0.5431
14	0.5318 *
16	0.5206

* Interpolated

For a spherical molecule, $\alpha = 1.0$. The counterions are assumed to be spherical and thus no parameterization is needed to describe the entropy change upon counterion compression. In the surfactant case, however, there is no means of determining α and it will be considered as a parameter. The computational procedure for determining this parameter by fitting experimental data is given in section 4.7.

The characteristic volume is another unknown quantity that needs to be determined. The Perturbed Hard-Chain theory developed by Beret and Prausnitz (1975) provides values for the hard body characteristic volumes for equation (3.19). Knowing that characteristic parameters determined from one equation of state can be different if another equation is used, we justify our choice by arguing that whatever error introduced in $\underline{V}^*$ is corrected by the experimental fitting of the parameter α.

Finally, the use of a hard-body equation of state ignores entropic effects associated with changes in orientational constraints of the chains in a micelle. However, we again lump these effects into α. Values of $\underline{V}^*$ used are listed in table 4.3.

4.4 Micelle Cavity Properties

The creation of a micelle cavity (Step 5) and its thermodynamic properties are discussed in this section. This step partially reverses step 2. However, unlike that step no experimental information such as solubility is available to use. If the cavity thermodynamic properties are assumed to be continuously changing from a macroscopic cavity of an

N-mer to a monomer cavity, we can relate the properties of the latter to the former by geometric considerations. This assumption, therefore, ignores discontinuities in the thermodynamic properties between microscopic and macroscopic sizes as is used in scaled particle theory (Reiss, 1977).

The micelle cavity thermodynamic properties are related to the monomer cavity properties by a geometric factor

$$\Delta\underline{G}^{o}\Big|_{\substack{\text{Micelle}\\\text{Cavity}}} = \Delta\underline{G}^{o}\Big|_{\substack{\text{Monomer}\\\text{Cavity}}} * f_r \qquad (4.29)$$

where

$$f_r = \frac{\text{Mean Radius of Curvature of N-mer/N}}{\text{Mean Radius of Curvature of Monomer}} \qquad (4.30)$$

The micelle radius of curvature is divided by N because the thermodynamic properties are on a monomer basis as discussed in section 3.5. The choice of radius of curvature was based on the work of Bruggman (1979) and the fact that the properties of aggregation could not be correlated with any other geometric factor.

The factor f_r depends on the shape and the size of the aggregate as given below for different geometries.

4.4.1 Spherical Aggregates

The radius of curvature, R_c, of an N-mer is obtained from its total volume, V_M, which is known from equation (4.27).

$$V_M = N\,V_m = \frac{4\pi}{3} R_M^3$$
$$R_c = R_M \qquad (4.31)$$

Solving for R_c and substituting it in equation (4.30), we can determine f_r:

$$f_r \simeq \frac{\left(\frac{3NV_m}{4\pi}\right)^{1/3}}{\left(\frac{3V_m}{4\pi}\right)^{1/3}} N^{1/3} = \frac{1}{N^{2/3}} \tag{4.32}$$

The spherical-nonspherical shape transition occurs when one surfactant molecule has an all-trans configuration. This fully extended chain length, ℓ_c, is given by Tanford (1973):

$$\ell_c = R_M \simeq (1.5 + 1.265\ N_c)\text{Å} \tag{4.33}$$

The micelle size at which this transition occurs is then given by

$$N_{transition} = \frac{4\pi}{3V_m}(1.5 + 1.265\ N_c)^3 \tag{4.34}$$

The nonspherical shapes that we considered are three: spherocylinder, prolate and oblate.

4.4.2 Spherocylindrical Micelle

The radius of curvature relation to the volume of a spherocylinder

$$V_M = N\,V_m \simeq \pi R_M^3\left(\alpha_s + \frac{4}{3}\right) \tag{4.35}$$

where $\alpha_s = \frac{L_M}{R_M}$ (L_M is the length of the cylindrical part)

$$R_c = R_M\left(\frac{\alpha_s}{4} + 1\right) \tag{4.36}$$

Solving for α_s in (4.35) and substituting in (4.36) gives that relation

$$R_c = R_M\left\{\left(\frac{NV_m}{\pi R_M^3} - \frac{4}{3}\right)/4 + 1\right\} \tag{4.37}$$

Replacing equation (4.37) in (4.30), f_r for a spherocylinder is obtained:

$$f_r = \left\{ \frac{1}{3^{1/3} R_M^2} \left(\frac{V_m}{4\pi} \right)^{2/3} \right\} + \frac{1}{N} \left\{ \frac{2}{3} R_m \left(\frac{4\pi}{3V_m} \right)^{1/3} \right\} - a^S_{o,r} + a^S_{1,r}/N \qquad (4.38a)$$

where $a^S_{o,r}$ and $a^S_{1,r}$ will be used from now on to represent the terms involved in f_r.

4.4.3 Prolate Micelle

The same procedure as in section 4.4.2 is followed to determine f_r for a prolate micelle:

$$V_M = N V_m = \frac{4\pi}{3} \alpha_p R_M^3 \qquad (4.39)$$

where $\alpha_p = \frac{L_M}{R_N}$ (L_M is the length of the major axis)

$$R_c = \frac{R_M}{2} \left[\alpha_p + \frac{\ln\left(\alpha_p + \sqrt{\alpha_p^2 - 1}\right)}{\sqrt{\alpha_p^2 - 1}} \right] \qquad (4.40)$$

The function f_r obtained after the radius of curvature is substituted in equation (4.30) has no direct (1/N) relation as in the spherocylinder case but it can be fitted to such a dependence:

$$f_r = a^P_{o,r} + a^P_{1,r}/N \qquad (4.38b)$$

where $a^P_{o,r}$ and $a^P_{1,r}$ are different in values than those in equation (4.38a).

4.4.4 Oblate Micelle

Similar to prolate micelle, the function f_r dependence on the size of an oblate micelle is

$$V_m = N V_m = \frac{4}{3} \alpha_o^2 R_M^3$$

$$\alpha_o = \frac{L_M}{R_M}$$

$$R_c = \frac{\alpha_o R_M}{2}\left(\frac{1}{\alpha_o} + \frac{\cos^{-1}(1/\alpha_o)}{\sqrt{1 - 1/\alpha_o^2}} \right)$$

$$f_r = a^o_{o,r} + a^o_{1,r}/N \qquad (4.38c)$$

The values of the geometrical parameters, $a_{o,r}$ and $a_{1,r}$, for the three shapes discussed above are illustrated below for a chain of 12 carbons.

Carbon Number	Spherocylinder		Prolate		Oblate	
	$a^S_{o,r}$	$a^S_{1,r}$	$a^P_{o,r}$	$a^P_{1,r}$	$a^O_{o,r}$	$a^O_{1,r}$
12	0.0229	2.543	0.0312	2.004	0.0127	3.224

The micelle cavity thermodynamic properties have been related to the monomer cavity properties by equation (4.29). This term is added to equation (4.11).

4.5 Micelle Surface Properties

The thermodynamic properties associated with the surface of a micelle (step 6 and part of step 3) are discussed in this section. They include three effects: chain-solvent interactions at the surface of a micelle, chain-chain interactions in the interior of the micelle and head group repulsions at the surface. Modeling of the first two effects are similar for nonionic and ionic surfactant systems. However, the head group repulsions are of a different nature in these

two systems because electrostatic interactions dominate the charged head groups in ionic systems where there are dipole-dipole interactions and steric repulsions between the uncharged head groups in nonionic systems.

4.5.1 Chain-Solvent and Chain-Chain Interactions

The interphase model concerning the surfactant conformations in a micelle was discussed in chapter II. We concluded from that model that solvent/hydrocarbon contact occurs at the surface of a micelle and solvent penetration into the micellar core can be ignored. If a hydrocarbon chain in a micelle does not contact the solvent, it contacts other chains. As the aggregate size increases, the amount of solvent-chain interaction decreases as the chain-chain interaction increases. The variation in chain/solvent interaction in a micelle can be simply modeled by relating it to the monomer/solvent interaction with a fraction f_s similar to f_r introduced in section 4.4 except it varies as the surface areas. The relation is as follows:

$$\Delta G^{o}_{tr}\Big|_{\substack{\text{Micelle}\\ \text{chain/solvent}}} = \Delta G^{o}_{tr}\Big|_{\substack{\text{Monomer}\\ \text{chain/solvent}}} * f_s \qquad (4.41)$$

where

$$f_s = \frac{\text{Surface Area of N-mer/N}}{\text{Surface Area of Monomer}} \qquad (4.42)$$

The micelle surface area is again divided by N because the properties are on a monomer basis.

The variation of chain-chain interaction with aggregate size is then related to $(1 - f_s)$. This interaction is modeled by the heat of vaporization of n-alkanes. The errors in this are small because the

difference between the interior of a micelle and liquid hydrocarbon is in ordering effects of the chains (entropic) which have been included in $-\frac{\Delta S^{\circ}}{R}\Big|_{comp}$. Therefore,

$$\Delta \underline{G}^{\circ}\Big|_{\substack{\text{Micelle} \\ \text{chain/solvent}}} = (-\Delta \underline{H}^{vap}) * (1-f_s) \qquad (4.43)$$

Heat of vaporization data are given by Hossenlopp and Scott (1981) and Sokolov et al. (1981). We chose to use the expression developed by Sokolov because it is valuable for most n-alkanes ($C_5 - C_{20}$) and it compares very well with experimental data:

$$\Delta \underline{H}^{vap} = 1280 + 100\, N_a\, (15.7 - 17.2\, T_r^2)^{0.5}$$

where N_a is the number of atoms in the molecule

T_r is the reduced temperature

The function f_s depends on the shape and the size of a micelle and is determined for spherical and nonspherical micelles similarly to the f_r of section 4.4.

Spherical Micelle

The surface area, S_M, of an N-mer micelle is related to N by using equation (4.31):

$$V_M = N\, V_m = \frac{4\pi}{3} R_M^3$$
$$S_M = 4\pi R_M^2 = 4\pi \left(\frac{3N\, V_m}{4\pi}\right)^{2/3} \qquad (4.44)$$

Substituting equation (4.44) in (4.42), f_s can be determined:

$$f_s = \frac{4\pi \left(\frac{3NV_m}{4\pi}\right)^{2/3} / N}{4\pi \left(\frac{3V_m}{4\pi}\right)^{2/3}} = \frac{1}{N^{1/3}} \qquad (4.45)$$

Spherocylinder Micelle

The volume to surface area relation in a spherocylindrical geometry is

$$V_M = N\,V_m = \pi R_M^3\left(\alpha_s + \frac{4}{3}\right)$$

$$S_M = 4\pi R_M^2\left(\frac{\alpha_s}{2} + 1\right) = 4\pi R_M^2\left(\frac{NV_m}{2\pi R_M^3} + \frac{1}{3}\right) \qquad (4.46)$$

Solving for f_s:

$$f_s = \frac{4\pi R_M^2\left(\frac{NV_m}{2\pi R_M^3}\right) + \frac{1}{3}\Big)/N}{4\pi\left(\frac{3V_m}{4\pi}\right)^{2/3}} = \frac{V_m}{2\pi R_M\left(\frac{3V_m}{4\pi}\right)^{2/3}} + \frac{1}{N}\,\frac{R_M^2}{3\left(\frac{3V_m}{4\pi}\right)^{2/3}}$$

$$\equiv a^S_{o,s} + a^S_{1,s}/N \qquad (4.47a)$$

where $a^S_{o,s}$ and $a^S_{1,s}$ are used to represent the geometrical terms involved in f_s.

Prolate Micelle

Following the same procedure as before, we get:

$$V_M = N\,V_m = \frac{4\pi}{3}\,\alpha_p\,R_M^3$$

$$S_M = 2\pi R_M^2\left[1 + \frac{\alpha_p^2}{(\alpha_p^2 - 1)^{1/2}}\cos^{-1}\left(\frac{1}{\alpha_p}\right)\right] \qquad (4.48)$$

Solving for α_p in equation (4.39) and substituting it in (4.48), we can obtain S_M as a function of N and thus f_s can be fitted to the form

$$f_s = a^P_{o,s} + a^P_{1,s}/N \qquad (4.47b)$$

Oblate Micelle

$$S_M = 2\pi\alpha_o^2 R_M^2\left\{1 + \frac{1}{\alpha_o(\alpha_o^2-1)^{1/2}}\ln\left[\alpha_o + (\alpha_o^2-1)^{1/2}\right]\right\}$$

$$f_s = a^O_{o,s} + a^O_{1,s}/N \qquad (4.47c)$$

The values of the geometrical parameters, $a_{o,s}$ [illegible] $a_{1,s}$, are given below for the three shapes discussed above:

Carbon Number	Spherocylinder		Prolate		Oblate	
	$a^S_{o,s}$	$a^S_{1,s}$	$a^P_{o,s}$	$a^P_{1,s}$	$a^O_{o,s}$	$a^O_{1,s}$
12	0.175	4.850	0.199	3.302	0.146	6.726

4.5.2 Dipole-Dipole Interactions

The uncharged head group of a nonionic amphiphile is polar and its interaction with a neighboring head group at the micelle surface is considered as a dipole-dipole interaction. The interaction energy between two dipoles i and j at a fixed separation r is given by (Reed and Gubbins, 1973)

$$\frac{E}{KT} = \frac{\mu_i \mu_j}{r^3 KT} (\sin \theta_i \sin \theta_j \cos \phi_{ij} - 2 \cos \theta_i \cos \theta_j) \qquad (4.49a)$$

where μ is the dipole moment

θ is the relative orientation polar angle

ϕ is the azimuthel angle

K is the Boltzmann constant

For single surfactant micelle

$$\mu_i = \mu_j = \mu$$

$$\frac{E}{KT} = \frac{\mu^2}{r^3 KT} (\sin \theta_i \sin \theta_j \cos \phi_{ij} - 2 \cos \theta_i \cos \theta_j)$$

The head groups have only one possible orientation which is normal to the surface of a micelle so that:

$$\theta_i = \theta_j = \frac{\pi}{2} ; \qquad \phi_{ij} = 0$$

$$\frac{E}{KT} = \frac{\mu^2}{r^3 KT} \tag{4.49b}$$

The separation distance r is related to the aggregate size, N, by the following equations:

$$r = R_M \delta(N) = \left(\frac{3N V_s}{4\pi}\right)^{1/3} \delta(N) \tag{4.50}$$

where $\delta(N)$ is the angle between two head groups from the center of the micelle and V_s is the surfactant volume.

If the head groups are assumed to be uniformly distributed around a spherical micelle, $\delta(N)$ can be expressed by

$$\delta(N) = \frac{2\pi}{\left[1 + \frac{N}{Z}\right]} \tag{4.51}$$

For a typical nonionic surfactant, equation (4.49b) shows that the contribution of head group interactions is negligible comparing to other surface properties discussed earlier even for very large aggregates. Values for $\frac{E}{KT}$ as a function of N are shown below for a dipole moment of 2 Debyes at a temperature of 298° K (V_s = 415 Å^3). They are small enough that we ignore them in our model.

$\frac{E}{KT}$	N
1.58(-02)	2
5.04(-02)	10
1.00(-01)	50
1.34(-01)	100

4.1.3 Electrostatic Interactions

The electrostatic interactions associated with ionic aggregates were described in section 3.4. The Poisson-Boltzmann equation (3.24) is used to compute the surface electrostatic effects. These effects are constrained by the boundary conditions given in equation (3.25). Their dependence on the aggregate size, N, and the fraction of counterions bound to the surface, β, is related to the surface charge density dependence on these variables. Assuming that for each "bound" counterion a surfactant head group is electrostatically neutralized (1:1 electrolyte) the surface charge density, σ, can be formulated as follows:

$$\sigma = \frac{N(1 - \beta)e}{S_M} \tag{4.52}$$

For a spherical micelle

$$\sigma = \frac{N(1 - \beta)e}{4\pi\left(\frac{3NV_m}{4\pi}\right)^{2/3}} \tag{4.53}$$

In a dimensionless form, σ becomes (Equation 3.25)

$$S = \frac{4\pi\sigma e}{\varepsilon\kappa\ KT} = \frac{1}{\left(\frac{3V_m}{4\pi}\right)^{2/3}} \frac{e^2}{\varepsilon\kappa\ KT}\ (1-\beta)N^{1/3} \tag{4.54}$$

An algorithm was developed to solve equations (3.24), (3.25) and (4.54) numerically as a function of the following independent variables : aggregate size, fraction of counterions bound, temperature, surfactant and salt concentrations and surfactant chain length. A hard copy

or this algorithm is given in Appendix A with an explanation for the numerical techniques and equations in it.

The electrostatic free energy change given in equation (3.27) is function of the independent variables mentioned above. These variations are discussed next

The surface charge density has a $N^{1/3}$ dependence on the aggregate size of a spherical micelle. The free energy dependence on N is not clear from equation (3.27). However the numerical solution showed a ln(N) dependence for N from 2 to $N_{transition}$. $\frac{\Delta G^{o}_{el}}{RT}$ at fixed T, P, C_t and β is then fitted to the form $(a_o + a_1 \ln N)$. We did not solve the Poisson-Boltzmann equation for nonspherical shapes because the ionic aggregate distributions lie in the spherical region. For large ionic aggregates the equation $(a_o + a_1 \ln N)$ is extrapolated. A typical variation of $\frac{\Delta G^{o}_{el}}{RT}$ with N at any condition is shown in figure 4.1.

Equation (4.54) shows that the surface charge density is linearly dependent on β. However, the free energy has a second order dependence on it. Over the range of β from 0 to 1 the typical change of $\frac{\Delta G^{o}_{el}}{RT}$ shown in figure 4.2.

The electrostatic free energy dependence on temperature varies from solvent to solvent due to the difference in the dielectric constant, ε, and its dependence on temperature. Generally $\frac{\Delta G^{o}_{el}}{RT}$ changes are negligible with temperature because ε decreases as temperature increases but the $\varepsilon \cdot T$ product used in equation (4.54) is relatively constant.

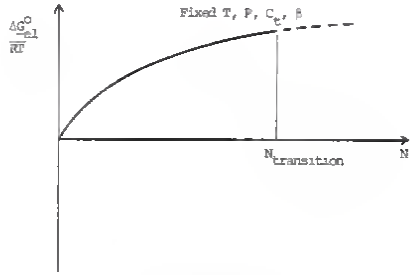

Figure 4.1 Electrostatic Free Energy Change with Aggregate Size

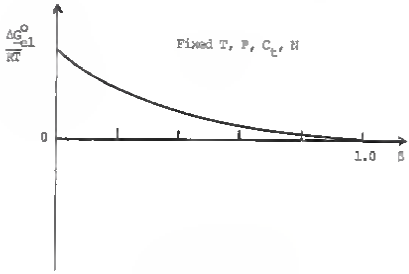

Figure 4.2 Electrostatic Free Energy Change with Counterion Binding

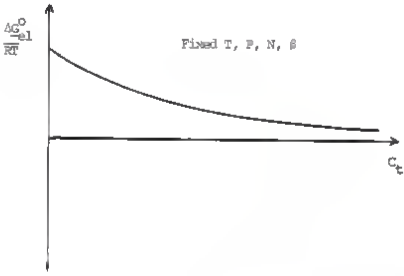

Figure 4.3 Electrostatic Free Energy Change with Surfactant and/or Salt Concentration

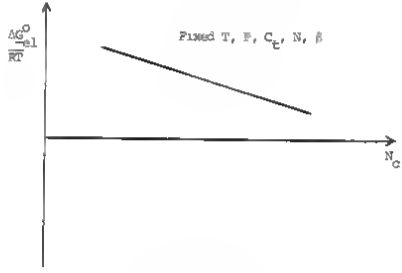

Figure 4.4 Electrostatic Free Energy Change with Chain Length

The addition of surfactant and salt to an amphiphile solution decreases the electrostatic effects on the micelle surface by decreasing the Debye length (Equation 3.23). The effect of these added solutes on $\frac{\Delta G^{o}_{el}}{RT}$ is shown in figure 4.3.

The surface charge density is inversely proportional to the molar volume of a surfactant. The electrostatic free energy, therefore, decreases with chain length and this change is shown in figure 4.4.

4.5.4 Counterion Binding

The results obtained from free ion electrode measurements are related to the fraction of counterions adsorbed at the surface. Data for β from these measurements are averaged values over the aggregate distribution, so the fraction for each N is not available. The dependence of β on the aggregate size can be obtained by minimizing the overall free energy in equation (4.7) with respect to β. The formulation for this minimization is as follows:

$$\frac{\partial}{\partial \beta}\left[\frac{\Delta G^{o}}{RT}\text{ overall}\right]_{T,P,N} = 0 \qquad (4.55)$$

so

$$-\frac{\partial}{\partial \beta}\frac{\Delta G^{o}_{el}}{RT}\bigg|_{T,P,N} - \frac{\partial}{\partial \beta}\frac{\Delta G^{o}}{RT}\text{ Dehydration}\bigg|_{T,P,N} + \ln X_{c}$$

$$+ \beta \frac{\partial}{\partial \beta}\ln X_{c}\bigg|_{T,P,N} + \ln C_{o} = 0 \qquad (4.56)$$

The electrostatic free energy dependence on β (Figure 4.2) has been fitted for each aggregate size to the following form

$$\frac{\Delta G^{o}_{el}}{RT} = C_{o,N} + C_{1,N}\,\beta + C_{2,N}\,\beta^{2} \qquad (4.57)$$

$$\frac{\partial}{\partial \beta}\left.\frac{\Delta G^{o}_{-\beta}}{RT}\right|_{T,P,N} = C_{1,N} + 2\,C_{2,N}\,\beta \qquad (4.58)$$

The counterion concentration, X_c, can be expressed in terms of the monomer concentration, X_1, and the overall concentration, X_t, and the fraction β by

$$X_c = X_1 + (1-\beta)(X_t - X_1) \qquad (4.59)$$

so that

$$\frac{\partial}{\partial \beta} \ln X_c\Big|_{T,P,N} = -\frac{(X_t - X_1)}{X_1 + (1-\beta)(X_t - X_1)} \qquad (4.60)$$

We did not model the free energy change upon dehydration due to the counterion adsorption. Instead, we determined the change by assuming a basis of one counterion adsorbed for each dimer and $\frac{\Delta G^{o}}{RT}$-Dehydration is linearly dependent on β

$$\beta = 0.5 \quad \text{for} \quad N = 2 \qquad (4.61)$$

$$\frac{\Delta G^{o}}{RT}\text{ Dehyd} = A_o\,\beta \qquad (4.62)$$

$$\frac{\partial}{\partial \beta}\frac{\Delta G^{o}}{RT}\text{ Dehyd} = A_o \qquad (4.63)$$

Substituting equations (4.58), (4.60) and (4.63) in (4.56) we obtain the function that allows determination of β as a function of N

$$-C_{1,N} - 2\,C_{2,N}\,\beta - A_o + \ln\{X_1 + (X_t - X_1)(1-\beta)\}$$
$$-\frac{\beta(X_t - X_1)}{X_1 + (X_t - X_1)(1-\beta)} + \ln C_o = 0 \qquad (4.64)$$

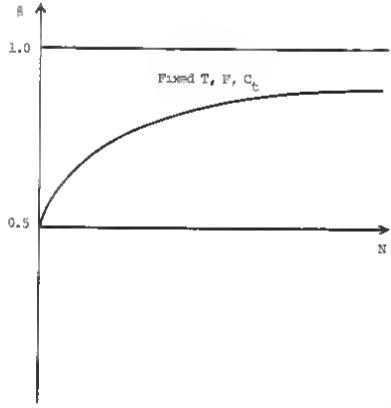

Figure 4.5 Counterion Binding Change with Aggregate Size

At a fixed X_t, X_1, and C_o, the procedure for calculating $\beta = \beta(N)$ starts by determining A_o in equation (4.64) with N = 2, $\beta = 0.5$. Then β is found for N > 2. A typical variation of β with N is shown in figure 4.5. In general, the fraction ranges from 0.50 to 0.75. The change of the β with minimum free energy is correlated with N in the form

$$\beta_{min} = A_1 + A_2 \ln N \tag{4.65}$$

This value is then used to calculate the electrostatic free energy from equation (4.57) using equation (4.65) for β_{min}

$$\left.\frac{\Delta G^o_{el}}{RT}\right|_{T,P,N} = C_{o,N} + C_{1,N}\,\beta_{min} + C_{2,N}\,\beta^2_{min} \tag{4.66}$$

$$= C_{o,N} + C_{1,N}\,A_1 + C_{1,N}\,A_2 \ln N + C_{2,N}\,A_1^2 + C_{2,N}\,A_2^2(\ln N)^2 + 2C_{2,N}\,A_1 A_2 \ln N \tag{4.67}$$

This can be approximated as

$$\left.\frac{\Delta G^o_{el}}{RT}\right|_{T,P,N} = A_3 + \frac{A_4}{N} + \frac{A_5}{N^2} \tag{4.68}$$

A_3, A_4 and A_5 are functions of T, C_t and n_c

Equations (4.62), (4.65) and (4.68) will be used in our model.

4.6 Total Free Energy Change Upon Micellization

Each term in equation (4.11) has now been modeled separately. The first two terms (monomer properties) are given by equation (4.22). The entropy of compression is modeled by equation (3.16) and its change is given by equation (3.19). The micelle cavity properties are related to the monomer properties by equation (4.29). The micelle surface

properties have two contributions for nonionic systems and they are calculated from equations (4.41) and (4.43). The two extra contributions for ionic micelles are computed from equations (4.62), (4.65) and (4.68). Adding all of these contributions, the total free energy changes upon micelle formation of spherical and nonspherical shapes are obtained.

Spherical Nonionic Micelles

$$\frac{\Delta G_M^o}{RT} = -\frac{\Delta G_{mc}^o}{RT} - \frac{\Delta G_{ms}^o}{RT} - \frac{\Delta S_{comp}^o}{R} + \frac{\Delta G_{mc}^o}{RT} * \frac{1}{N^{2/3}} + \frac{\Delta G_{ms}^o}{RT} * \frac{1}{N^{1/3}} - \frac{\Delta H^{vap}}{RT}\left(1 - \frac{1}{N^{1/3}}\right) \qquad (4.69)$$

where mc stands for monomer cavity

ms stands for monomer surface

comp stands for compression

Collecting terms gives the form

$$\frac{\Delta G_M^o}{RT} = \left(-\frac{\Delta G_{mc}^o}{RT}\right)\left(1 - \frac{1}{N^{2/3}}\right) + \left(-\frac{\Delta G_{ms}^o}{RT} - \frac{\Delta H^{vap}}{RT}\right)\left(1 - \frac{1}{N^{1/3}}\right) - \frac{\Delta S_{comp}^o}{R} \qquad (4.70a)$$

Spherical Ionic Micelles

For ionic micelles, the two extra terms are added to give

$$\frac{\Delta G_M^o}{RT} = \left(-\frac{\Delta G_{mc}^o}{RT}\right)\left(1 - \frac{1}{N^{2/3}}\right) + \left(-\frac{\Delta G_{ms}^o}{RT} - \frac{\Delta H^{vap}}{RT}\right)\left(1 - \frac{1}{N^{1/3}}\right) - \frac{\Delta S_{comp}^o}{R} + A_o\{A_1 + A_2 \ln N) + \left(A_3 + \frac{A_4}{N} + \frac{A_5}{N^2}\right) \qquad (4.70b)$$

Nonspherical Nonionic Micelles

The only difference in $\frac{\Delta G_M^o}{RT}$ between spherical and nonspherical shapes comes from the geometrical fractions f_r and f_s given in equations (4.30) and (4.42), respectively

$$\frac{\Delta G_M^o}{RT} = \left(-\frac{\Delta G_{mc}^o}{RT}\right)(1 - a_{o,r} - a_{1,r}/N) + \left(-\frac{\Delta G_{ms}^o}{RT} - \frac{\Delta H^{vap}}{RT}\right)(1 - a_{o,s} - a_{1,s}/N) - \frac{\Delta S_{comp}^o}{R} \tag{4.71a}$$

Nonspherical Ionic Micelles

The equation for this case is

$$\frac{\Delta G_M^o}{RT} = \left(-\frac{\Delta G_{mc}^o}{RT}\right)(1 - a_{o,r} - a_{1,r}/N) + \left(-\frac{\Delta G_{ms}^o}{RT} - \frac{\Delta H^{vap}}{RT}\right)(1 - a_{o,s} - a_{1,s}/N) - \frac{\Delta S_{comp}^o}{R} + A_o(A_1 + A_2 \ln N) + \left(A_3 + \frac{A_4}{N} + \frac{A_5}{N^2}\right) \tag{4.71b}$$

Equations (4.70) and (4.71) can be substituted in equation (4.7) to determine aggregate size distribution which is constrained by the material balance presented in equation (4.14). This substitution leads to

$$\left.\frac{X_N}{N}\right|_{spherical} = \exp\left\{N\left\{\frac{\Delta G_{mc}^o}{RT}\left(1 - \frac{1}{N^{2/3}}\right) + \left(\frac{\Delta G_{ms}^o}{RT} + \frac{\Delta H^{vap}}{RT}\right)\left(1 - \frac{1}{N^{1/3}}\right) + \frac{\Delta S_{comp}^o}{R} - A_o(A_1 + A_2 \ln N) - A_3 - \frac{A_4}{N} - \frac{A_5}{N^2} + \ln X_1 + (A_1 + A_2 \ln N) \ln [X_1 + (X_L - X_1)(1 - A_1 - A_2 \ln N)] + \ln C_o [N + N(A_1 + A_2 \ln N) - 1]/N\right\}\right\} \tag{4.72}$$

A similar equation can be written for $\left.\frac{X_N}{N}\right|_{\text{Nonspherical}}$. For nonionic systems the coefficients A_0, A_1, A_2, A_3, A_4, and A_5 are equal to zero.

The formulation of the model is now complete. The parameters involved and the computational technique used to determine these parameters are discussed next.

4.7 Model Parameters

There are three unknown quantities in equation (4.72). They are the monomer cavity term, $\frac{\Delta G^o_{mc}}{RT}$, the monomer surface term, $\frac{\Delta G^o_{ms}}{RT}$, and the nonsphericity factor α, defined in equation (3.16). For a given surfactant system (head group, solvent, and added salt if any) these parameters are determined by fitting three experimental measurements :

1. The hydrocarbon solubility in equation (4.22) relating $\frac{\Delta G^o_{mc}}{RT}$ and $\frac{\Delta G^o_{ms}}{RT}$
2. The Critical Micelle Concentration in equation (4.14) where $X_t = X_{CMC}$ and X_1 is given by equation 2.1
3. The mean aggregate size, $\bar{N}$ in equation (4.16)

The computation starts with a guess for the surface property, $\frac{\Delta G^o_{ms}}{RT}$. The cavity property, $\frac{\Delta G^o_{mc}}{RT}$, is then calculated from equation (4.22) and the solubility data. The parameter α is then fitted to the CMC. Then the mean aggregate size is compared to the experimental $\bar{N}$. If the agreement is not satisfactory, a new guess has to be made for $\frac{\Delta G^o_{ms}}{RT}$. An increase in its value means a more favorable solvent/monomer interaction or a smaller mean aggregate size. This dependence suggests the choice of a new guess. If $\bar{N}$ data are not available, calorimetric heat measurements can be used in place of it and equation (2.18) which

represents the enthalpy change associated with micelle formation will replace equation (4 16)

The present model has been used to correlate and predict aggregate properties such as free energies and enthalpies of micelle formation and the aggregate size distribution along with their dependence on conditions such as temperature, salt and surfactant concentrations, chain length and head group type. This is presented in chapter V.

CHAPTER V
CORRELATION AND PREDICTION OF AGGREGATE PROPERTIES

5.1 Nonionic Systems

The thermodynamic properties of nonionic surfactant solutions have not been studied extensively compared to ionic systems due to the difficulty of obtaining highly purified nonionic compounds. Polyoxyethylenated nonionic surfactants are those most used because of their considerable commercial importance. Corkill et al. (1961), Balmbra et al. (1962 and 1964), Becher (1970), Rosen et al. (1982), Fujimatsu et al. (1983) and Corti et al. (1984) studied this family of surfactants and some of their reported CMC and mean aggregate size data are collected and reported in table 5.1.

The hydrocarbon solubility data given in table 4.2 along with the CMC and $\bar{N}$ data given in table 5.1 can be used to determine the parameters of the model presented in chapter IV following the procedure described in section 4.7. These parameters involve the three unknown quantities : the monomer cavity term, $\Delta G^{o}_{mc}/RT$, the monomer surface term, $\Delta G^{o}_{ms}/RT$, and the entropy of compression, $-\Delta S^{o}/R\big|_{comp}$. The values of these parameters for each system in table 5.1 are given in table 5.2. Note that the shape of nonspherical aggregates is assumed to be spherocylindrical as justified in section 5.1.1.

Table 5-1
Data Collected on Polyoxyethylenated Surfactants $C_xH_{2x+1}(OC_2H_4)_6OH$ in Aqueous Solutions

x	T (°K)	CMC (M)	$\bar{N}$
8	298	9.9(-03) [a]	35 [a]
	313	7.2(-03) [b]	51 [b]
	323	6.3(-03) [b]	82 [b]
10	298	9.0(-04) [b]	73 [b]
	308	6.5(-04)	260
	318	6.4(-04)	640
12	288	1.1(-04) [a]	140 [c]
	298	8.7(-05)	400
	308	7.2(-05)	1400
	318	5.7(-05)	4000
14	298	1.1(-05) [b]	3100 [b]
	308	8.9(-06)	7500
	313	8.2(-06)	11700
16	298	1.4(-06) [a]	10500 [b] 2430 [d]
	305	1.2(-06)	13300 [b]
	307	1.1(-06)	16600 [b]

a : Corkill et al. (1961)

b : Balmbra et al. (1964)

c : Balmbra et al. (1962)

d : Elworthy and Macfarlane (1963)

Table 5.2
Parameter Values for $C_xH_{2x+1}(OC_2H_4)_6OH$ Surfactant Systems in Aqueous Solutions

x	T (°K)	$\frac{\Delta G^{o}_{mc}}{RT}$ [a]	$\frac{\Delta G^{o}_{mc}}{RT}$ [b]	$\frac{\Delta G^{o}_{ms}}{RT}$ [a]	$\frac{\Delta G^{*}_{ms}}{RT}$ [c]	$-\frac{\Delta S^{o}}{R}\Big\vert_{comp}$ [a]
8	298	87.85	88.01	- 71.99	- 55.28	36.36
	313	87.87	88.28	- 70.05	- 54.45	36.67
	323	87.58	88.44	- 68.60	- 53.70	36.81
10	298	88.30	88.01	- 68.49	- 47.85	39.58
	308	87.88	88.19	- 66.31	- 46.55	39.89
	318	87.16	88.36	- 64.53	- 45.60	39.92
12	288	87.85	87.81	- 67.83	- 42.20	41.21
	298	87.68	88.01	- 66.04	- 41.49	41.41
	308	87.46	88.19	- 64.31	- 40.77	41.59
	318	87.55	88.36	- 62.90	- 40.32	41.82
14	298	88.00	88.01	- 65.66	- 37.20	42.92
	308	88.22	88.19	- 64.30	- 36.98	43.12
	313	88.26	88.28	- 63.60	- 36.83	43.21
16	298	91.26	88.01	- 67.88	- 35.39	45.40
	305	91.52	88.14	- 67.00	- 35.41	45.52
	307	91.65	88.17	- 66.73	- 35.39	45.59

a : Nonspherical micelles are spherocylindrical

b : Values obtained from equation (5.1)

c : $\Delta G^{*}_{ms}/RT = \Delta G^{o}_{ms}/RT + \Delta H^{vap}/RT$

The solubility data are available at only one temperature (298 K). The assumption that had to be made in order to compute the model parameters at temperatures different than 298 K is that the nonsphericity factor, α, involved in the entropy of compression is independent of temperature. It is dependent, however, on the surfactant chain length and head group. This assumption makes $-\Delta\underline{S}^{o}/R\big|_{comp}$ a function of only the overall surfactant concentration or the CMC for a given surfactant molecule. The model parameters are then reduced from three to two at temperatures other than 298 K. In this case the CMC and $\bar{N}$ data are the only ones needed to describe the properties of the system.

The dependence of the cavity parameter on temperature and chain length shown in table 5.2 is not consistent from one surfactant to the other due to the experimental data being from different sources and having significant uncertainties. In fact, this parameter should be independent of chain length because this dependence has already been accounted for by the geometrical factors, $a_{o,r}$ and $a_{1,r}$, defined in chapter IV. By comparing its value from table 5.2 for different chain length at 298 K, we find that it is approximately constant (88.00 ± 0.30) except for the hexadecyl chain which is off by 4% probably due to uncertainty in the experimental data. Further, this parameter should increase with temperature because chain curvature increases with temperature as more gauche bonds and less of trans bonds occur. The values in table 5.2 show that the curvature parameter associated with tetradecyl and hexadecyl chains increases virtually linearly with temperature while it goes through an extremum for the other chains.

We will disregard this extremum and fit the parameter to the form

$$\frac{\Delta G^{o}_{mc}}{RT} = a + \frac{b}{T} \qquad \text{(All chain lengths)} \qquad (5.1)$$

From least-square fitting

$$a = 93.64$$

$$b = -1678.51$$

Equation (5.1) will be applied for ionic surfactants in section 5.2 reducing the ionic model parameters from three to one since the parameter α is assumed to be independent of temperature.

5.1.1 Free Energy Change and Aggregate Distribution

The free energy change upon micelle formation of spherical and nonspherical shapes and the aggregate population density are given in equations (4.70a), (4.71a) and (4.72), respectively. Using the parameters of table 5.2, these properties can be determined as a function of aggregate size, N. This dependence is shown in figures 5.1a, 5.1b, 5.2 and 5.3. The free energy plots are similar to figure 3.4 where small aggregates (N<6) with a positive $\Delta G^{o}_{N}/RT$ are thermodynamically unfavorable, while large aggregates (N>6) with a negative $\Delta G^{o}_{N}/RT$ are thermodynamically favorable. It is the material balance constraint that does not allow very large aggregate sizes to be formed as can be seen from the distributions of figures 5.2 and 5.3. The free energy change can be averaged over all aggregate sizes by the equation

$$\left.\frac{\Delta G_M^o}{RT}\right|_{Avg.} = \int_2^{\infty} \frac{\Delta G_M^o}{RT}\left(\frac{X_N}{\bar{N}}\right) dN \Big/ \int_2^{\infty}\left(\frac{X_N}{\bar{N}}\right) dN \qquad (5.2)$$

$$\frac{\int_2^{N_{sph}} \frac{\Delta G_M^o}{RT}\left(\frac{X_N}{\bar{N}}\right) dN + \int_{N_{sph+1}}^{\infty} \frac{\Delta G_M^o}{RT}\left(\frac{X_N}{\bar{N}}\right) dN}{\int_2^{N_{sph}}\left(\frac{X_N}{\bar{N}}\right) dN + \int_{N_{sph+1}}^{\infty}\left(\frac{X_N}{\bar{N}}\right) dN} \qquad (5.3)$$

These averaged values are shown in figures 5.1c and 5.1d.

The parameters of table 5.2 and figures 5.1, 5.2 and 5.3 are based on the spherocylinder shape for nonspherical micelles. The effect of other shapes such as prolate or oblate on these parameters and the average free energy changes are shown in table 5.3. The free energy change and the aggregate population density obtained for these different shapes are plotted in figures 5.4 and 5.5, respectively. Since the experimental CMC and $\bar{N}$ data are fitted in the model, we expect that the difference in the free energy change between the three shapes to be small. The prolate geometry has the least favorable free energy for nonspherical aggregates (N>57) while oblate and spherocylinder shapes give identical properties. This small difference in the free energy between prolate in one hand and oblate and spherocylinder in the other has a noticeable effect on the distribution of these nonspherical aggregates. To satisfy the material balance, the small aggregate population (N<57) for the prolate system must be greater than those of the oblate or spherocylinder systems as seen in figure 5.5.

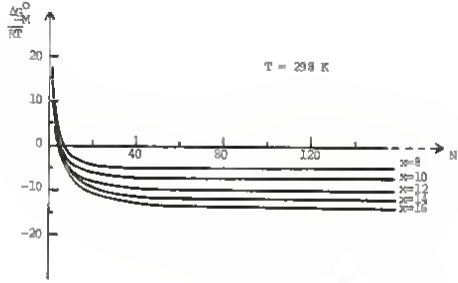

Figure 5.1a Free Energy Change Upon Micelle Formation of $C_xH_{2x+1}(OC_2H_4)_6OH$ in Aqueous Solutions

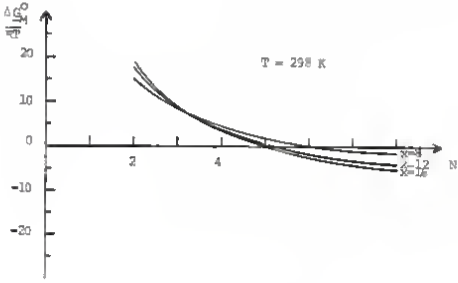

Figure 5.1b Free Energy Change Upon Micelle Formation of $C_xH_{2x+1}(OC_2H_4)_6OH$ in Aqueous Solutions (Small aggregates)

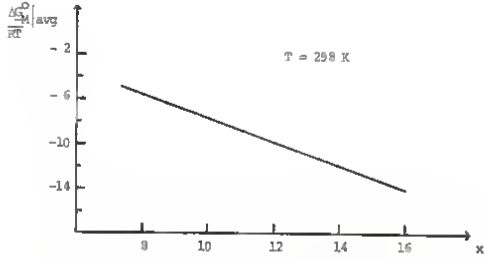

Figure 5.1c Free Energy Change Upon Micelle Formation of $C_xH_{2x+1}(OC_2H_4)_6OH$ (Averaged Values) for different chain length

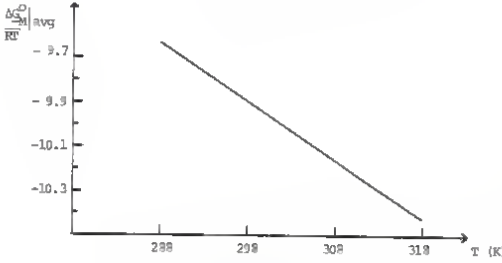

Figure 5.1d Free Energy Change Upon Micelle Formation of $C_{12}H_{25}(OC_2H_4)_6OH$ (Averaged Values) at Different Temperatures

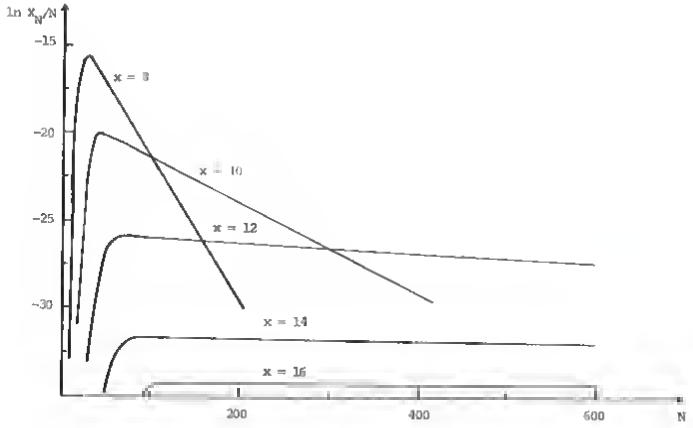

Figure 5.2 Aggregate Population Density of $C_xH_{2x+1}(OC_2H_4)_6OH$ at 298 K

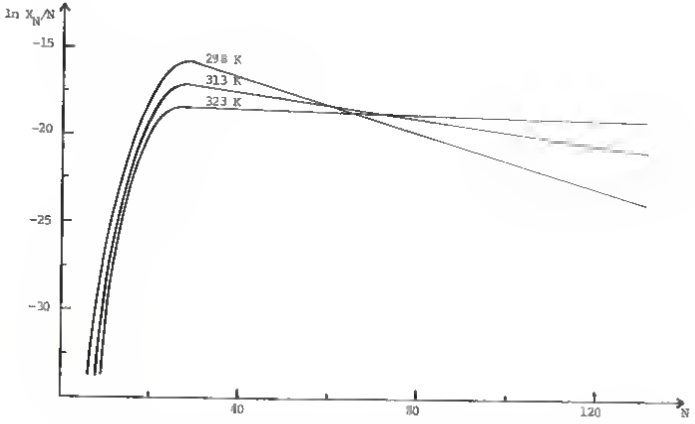

Figure 5.3 Aggregate Population Density of $C_8H_{17}(OC_2H_4)_6OH$ at Different Temperatures

Table 5.3
Parameter Values for $C_{12}H_{25}(OC_2H_4)_6OH$ Surfactant System for Different Nonspherical Aggregate Shapes

Shape [a]	$\frac{\Delta G^{\circ}_{mc}}{RT}$	$\frac{\Delta G^{\circ}_{ms}}{RT}$	$\frac{\Delta G^{*}_{ms}}{RT}$	$-\frac{\Delta S^{\circ}}{R}\Big\vert_{comp}$	$\frac{\Delta G^{\circ}_{M}}{RT}\Big\vert_{avg}$
Spherocyl	87.68	-66.04	-42.49	41.41	-9.91
Prolate	98.28	-76.64	-52.09	43.45	-9.66
Oblate	82.50	-60.86	-36.31	40.41	-9.91

a : T = 298 $^{\circ}$K

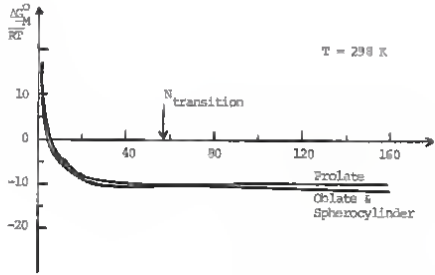

Figure 5.4 Free Energy Change of $C_{12}H_{25}(OC_2H_4)_6OH$ Micelle Formation for Different Nonspherical Shapes

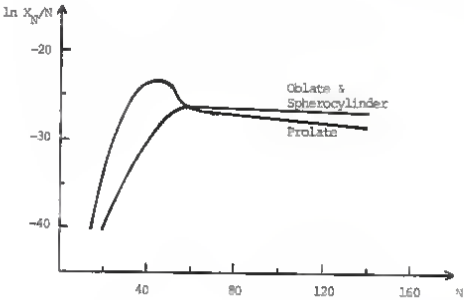

Figure 5.5 Aggregate Population Density of $C_{12}H_{25}(OC_2H_4)_6OH$ for Different Nonspherical Shapes

The option for the nonspherical shape is then between oblate and spherocylinder and we chose the latter simply because its geometrical factors, $a^S_{o,r}$, $a^S_{1,r}$, $a^S_{o,s}$ and $a^S_{1,s}$ defined in chapter IV (Equations 4.38a and 4.47a) are directly related to the size of the surfactant and can be exactly calculated while they are fitted in the case of oblate as shown in equations (4.38 c) and (4.47c). Thus, spherocylindrical shape is used in all modeling of the nonspherical aggregates.

5.1.2 Enthalpy Change Upon Aggregation

The enthalpy change upon aggregation was derived in chapter 2 (Equation 2.18) for a fixed surfactant concentration and it is reduced to the following form:

$$\left.\frac{\Delta H^o_M}{RT}\right|_{T,P,N} = \frac{1}{T}\left.\frac{\partial \Delta G^o_M/RT}{\partial(1/T)}\right|_{P,N} + \frac{1}{T}\left.\frac{\partial \Delta G^o_M/RT}{\partial(C_N/N)}\right|_{T,P,N,C_{N'\neq N}} \left.\frac{\partial(C_N/N)}{\partial(1/T)}\right|_{P,N} \qquad (5.4)$$

The free energy dependence on temperature at a constant pressure and aggregate size is fitted for selected N to the form

$$\left.\frac{\Delta G^o_M}{RT}\right|_{P,N} = K_o + \frac{K_1}{T} + \frac{K_2}{T^2}$$

so that

$$\left.\frac{\partial \Delta G^o_M/RT}{\partial(1/T)}\right|_{P,N} = K_1 + 2\,\frac{K_2}{T} \qquad (5.5)$$

The second term in equation (5.4) can be simplified to

$$\left.\frac{\partial \Delta G_M^o/RT}{\partial (C_N/N)}\right|_{T,P,N,C_{N'\neq N}} \left.\frac{\partial (C_N/N)}{\partial (1/T)}\right|_{P,N} = \left.\frac{\partial \Delta G_M^o/RT}{\partial \ln (X_N/N)}\right|_{T,P,N,X_{N'\neq N}} \left.\frac{\partial \ln (X_N/N)}{\partial (1/T)}\right|_{P,N} \tag{5.6}$$

From equation (4.2) we know that

$$\frac{\Delta G_M^o}{RT} = \frac{1}{N} \ln \frac{X_N}{N} - \ln X_1 = \beta \ln X_c$$

so that

$$\left.\frac{\partial \Delta G_M^o/RT}{\partial \ln (X_N/N)}\right|_{T,P,N,C_{N'\neq N}} = \frac{1}{N} \tag{5.7}$$

Finally, the micelle mole fraction ($\ln X_N/N$) dependence on temperature is fitted for selected N to the form

$$\ln \left(\frac{X_N}{N}\right)\Bigg|_{P,N} = K_3 + \frac{K_4}{T} + \frac{K_5}{T^2}$$

so that

$$\left.\frac{\partial \ln (X_N/N)}{\partial (1/T)}\right|_{P,N} = K_4 + 2\,\frac{K_5}{T} \tag{5.8}$$

Substituting equations (5.5), (5.7) and (5.8) in (5.4), we get

$$\left.\frac{\Delta H_M^o}{RT}\right|_{T,P,N} = \frac{1}{T}\left[K_1 + 2\,\frac{K_2}{T}\right] + \frac{1}{T}\left[\frac{1}{N}\left(K_4 + 2\,\frac{K_5}{T}\right)\right] \tag{5.9}$$

Equation (5.9) has been used for some of the systems in table 5.1 and the results are plotted in figures 5.6 and 5.7. In figure 5.6 the

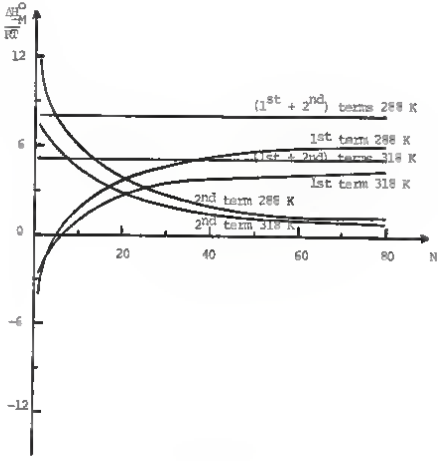

Figure 5.6 Enthalpy Change Upon Aggregation of $C_{12}H_{25}(OC_2H_4)_6OH$

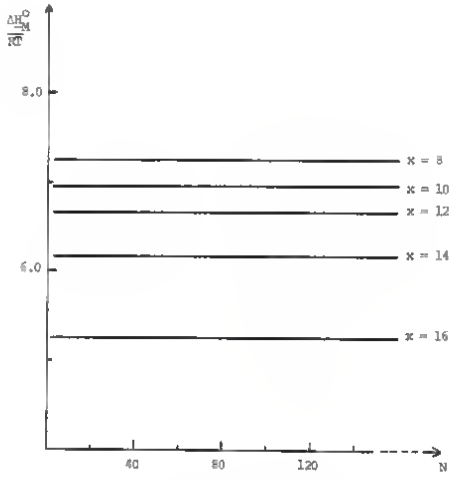

Figure 5.7 Enthalpy Change Upon Aggregation of $C_xH_{2x+1}(OC_2H_4)_6OH$ at 298 K

contribution from each term of equation (5.9) is shown. The second term approaches zero as N approaches infinity because it has a 1/N dependence. The sum of these two terms give a constant enthalpy change as a function of aggregate size at fixed temperature. This enthalpy behavior was predicted in chapter III (Figure 3.3) where two opposing effects with an $N^{1/3}$ dependence cancel each other so to make the enthalpy independent of size. These effects are water/hydrocarbon and hydrocarbon/hydrocarbon interactions (Steps 1 and 3). The cavity effect of step 2 is negligible at low temperatures comparing to 1 and 3, as discussed in chapters II and III, and its contribution does not effect the enthalpy change at these temperatures. At higher temperatures, however, this effect gets larger and its contribution starts to show a decrease in the enthalpy with respect to aggregate size and that will be seen in section 5.2 for ionic systems as the temperature is increased up to 368 K. Also in nonaqueous media, where the cavity contribution to the enthalpy is large, the enthalpy decreases with aggregate size more than in aqueous media and this will be seen in section 5.2.3. The enthalpy change also decreases with increasing temperature and that is mainly due to the temperature dependence of step 2 (cavity removal) as discussed in chapter III (Figures 3.3 and 3.6). Figure 5.7 shows that the enthalpy change decreases with increasing chain length at a fixed temperature and that is because of the more favorable chain-chain interaction. This enthalpy change can be compared to calorimetric measurements (Birdi, 1983). Desnoyers et al. (1983) reported some of these measurements on alkyldimethylamine oxides in water and their results compared relatively well with our results for polyoxyethylenated systems.

recognizing that the head groups of the two surfactants are different. In particular, the dramatic change of the enthalpy with temperature is closely followed.

	$\Delta H_M^o/RT$			
T (K)	C_8DAO [a]	C_8OEH [b]	$C_{10}DAO$ [a]	$C_{10}OEH$ [b]
298	6.66	7.24	5.43	6.96
323	1.81	1.98		

a : Desnoyers et al. (1983)

b : Equation 5.9 averaged over all sizes

5.1.3 Aggregate Properties Dependence on Surfactant Concentration

We have described so far the aggregate properties of nonionic surfactants at one concentration and that is the CMC. In this section, the dependence of the properties on the surfactant concentration above and below the CMC is addressed.

At the CMC, the monomer concentration, x_1, is a known quantity and is given by the CMC definition of Hall and Pethica (Equation 2.1). However, at different concentrations, this definition is not appropriate and x_1 is expected to vary with concentration as observed experimentally by Cutler et al. (1978), Kale et al. (1980) and Backlund and Rundt (1981). The model of chapter IV (Equation 4.14) should then be solved for x_1 using the three model parameters which are determined only at the CMC. Then the aggregate size distribution and its mean can be computed from equations (4.72) and (4.16), respectively. The results for various surfactant concentrations are shown in figure 5.9.

Note that adding surfactant at the CMC does not effect the small aggregate distribution (N<56) since the surfactant surplus only creates larger size aggregates. Since the model parameters are unchanged with concentration, the free energy change for a fixed aggregate size is the same at all concentrations as can be seen from equations (4.70) and (4.71) and figure 5.8. Therefore, it is clear that large aggregates were not thermodynamically constrained below the CMC; rather they are not favored because there is insufficient surfactant in the solution to create them. The average free energy change defined in equation (5.3) does vary with concentration since it is a function of the aggregate distribution as shown in figure (5.10). The sharp drop in $\Delta G_M^o/RT\big|_{avg}$ at C_t = 1.5(-05) M is due to the fact that $\Delta G_M^o/RT$ decays very rapidly between N=2 and N=20 (Figure 5.8) while the mean aggregate size, $\bar{N}$, increases from 6 to 21 between C_t = 1.2(-05) M and 1.7(-05) M (Figure 5.11). However even this dramatic thermodynamic change does not overcome the material balance constraint and, as it can be seen from figure 5.9, the micelle mole fraction is still negligible at that surfactant concentration

Ruckenstein and Nagarajan (1975) defined the CMC as the concentration at which an inflection point occurs in the aggregate size distribution as surfactant is added. Such a point is seen in figure 5.9 but it occurs at 1/7 the concentration of the CMC. Ruckenstein and Nagarajan assigned a value for the monomer concentration, x_1, at each overall surfactant concentration and arbitrarily defined the CMC at that inflection point Ben-Naim and Stillinger (1980) criticized that definition noting that x_1 should be a dependent variable on the overall

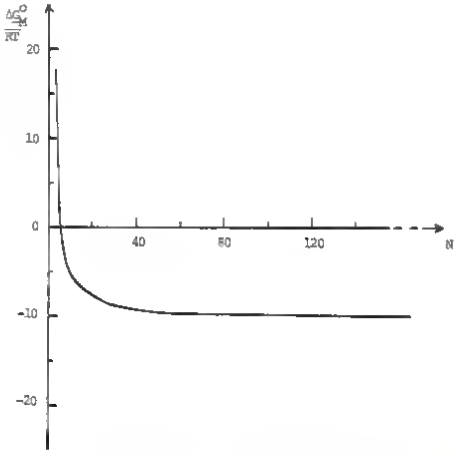

Figure 5.8 Free Energy Change Dependence on Surfactant Concentration ($C_{12}H_{25}(OC_2H_4)_6OH$ at 298 K)

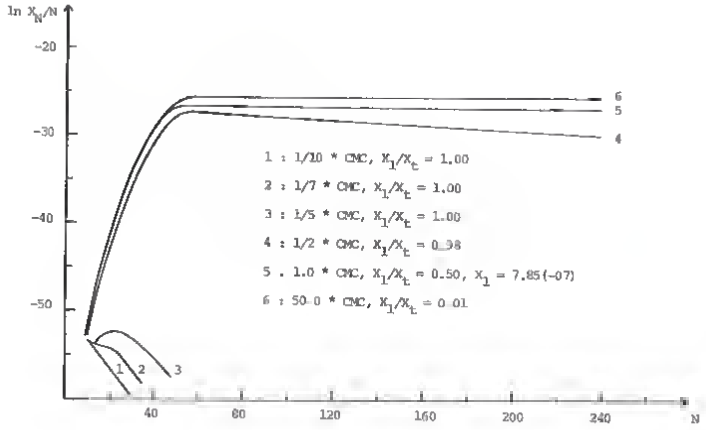

Figure 5.9 Aggregate Population Density of $C_{12}H_{25}(OC_2H_4)_6OH$ at Different Concentrations (T = 298 K)

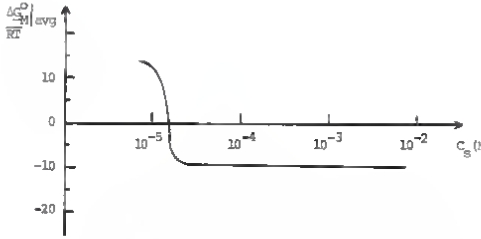

Figure 5.10 Average Free Energy Change with Surfactant Concentration ($C_{12}H_{25}(OC_2H_4)_6OH$ at 298 K)

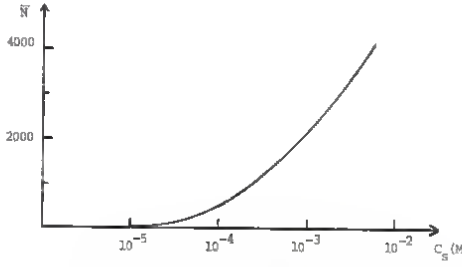

Figure 5.11 Mean Aggregate Size Dependence on Surfactant Concentration ($C_{12}H_{25}(OC_2H_4)_6OH$ at 298 K)

surfactant concentration and they concluded that the CMC can be far above the concentration at which that point occurs. Our results agree with Ben-Naim and Stillinger argument and with experimental results as shown in the next section for ionic surfactant systems.

5.2 Ionic Systems

Ionic surfactant solutions have been studied far more extensively than nonionic solutions and experimental data are available for a diversity of systems. Alkyltrimethylammonium bromide and sodium alkyl sulfate surfactant systems have assumed, however, more emphasis than others because of their high purity and monodispersity. Evans et al. (1983 and 1984) used a flow conductance cell and tracer diffusion methods to measure the CMC and $\bar{N}$ for the alkyltrimethylammonium bromide systems at different temperatures in aqueous and nonaqueous solutions. Lianos and Zana (1981 and 1982) used fluorescent probes to also measure these system properties. The most recent reported measurements on the sodium alkyl sulfate systems are given by Bardi et al. (1980), Hayashi and Ikeda (1980), Lianos and Zana (1980), Missel et al. (1980), Backlund et al. (1981), Mitchell and Ninham (1983) and Evans et al. (1983a). Our model has been applied to both types of head groups and the results are presented separately.

5.2.1 Alkyltrimethylammonium Bromide Systems

The collected data for these systems in aqueous solutions are given in table 5.4. Their aggregate properties in nonaqueous media are separately discussed in section 5.2.3. In ionic systems, our model is

Table 5.4
Data Collected, Parameter Values and Predicted $\bar{N}$ for Alkyltrimethylammonium Bromide Systems in Aqueous Solutions

x	T (°K)	CMC (M) [a]	$\bar{N}_{exp}$	$\frac{\Delta G^{o}_{mc}}{RT}$	$\frac{\Delta G^{o}_{ms}}{RT}$	$\frac{\Delta G^{*}_{ms}}{RT}$	$\frac{\Delta G^{o}}{R}\|_{comp}$	$\bar{N}_{pred}$
10	298	6.76(-02)	40	88.01	-68.74	-48.10	41.30	
	338	7.79(-02)		88.67	-66.96	-49.58	41.01	36
	368	9.36(-02)		89.08	-66.29	-50.98	40.65	33
12	298	1.54(-02)	55	88.01	-66.10	-41.55	43.41	
	338	2.19(-02)		88.67	-64.96	-44.15	42.71	47
	368	3.42(-02)		89.08	-65.41	-46.96	41.82	41
14	298	3.79(-03)	70	88.01	-64.16	-35.70	45.28	
	313	4.22(-03)	64	88.28	-63.34	-36.57	45.06	67
	327	4.94(-03)	60	88.51	-62.96	-37.65	44.75	63
	349	6.67(-03)	55	88.83	-62.80	-39.58	44.15	58
	368	9.83(-03)	50	89.08	-63.46	-41.88	43.37	52
16	298	9.55(-04)	90	88.01	-64.09	-31.60	45.96	
	338	1.55(-03)		88.67	-62.66	-34.86	45 00	73
	368	2.61(-03)		89.08	-62.92	-38.05	43.96	62

a : Evans et al. (1983 and 1984)

Table 5.5
Electrostatic Interaction Parameters for the Systems in Table 5.4

x	T (°K)	A_0	A_1	A_2	A_3	A_4	A_5
10	298	-1.133	0.444	0.0865	0.428	1.269	-1.759
	338	-0.966	0.444	0.0865	0.411	1.087	-1.517
	368	-0.841	0.444	0.0865	0.374	0.920	-1.290
12	298	-1.441	0.444	0.0863	0.637	2 732	-3.645
	338	-1.329	0.444	0.0859	0.595	2.426	-3.252
	368	-1.197	0.445	0.0853	0.538	2.047	-2.754
14	298	-1.749	0.442	0.0869	0.846	4.195	-5.531
	313	-1.724	0.443	0.0870	0.828	4.077	-5.368
	327	-1.692	0.443	0.0870	0.803	3.915	-5 175
	349	-1.631	0.443	0.0870	0.756	3.620	-4 799
	368	-1.553	0.443	0.0870	0.702	3.174	-4.218
16	298	-2.057	0.444	0.0865	1.055	5.658	-7.417
	338	-1.995	0.444	0.0865	0.964	5.113	-6.722
	368	-1.909	0.444	0.0865	0.866	4.301	-5.682

reduced from three parameters to two at 298 K because the monomer cavity term which was determined in section 5.1 (Equation 5.1) for nonionic surfactants is universal for all surfactants. Assuming that the entropy of compression is independent of temperature will further reduce the parameters from two to one at temperatures different than 298 K. The CMC and $\bar{N}$ data are, therefore, fitted by our model at 298 K and only the CMC is needed at other temperatures where the model is able to predict the mean $\bar{N}$ at these temperatures. Note that the CMC data are needed at all temperatures and the model has not the ability to predict that property. This is because it is too sensitive to the parameter values by its "small difference of large numbers" problem leading to an unacceptable error in the CMC for slight variations of the parameters.

Free Energy Change and Aggregate Distribution

Except for $C_{14}TAB$, the mean aggregate size $\bar{N}$ data are known at one temperature (298 K) while the CMC data are given at other temperatures. By reducing the model parameters from three to one we can predict $\bar{N}$ at any temperature other than 298 K at which the CMC is known. Table 5.4 shows the parameters, the predicted and experimental $\bar{N}$ for the alkyltrimethylammonium bromide systems. The electrostatic interaction parameters (A_0, A_1, A_2, A_3, A_4 and A_5) defined in chapter IV are given in table 5.5. Note that the assumption that α is independent of temperature allowed us to predict $\bar{N}$ for $C_{14}TAB$ that is within 5% of the experimental value up to a temperature of 368 K, probably within the experimental uncertainty. This is particularly supportive of the assumptions in the model.

The free energy change upon micellization and its average value and the aggregate population density for these systems are shown in figures (5.12a), (5.12b), (5.13a), (5.13b), (5.14) and (5.15). The free energy change for ionic systems shows behavior similar to nonionic systems (Figures 5.1 and 5.12). However the total change is less favorable for ionics due to the long ranged electrostatic forces. This difference leads to smaller ionic aggregates. Spherocylinder and oblate shapes show again more favorable free energy then the prolate for these systems and the former is chosen for nonspherical aggregates for the same reason given for the nonionic systems of section 5.1.1. Further, the free energy dependence on temperature is reversed from nonionic to ionic surfactant systems (Figures 5.1d and 5.13b) due to cancelling of the effect of temperature on the free energy of solution (Equation 4.22, more favorable with increasing temperature) by the electrostatic free energy (less favorable with increasing temperature). Only the first appears in nonionic systems leading to a decrease of free energy with temperature. In ionic systems, however, the electrostatic effect overcomes the solution effect and the free energy increases with temperature. This increase reduces the mean aggregate size and increases the CMC with temperature and, as seen in figure 5.15, the distribution of large aggregates gets smaller with higher temperatures. This forces the distribution of small aggregates to be larger with increasing temperature in order to satisfy the material balance constraint. Similar effects are observed when the thein length is increased (Figure 5.14). The CMC gets smaller and the mean aggregate size gets larger with increasing thein length. This leads to a higher distribution for large aggregates and a smaller distribution for small aggregates when chain length is increased.

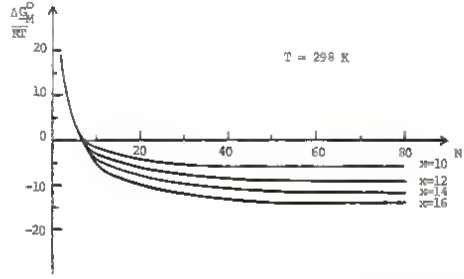

Figure 5.12a Free Energy Change Upon Micelle Formation of $C_xH_{2x+1}N^+(CH_3)_3\ Br^-$ in Aqueous Solutions

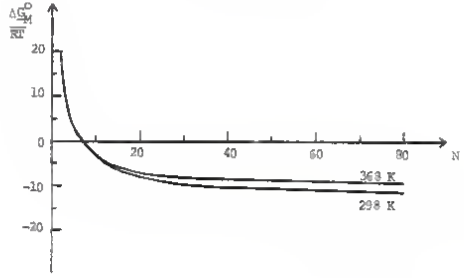

Figure 5.12b Free Energy Change Upon Micelle Formation of $C_{14}H_{29}N^+(CH_3)_3\ Br^-$ at Different Temperatures

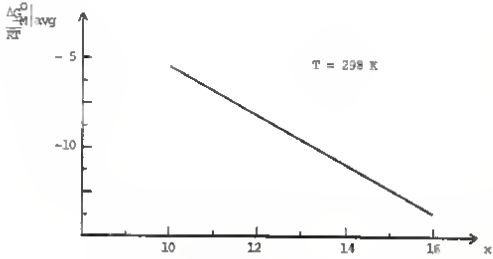

Figure 5.13a Average Free Energy Change Upon Micelle Formation of $C_xH_{2x+1}N^+(CH_3)_3\ Br^-$ (At Different Chain Length)

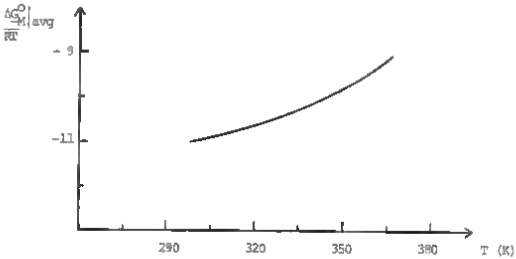

Figure 5.13b Average Free Energy Change Upon Micelle Formation of $C_{14}H_{29}N^+(CH_3)_3\ Br^-$ at Different Temperatures

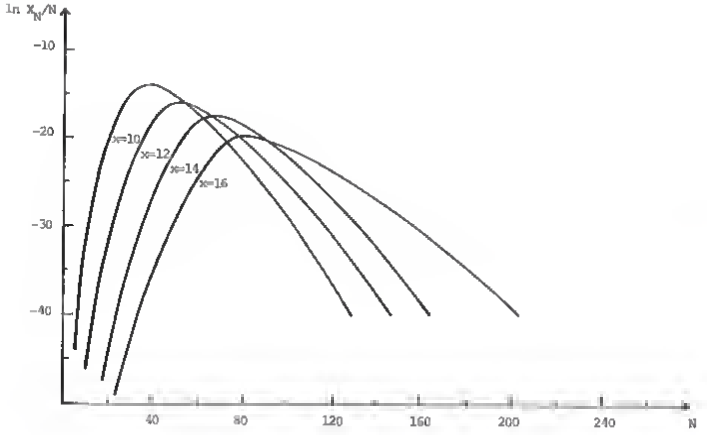

Figure 5.14 Aggregate Population Density of $C_xH_{2x+1}N^+(CH_3)_3\ Br^-$ at 298 K

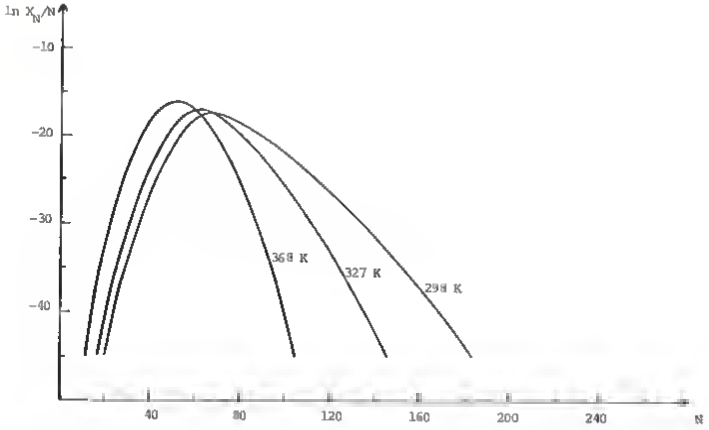

Figure 5.15 Aggregate Population Density of $C_{14}H_{29}N^{+}(CH_3)_3\ Br^{-}$ at Different Temperatures

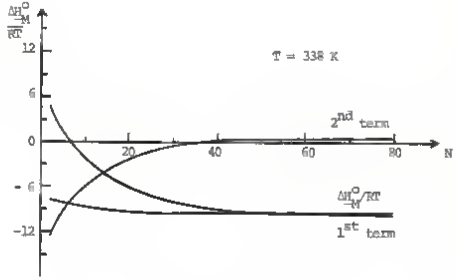

Figure 5.16 Enthalpy Change Upon Aggregation of $C_{14}H_{29}N^+(CH_3)_3\ Br^-$

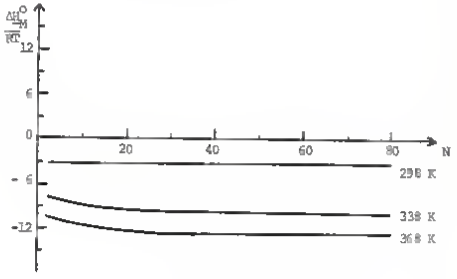

Figure 5.17 Temperature Effect on the Enthalpy Change ($C_{14}H_{29}N^+(CH_3)_3\ Br^-$)

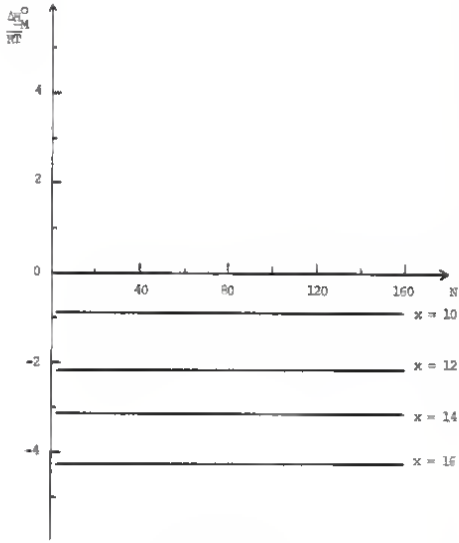

Figure 5.18 Chain Length Effect on the Enthalpy Change (C_xTAS at 298 K)

Enthalpy Change Upon Aggregation

Equation (5.9) is used to determine the enthalpy change upon aggregate formation of C_xTAB systems. This change is shown in figures (5.16), (5.17) and (5.18). Comparing figures (5.16) and (5.6), we find that the contributions from the first and the second terms of equation (5.8) are reversed from ionic to nonionic systems due to the difference in the temperature dependence of the free energy in the two systems. Similar to nonionic surfactants, the enthalpy change decreases with increasing temperature due to the high dependence of step 2 in the thermodynamic process on temperature. Calorimetric measurements are not available for C_xTAB systems so we cannot verify the accuracy of our results. Most of these measurements have been done on sodium alkyl sulfate systems and this family of surfactants is discussed next.

5.2.2 Sodium Alkyl Sulfate Systems

More measurements have been accumulated on this system of surfactants than for any other system. Salt and surfactant concentration effects on aggregate properties and calorimetric studies are the type of measurements that we focus on here. The collected CMC and $\bar{N}$ data for this system in aqueous solutions are given in table 5.6.

Salt Effects

Adding salt to an ionic surfactant solution reduces the long ranged electrostatic forces on the micelle surface by increasing the bulk electrolyte concentration and, therefore, reducing the Debye length κ^{-1} (Equation 3.23). This effect then transforms these long

Table 5.6
Data Collected on Sodium Sulfate Systems ($C_xH_{2x+1}SO_4^- Na^+$) in Aqueous Solutions

System	x	T (°K)	C_s (M) [a]	CMC (M)	$\bar{N}$
1	8	298	0	1.34(-01) [b]	24 [c]
2	8	298	0.03	1.21(-01)	29
3	8	298	0.30	6.89(-02)	48
4	12	288	0	8.44(-03) [b]	58 [c]
5	12	298	0	8.11(-03)	
6	12	308	0	8.39(-03)	
7	12	318	0	8.83(-03)	
8	12	338	0	1.09(-02)	
9	12	298	0.03	3.11(-03) [b]	71 [c]
10	12	298	0.10	1.50(-03)	93
11	12	298	0.30	7.00(-04)	123
12	12	298	0.60	1.20(-04) [d]	174 [d]
13	12	303	0.60	1.20(-04) [d]	151 [d]

a : C_s is the NaCl salt concentration in moles/liter

b : Mukerjee and Mysels (1971)

c : Mitchell and Ninham (1983)

d . Hayashi and Ikeda (1980)

range interactions into short range ones which enhances the formation of size aggregates. Examining table 5.6 we find that $\bar{N}$ increases from 58 to 174 as salt concentration is increased from 0 to 0.6M. Also, less overall surfactant concentration is needed to form these aggregates as we find that the CMC decreases from 8.11(-03) M to 1.20(-04) M over that range of salt concentration.

The temperature effect on aggregate properties was well predicted in our model (Section 5.2.1) even though only one parameter was used. In the case of salt effects, a similar procedure is followed. The monomer cavity term is considered independent of salt concentration and equation (5.1) is universal for all surfactants at any concentration. The change in the entropy of compression due to added salt is determined from the change in the CMC and, therefore, if the salt effect on the CMC of a particular surfactant is known, $-\Delta\underline{S}^{o}/R\big|_{comp}$ can be easily calculated. These two arguments reduce the number of parameters to only one in order to study salt effects on aggregate properties. The CMC measurements and its dependence on salt concentration is the only information needed to allow our model to predict $\bar{N}$ and other aggregate and thermodynamic properties as a function of salinity.

It has been determined experimentally that the fraction of bound counterion is insensitive to added NaCl salt to a sodium dodecyl sulfate solution (Backlund et al., 1981). However, by using equation (4.61) to obtain the value of β for dimers the fraction increases with salinity, approaching 1.0 at 0.6 M salt. Using these results, $\bar{N}$ does not increase as fast as experiment. Better agreement for $\bar{N}$ is obtained

Table 5.7
Experimental and Predicted $\bar{N}$ for Sodium Dodecyl Sulfate Aggregates as a Function of NaCl Concentration

C_s (M) [a]	$\bar{N}_{exp}$	$\bar{N}_{pred}$ [b]	$\bar{N}_{pred}$ [c]	$\bar{A}_{exp}$ [d]	$\bar{\beta}_{(Eq.\ 4.61)}$
0	58			0.78	0.79
0.03	71	63	67	0.75	0.90
0.10	93	73	86	0.77	0.92
0.30	123	92	122	0.79	0.96
0.60	174	122	178		0.99

a : $T = 298\ ^{o}K$

b : $\bar{\beta}$ increases

c : $\bar{\beta} = 0.79$

d — Backlund et al. (1981)

when $\bar{\beta}$ is set to 0.79 for all salt concentrations. This is done by adjusting the value of β for dimers, though a value of 0.5 gives good agreement at 298 K and no added salt. We also note here that $\bar{\beta}_{exp}$ obtained from Backlund et al. has been adjusted to ideal solution. They did not make that assumption and have slightly different values which are not strictly comparable with ours.

A similar procedure is followed for sodium octyl sulfate though there are no available experimental data for $\bar{\beta}$ in this system. We assume it is constant at 0.79 as in the case of dodecyl chain and the predicted $\bar{N}$ is shown below:

C_s (M)	$\bar{N}_{exp}$	$\bar{N}^a_{pred}$	$\bar{N}^b_{pred}$
0	24	24	28
0.03	29	26	33
0.30	48	34	48

a : N = 24 at C_s = 0M is fitted

b : N = 48 at C_s = 0.30M is fitted

Contrary to the case of dodecyl chain aggregates, the model does not predict an acceptable mean aggregate size comparing to experimental values. Two reasons might contribute to this problem. First, the experimental fraction $\bar{\beta}$ is not available to compare it to the value of 0.79 that we calculated from the model. Second, we believe that our model is not adequate for systems with mean aggregate size less than about 30 because we have assumed spherical configuration for all small aggregates up to $N_{transition}$. Such a configuration is not likely to be appropriate for these small entities. In fact, when we fitted $\bar{N}$=48 at

the salt concentration of 0.30M and predicted its value at 0M and 0.03M salt the model does a more adequate description of the properties due to the fact that we started at N>30.

The parameter values obtained for all the systems in table 5.6 are shown in table 5.8 and in table 5.9 their electrostatic terms are given. The predicted $\bar{N}$ and the calculated average free energy change for these systems are also given in table 5.10 along with the experimental values. The free energy change shows a satisfactory comparison with the reported data in the literature. The small difference is due to the assumption in Backlund et al. that surfactant micelle concentration is 2% of the overall surfactant concentration while we used Hall and Pethica value given in equation (2.1). In fact, when we adjust Backlund et al. values according to Hall and Pethica definition, the agreement is even better.

From the parameters of table 5.8 and 5.9, all of the aggregate properties for these systems can be determined. The salt effect on the free energy change and aggregate population density is shown in figures 5.19 and 5.20 for sodium dodecyl sulfate solutions at 298 K. Also from the temperature effect on these solutions, the enthalpy change is calculated for the temperature range of 288-338 K at no added salt and the results are shown in figure 5.21. Birdi (1983) reported a calorimetric value of 0.17 for $\Delta\bar{H}_m^o/RT$ at 298 K comparing to 0.20 obtained by our model. Also at 0.60 M salt, Mazer and Olofsson (1982) measured that quantity and found it equal to -3.92 at 313 K comparing to -3.02 value that we calculated at 303 K from the two available CMC and $\bar{N}$ data given in table 5.6 at 0.60 M salt.

Table 5.8
Parameter Values for Sodium Alkyl Sulfate Systems in Aqueous Solutions

System [a]	$\frac{\Delta G^{o}_{-mc}}{RT}$	$\frac{\Delta G^{o}_{-ms}}{RT}$	$\frac{\Delta G^{*}_{-ms}}{RT}$	$-\frac{\Delta S^{o}}{R}\Big\vert_{comp}$
1	88.01	-74.01	-57.30	36.05
2	88.01	-72.70	-55.99	36.24
3	88.01	-68.51	-51.80	36.84
4	87.81	-66.20	-40.57	42.81
5	88.01	-65.15	-40.60	42.89
6	88.19	-64.53	-40.99	42.82
7	88.36	-64.04	-41.46	42.72
8	88.67	-63.74	-42.93	42.30
9	88.01	-63.65	-39.10	43.85
10	88.01	-62.93	-38.38	44.57
11	88.01	-61.50	-36.95	45.33
12	88.01	-57.02	-32.47	47.09
13	88.10	-58.65	-34.10	45.88

a : See table 5.6 for conditions

Table 5.9
Electrostatic Interaction Parameters for the Systems in table 5.6

System	A_0	A_1	A_2	A_3	A_4	A_5
1	-0.870	0.516	0.0774	0.298	1.182	-1.631
2	0.000	0.501	0.0774	0.272	1.426	-1.918
3	1.100	0.462	0.0774	0.164	1.518	-1.988
4	-1.484	0.443	0.0850	0.762	3.359	-4.440
5	-1.474	0.442	0.0849	0.772	3.512	-4.703
6	-1.468	0.441	0.0858	0.760	3.519	-4.712
7	-1.455	0.441	0.0859	0.752	3.442	-4.596
8	-1.410	0.442	0.0858	0.716	3.243	-4.349
9	-0.295	0.309	0.1210	0.484	3.840	-4.954
10	0.050	0.233	0.1270	0.400	2.620	-2.940
11	0.762	0.200	0.1270	0.381	2.126	-2.353
12	1.700	0.130	0.1270	0.372	2.108	-2.285
13	1.700	0.130	0.1270	0.372	2.108	-2.285

Table 5.10
Predicted $\bar{N}$ and Average Free Energy Change

System	$\bar{N}_{exp}$	$\bar{N}_{pred}$	$\frac{\Delta G^{o}_{M}}{RT}\Big\|^{*}_{avg,exp}$	$\frac{\Delta G^{o}_{M}}{RT}\Big\|^{+}_{avg,exp}$	$\frac{\Delta G^{o}_{M}}{RT}\Big\|_{avg,pred}$
1	24				-4.24
2	29	26			-4.14
3	48	34			-3.84
4		57			-9.38
5	58		-8.42 [a] -8.40 [b]	-9.09	-9.45
6		56			-9.39
7		54			-9.27
8		49			-8.84
9	71	67	-8.22 [a] -8.40 [b]	-8.77	-9.06
10	93	86	-8.32 [a]	-8.80	-8.83
11	123	122	-8.58 [a]	-9.03	-8.78
12	174	178			-10.01

a : Backlund et al. (1981)

b : Backlund and Rundt (1981)

* : 2% of the total surfactant is present as micelles

\+ : 50% of the total surfactant is present as micelles

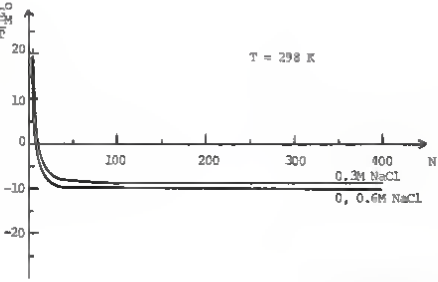

Figure 5.19 Free Energy Change Upon $C_{12}SO_4^- Na^+$ Aggregate Formation as a Function of Salt Concentration

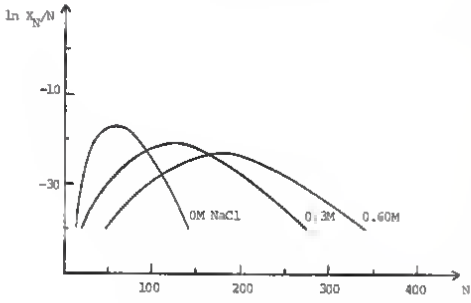

Figure 5.20 Aggregate Population Density of $C_{12}SO_4^- Na^+$ as a Function of Salt Concentration

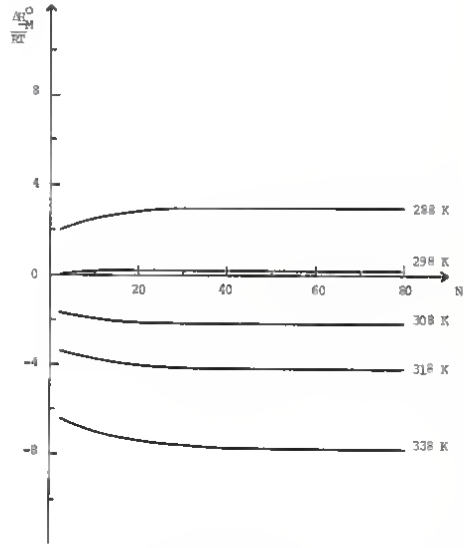

Figure 5.21 Enthalpy Change Upon $C_{12}SO_4^- Na^+$ Aggregation with no Added Salt

Thus, the model predicts temperature and salinity effects on aggregate properties such as mean aggregate size, enthalpy and free energy changes by using only one parameter obtained from the CMC as the only experimental measurement.

Surfactant Concentration Effect

The aggregate properties dependence on $C_{12}SO_4^-$ Na^+ concentration at 298 K above and below the CMC is discussed in this section. Similar to the procedure discussed in section 5.1.3 for nonionic surfactant systems, the three model parameters are predetermined at the CMC and kept constant. The monomer concentration, x_1, is solved for at different surfactant concentrations. The fraction $\bar{N}$ is kept constant at all concentrations as in the case of added salt because of the observations made by Backlund and Rundt (1981). The free energy change and its average value and the aggregate size distribution obtained from these calculations are shown in figures 5.22 and 5.23, respectively, at different overall surfactant concentrations (The parameters are given in table 5.11). From these plots we can note that the monomer concentration decreases as surfactant is added to the solution above the CMC and that behavior was observed experimentally by Kale et al. (1980). The mean aggregate size increases slightly at a concentration that is an order of magnitude larger than the CMC. It varies from 58 to 68 over that range of concentration as shown in figure 5.24. Llanos and Zana (1981) reported an increase from 60 to 64 in $\bar{N}$ for that same range.

Table 5.11

Model Parameters for $C_{12}SO_4^- Na^+$ at Different Concentrations

(T = 298 K and C_s = 0 M)

$\frac{\Delta G^o_{mc}}{RT}$	$\frac{\Delta G^o_{ms}}{RT}$	$\frac{\Delta G^*_{ms}}{RT}$	$-\frac{\Delta S^o}{R}\|_{comp}$
88.01	-65.15	-40.60	42.89

C_t (M)	A_o	A_1	A_2	A_3	A_4	A_5
8.11(-04)	-0.550	0.442	0.0849	1.384	4.970	-6.151
1.62(-03)	-0.530	0.442	0.0849	1.232	4.247	-5.266
2.03(-03)	-0.516	0.442	0.0849	1.175	3.913	-4.865
4.06(-03)	-0.315	0.442	0.0849	1.115	3.385	-4.792
6.06(-03)	-0.338	0.442	0.0849	0.827	3.841	-5.211
8.11(-03)	-1.474	0.442	0.0849	0.772	3.512	-4.703
1.62(-02)	-4.000	0.442	0.0849	0.646	2.806	-3.858
8.11(-02)	-4.700	0.442	0.0849	0.407	1.325	-1.885
4.06(-01)	-3.820	0.408	0.0849	0.200	0.684	-0.997

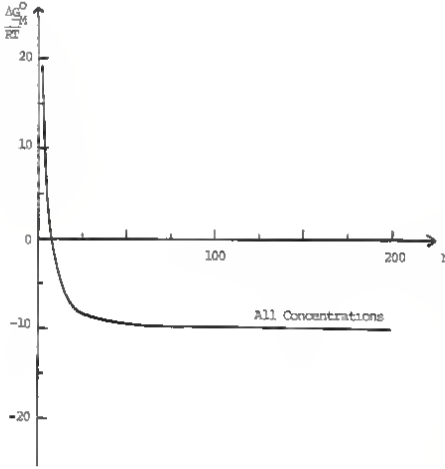

Figure 5.22 Free Energy Change Dependence on $C_{12}SO_4^-$ Na^+ Concentration

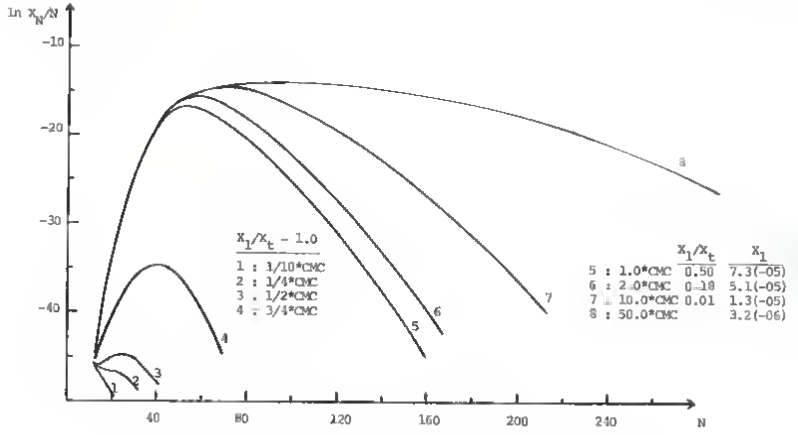

Figure 5.23 Aggregate Distribution of $C_{12}SO_4^-$ Na^+ at Different Concentrations

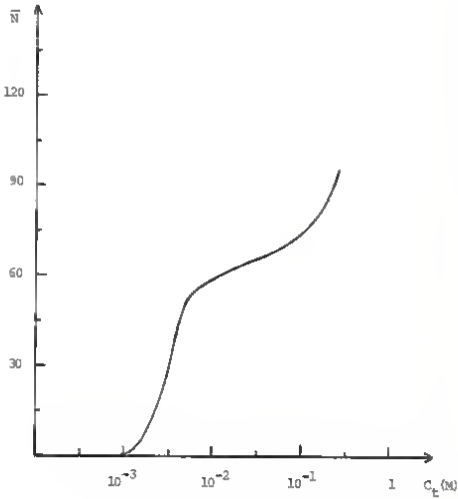

Figure 5.24 Mean Aggregate Size Dependence on Surfactant Concentration ($C_{12}SO_4^-Na^+$ at 298 K)

Sphere-to-Rod Transition

Even though the mean aggregate size for sodium dodecyl sulfate increases only slightly from the CMC to about one order of magnitude larger, it increases more rapidly at higher concentrations as seen in figure 5.24. The slope stays constant beyond the transition point that has been called "2nd CMC" (Miura and Kodama, 1972; Porte and Poggi, 1978). This transition can be ascribed to the shift in shape from spherical to nonspherical because, at this concentration, $\bar{N} = N_{transition}$.

Missel et al. (1983) studied the influence of the chain length on the spherical-to-nonspherical transition and concluded that with increasing chain length, the "2nd CMC" approaches the CMC. We studied the surfactant concentration effect on $\bar{N}$ in C_xTAB systems and the results are shown in figure 5.25. The transition points occur at a concentration of (40*CMC) for the octyl chain, (20*CMC) for the dodecyl chain and (7*CMC) for the hexadecyl chain. Thus, in agreement with Missel et al., we find that less surfactant is needed above the CMC for the transition to occur for longer chain lengths. This dependence is similar to the mean aggregate size dependence on temperature and added salt for various chain lengths. For short chains, the mean aggregate size is small and the free energy difference between two adjacent aggregate sizes is large (Figure 5.12a). Therefore, it takes larger changes in temperature and added salt or surfactant to effect the system free energy change enough to significantly change the mean aggregate size. For larger aggregates, however, the free energy difference is much smaller and any change in these variables can have a dramatic change in $\bar{N}$. This also explains the difference in the

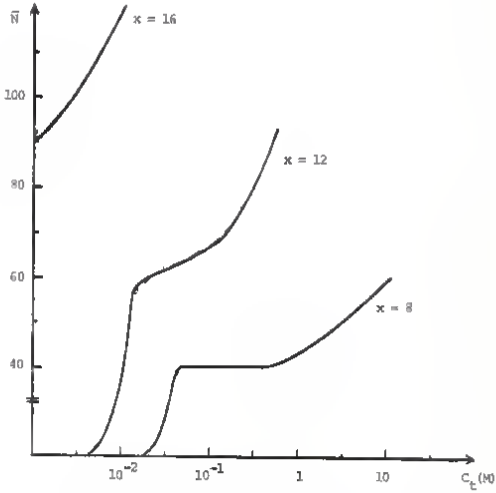

Figure 5.25 Spere-to-Rod Transition in C_xTAB as a Function of Chain Length

temperature dependence for head groups of different length in the polyoxyethylenated surfactant systems. Here, $\bar{N}$ is large for short length head groups and their temperature dependence is large while $\bar{N}$ is small for longer head groups and their temperature dependence is small. Finally, when salt is added, $\bar{N}$ changes very little with the initial amounts However, the effect increases as the size grows until a spherical-nonspherical transition is obtained (Lianos and Zana, 1980).

5.2.3 Aggregate Properties in Nonaqueous Media

So far, the properties of aggregate formation in aqueous media have been discussed. In this section, we direct the attention to these properties in nonaqueous media. Amphiphilic molecules associate in nonaqueous solvents of relatively high polarity such as hydrazine, glycerol and ethylammonium nitrate. Evans et al. (1982 and 1983) have studied aggregate formation in hydrazine and ethylammonium nitrate and have reported some CMC measurements in the former and both CMC and $\bar{N}$ measurements in the latter. Mean aggregate sizes in ethylammonium nitrate solutions are very small ($\bar{N}$<25) and, as we discussed earlier, our model is incorrect for such small aggregates because it assumes sphericity for all sizes up to the transition Also, there is not a known or measured dielectric constant for these solutions and, therefore, the electrostatic interactions cannot be determined. Because of these difficulties we chose to study aggregate formation in hydrazine only. Aggregate sizes in hydrazine have not been yet measured because the refractive index of hydrazine is very close to that of most surfactants, thus eliminating most of the conventional methods used for determining aggregate numbers. These numbers will be

predicted by our model by using only the CMC and solubility measurements in hydrazine solutions and that is accomplished by reducing the model parameters from three to two in nonaqueous media.

The surfactant entropy of compression is independent of the solvent and that can be best explained by examining the thermodynamic process presented in figure 3.1. In step 1, the surfactant has been removed from the solvent and then compressed to the micelle density in step 3 which is independent of the solvent. Therefore, once that quantity is determined for a specific surfactant, it is kept constant for all solvents. It is, however, dependent on the overall surfactant concentration but that can be easily taking care of from the difference in the CMC from one solvent to the other. This procedure reduces the model parameters to two for surfactants in nonaqueous solutions if these surfactants have already been studied in aqueous solutions. The CMC and solubility data are then used to determine the other two unknown quantities which are $\Delta G^{o}_{mc}/RT$ and $\Delta G^{o}_{mb}/RT$.

In table 4.2, the solubilities of helium, nitrogen and argon in hydrazine are given and these are the only known solubility measurements in hydrazine up to date. The comparison with their solubility in water at 298 K is shown below:

	$-\ln(x_1)$			
Solute	Water	Hydrazine	Difference	ε/K (^{o}K)
He	11.86	12.16	0.30	14.6
N	11.35	11.84	0.49	96.3
Ar	10.59	11.30	0.71	116.1
$C_{12}H_{26}$	21.64			529.0

The surfactant $C_{12}TAB$ aggregate properties in hydrazine are examined in this section and that requires knowledge of the solubility of the dodecyl chain in N_2H_4, which is not available. This difficulty is overcomed by extrapolating the data given above to the Leanord-Jones intermolecular potential energy parameter (ε/K) of dodecane because we can note that the difference between the solubility in hydrazine and water varies linearly with the solute (ε/K). Such a variation is fitted to the following equation:

$$(-\ln x_1)_{N_2H_4} - (-\ln x_1)_{H_2O} = 0.232 + 0.00351*(\varepsilon/K) \qquad (5.10)$$

This equation gives a solubility for dodecane in hydrazine equal to

$$(-\ln x_1)_{C_{12}H_{26} \text{ in } N_2H_4} = 23.73 \qquad (5.11)$$

Equation (5.11) and the CMC data given by Evans et al. (1983) for $C_{12}TAB$ in N_2H_4 are used to determine the two parameters of the model which, in turn, allow to compute all of the aggregate and thermodynamic properties of these solutions. The data and parameters are given in table 5.12. From these values, the free energy change and its average value, the aggregate population density and the enthalpy change are calculated and plotted in figures 5.26, 5.27 and 5.28, respectively, and compared to aqueous solution results.

From the values in table 5.12 and figures 5.26 to 5.28 we can conclude that there are major differences between the driving forces for aggregate formation in water compared to hydrazine and between their properties. The solvophobic interactions between the surfactant and hydrazine appear to be weaker than that in water as it can be seen

Table 5.12
CMC and Parameter Values for C_{12}TAB in Hydrazine

T (K)	CMC (M)	$\frac{\Delta G^{o}_{mc}}{RT}$	$\frac{\Delta G^{o}_{ms}}{RT}$	$\frac{\Delta G^{*}_{ms}}{RT}$	$-\frac{\Delta S^{o}}{R}\|_{comp}$
308	6.45(-02)	50.41	-26.06	- 2.52	40.55
(*)	1.54(-02)	88.01	-66.10	-41.55	43.41
318	8.23(-02)	50.51	-26.37	- 3.79	40.05

(*) Aqueous solution results at 298 K

T (K)	$\bar{N}_{calc}$	A_0	A_1	A_2	A_3	A_4	A_5
308	352	-0.831	0.444	0.086	0.479	1.800	-2.435
318	349	-0.758	0.444	0 086	0.446	1.636	-2.206

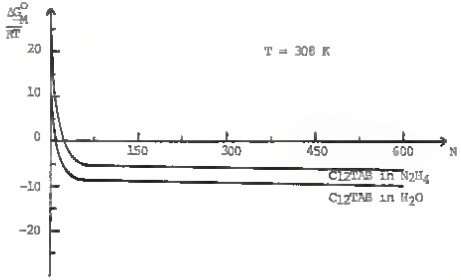

Figure 5.26 Free Energy Change Upon $C_{12}TAB$ Aggregate Formation in N_2H_4 and H_2O

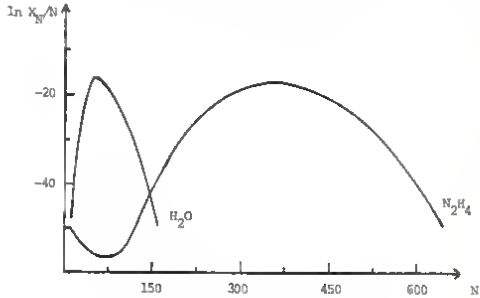

Figure 5.27 Aggregate Population Density of $C_{12}TAB$ in N_2H_4 and H_2O

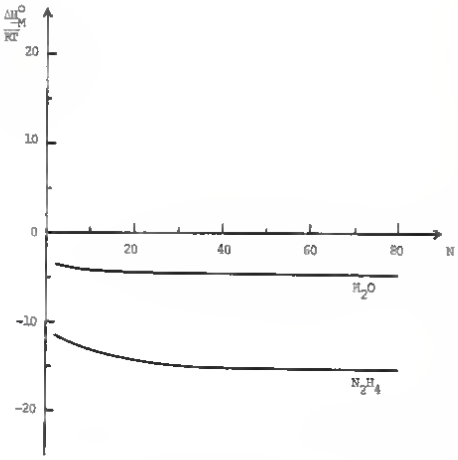

Figure 5.28 Enthalpy Change Upon C_{12} TAB Aggregate Formation in N_2H_4 and H_2O

from the smaller values of $\Delta G^{o}_{mic}/RT$ and $\Delta G^{o}_{mic}/RT$ for hydrazine. Also, the enthalpy change upon aggregate formation is strikingly different in the two systems. While it is small and negative in H_2O, it is large and negative in N_2H_4 and the formation of aggregates in the latter appears to be entirely a result of a favorable enthalpy change. This large difference, however, has a small impact on the free energy change between the two systems which are equally lipophobic.

The solubility data show that nonpolar molecules are less soluble in hydrazine than in water and that drives the surfactant out of the bulk solution to form more aggregates in the case of hydrazine. We have determined a mean aggregate size of 352 at 308 K for $C_{12}TAB$ in hydrazine while it is equal to 55 in water. Evans et al. suggested a value close to 55 in hydrazine and our results disagree with that speculation. Similar reasoning exists for an ethylammonium nitrate solution (where the solubility is larger than in water; table 4.2) leading to less tendency for the surfactant to form aggregates. The mean aggregate size should then be smallest in this solution precisely what was determined experimentally by Evans et al. (1983b) where $\overline{N}$ is less than 17 for a dodecyl chain. Thus, solvophobic differences are the cause for the drastic differences in the aggregate population density shown in figure 5.27.

CHAPTER VI
SUMMARY AND CONCLUSIONS

A molecular thermodynamic process has been developed to describe properties of aggregate formation. This process provides a conceptual and calculational framework for the thermodynamic properties of aggregate formation, the mean and distribution of aggregate sizes and shapes and the degree of counterion binding in ionic systems. It includes all of the important effects such as changes in intermolecular interactions upon aggregation, restriction of surfactant head groups to the micelle surface, excluded volume effects associated with destroying monomer cavities and creating micelle cavities in the solvent, entropy changes for concentrating the surfactant from the solution density to the aggregate density and counterion binding in ionic systems

The mass-action model which allows to describe the properties of all aggregate sizes has been used. This model considers micellization as a reversible formation of aggregates to which reaction equilibrium thermodynamics can be applied. The standard state thermodynamic property changes upon aggregation are then calculated for each step in the above process. These steps are related to similar molecular phenomena and are modeled accordingly : the monomer-solvent interactions and solvent cavity formation are related to the solubility of organic substances in the solvent, the micelle-solvent interactions and cavity properties are correlated to monomer-solvent properties by

only geometrical considerations, an equation of state for nonspherical molecules is used for monomer and counterion compression, the Poisson-Boltzmann theory is used to account for the surface electrostatic interactions in ionic aggregates and salt effects. This procedure leads to expressions for the free energy change upon aggregation which, with the material balance constraint on the overall surfactant concentration in the solution, describes all factors of aggregate formation.

The model uses hydrocarbon solubility (here, normal paraffins), critical micelle concentration and mean aggregate size experimental measurements to determine values for its three parameters for each surfactant-solvent system. The model has been applied to nonionic polyoxyethylenated surfactant systems in aqueous solutions. Besides excellent agreement with data, a result of the analysis is a universal correlation for the monomer cavity parameter as a function of temperature. This correlation can be used for all surfactants, nonionic and ionic, because the model assumes that head group cavity size is unchanged upon aggregation. Thus the model actually has only two parameters for each head group which are determined from the CMC and a single mean aggregate measurement.

The calculated free energy change for these nonionic systems shows that small aggregates are thermodynamically unfavored ($\Delta G_M^o > 0$) while large ones are thermodynamically favored ($\Delta G_M^o < 0$). The value of ΔG_M^o decays asymptotically to a constant negative value. Very large aggregate sizes are not allowed simply because of the material balance constraint. The population density as a function of sizes shows two

extrema : a minimum at very small sizes and a maximum near the mean aggregate size. Larger sizes must be nonspherical and three geometries were considered : spherocylindrical, prolate and oblate ellipsoids. Over all distributions, the spherocylindrical shape showed the most favorable free energy change so it was chosen as the shape for large aggregates. The aggregate distribution dependence on the surfactant concentration shows that smaller aggregates can be formed far below the critical micelle concentration but their concentration is negligible. The size distribution shows a transition concentration well below the CMC. Below the transition the sizes monotonically decrease while above it there are two extrema. For nonionics, the monomer concentration above the CMC is found to be independent of surfactant concentration and the mean aggregate size increases continuously with added surfactant. The enthelpy change computed from the model compares well with experimental calorimetric measurements.

The model has been applied to ionic systems of alkyltrimethyl-ammonium bromide and sodium alkyl sulfate. In addition to using the nonionic cavity parameter, assuming that the nonsphericity factor associated with the surfactant entropy of compression is independent of temperature reduces the number of parameters to one. So the model can be used to predict aggregate properties such as the mean size from only the CMC measurement. It should be noted that the CMC cannot be predicted because of its sensitivity to the parameters, the model relations contain a small difference of large numbers for this property. However, the model predicts mean aggregate size for $C_{14}TAB$ to within 5% of the experimental data up to 368 K.

The dependence of free energy change on aggregate size in the ionic systems is similar to what we observed in nonionic surfactant systems. The major difference is quantitative since the long ranged electrostatic forces yield positive free energies of formation leading to smaller aggregate sizes for ionics. However, the CMC and aggregate size dependence on temperature are different for ionics and nonionics because the variation of free energy of solution dominates in nonionic systems while the temperature variation of the electrostatic forces dominates in ionic systems.

The model has also the ability to predict salt effects on ionic aggregate properties. By keeping the fraction of counterion bound to the aggregates independent of salt concentration as determined experimentally, the model predicts mean aggregate sizes for SDS to within 7% of the experimental data up to a salt concentrations of 0.6M. The enthalpy change and surfactant concentration effects obtained from the model also compare well with experimental observations. The monomer concentration above the CMC decreases continuously with added surfactant while the mean aggregate size increases in a manner consistent with a "2nd CMC" where the aggregate of mean size changes from a sphere to a spherocylinder.

Aggregate properties in nonaqueous media such as hydrazine have been studied. By extrapolating the available solubility data for helium, nitrogen and argon in hydrazine to larger molecules, and using surfactant entropies of compression that are independent of the solvent, the model has only one parameter. Thus, CMC measurements again determine all other aggregate properties. Major differences

appear between the aggregate properties in water and hydrazine primarily because the solvophobic interactions in hydrazine are weaker. Thus, the enthalpy change of formation is the driving force for aggregation in hydrazine at all temperatures while in water the driving force is entropy at low temperatures and enthalpy only at high temperatures. The mean aggregate size is found to be larger in hydrazine than in water. Preliminary analysis of aggregation in ethylammonium nitrate indicates that the mean size is smaller than in water.

The thermodynamic process and the model developed in this analysis can be applied to multicomponent aggregate systems. The equations presented in chapter IV are for single component systems but they can be extended to multicomponent systems. The mass-action law is recommended for this extension because it allows complete description of component distributions in all states.

APPENDIX A
NUMERICAL SOLUTION OF THE POISSON-BOLTZMANN EQUATION

The dimensionless form of the Poisson-Boltzmann equation and its boundary conditions are (Equations 3.24 and 3.25)

$$\frac{d^2y}{dx^2} + \frac{2}{x}\frac{dy}{dx} = \sinh y \qquad (A.1)$$

$$\left.\frac{dy}{dx}\right)_{x=\kappa R} = -S \qquad (A.2)$$

$$\left.\frac{dy}{dx}\right)_{x=\infty} = 0 \qquad (A.3)$$

Numerical methods for solving a nonlinear second order differential equation with boundary conditions are not available. The technique used to overcome that difficulty is to transform equation (A.1) to a set of four linear first order differential equations with four initial conditions replacing the boundary conditions. This set of equations in numerically solvable. The procedure is given below

Let $$Y_1 = y \qquad (A.4a)$$

$$Y_2 = x^2\frac{dy}{dx} \qquad (A.4b)$$

Taking the first derivative of Y_1 and Y_2 with respect to x we get

$$\frac{dY_1}{dx} = \frac{dy}{dx} = \frac{Y_2}{x^2} \qquad (A.5a)$$

$$\frac{dY_2}{dx} = \frac{d}{dx}\left(x^2\frac{dy}{dx}\right) = x^2\frac{d^2y}{dx^2} + 2x\frac{dy}{dx} \qquad (A.5b)$$

Note that equation (A.5b) is related to equation (A.1) by

$$x^2 \frac{d^2y}{dx^2} + 2x \frac{dy}{dx} = x^2 \sinh y$$

so that

$$\frac{dY_2}{dx} = x^2 \sinh y$$

Define $\frac{dY_1}{dx}$ and $\frac{dY_2}{dx}$ by the following functions

$$\frac{dY_1}{dx} = \frac{dy}{dx} = \frac{Y_2}{x^2} \equiv F(1) \qquad (A.6a)$$

$$\frac{dY_2}{dx} = x^2 \sinh Y_1 \equiv F(2) \qquad (A.6b)$$

The boundary conditions (A.2 and A.3) can now be replaced by

$$\left.\frac{dy}{dx}\right)_{x=\kappa R} = \left.\frac{dY_1(G)}{dx}\right)_{x=\kappa R} = -S \qquad (A.7)$$

$$\left.\frac{dy}{dx}\right)_{x=\infty} = \left.\frac{dY_1(G)}{dx}\right)_{x=a*\kappa R} = 0 \qquad (A.8)$$

where G is an initial guess for the dimensionless potential y at a distance "very far" from the charged surface. Thus "very far" distance is equal to $(a*\kappa R)$ where a is an integer that is large enough to make y at $(a*\kappa R)$ equal to 0.

The guess G is converged by a Newton-Raphson method, where

$$G_{m+1} = G_m - \frac{f(G_m)}{f'(G_m)} \qquad (A.9a)$$

and

$$f(G_m) = \left.\frac{dY_1(G_m)}{dx}\right)_{x=\kappa R} + S \qquad (A.9b)$$

so that

$$G_{m+1} = G_m - \frac{\left.\frac{dY_{1(G_m)}}{dx}\right|_{x=\kappa R} + S}{\left.\frac{d^2Y_{1(G_m)}}{dG_m dx}\right|_{x=\kappa R}} \qquad (A.9c)$$

A new set of variables, Y_3 and Y_4, and functions, F(3) and F(4), are defined as follows:

Let
$$Y_3 = \frac{dY_{1(G)}}{dG} \qquad (A.10a)$$

$$Y_4 = \frac{dY_2}{dG} \qquad (A.10b)$$

so that

$$\frac{d^2Y_{1(G)}}{dG\,dx} = \frac{d}{dx}\left(\frac{dY_{1(G)}}{dG}\right) = \frac{dY_3}{dx} = F(3) \qquad (A.11a)$$

$$\frac{dY_4}{dx} = \frac{d^2Y_2}{dx\,dG} = F(4) \qquad (A.11b)$$

Note that from these variables, equation (A.9c) can be rewritten as

$$\left.\frac{dY_{1(G_m)}}{dx}\right|_{x=\kappa R} = \left.\frac{Y_2}{x^2}\right|_{x=\kappa R} \qquad \text{(From A.4b)}$$

$$\left.\frac{d^2Y_{1(G_m)}}{dG_m\,dx}\right|_{x=\kappa R} = \frac{1}{x^2}\frac{d}{dG_m}\left(x^2\frac{dY_{1(G_m)}}{dx}\right) = \left.\frac{1}{x^2}\frac{dY_2}{dG_m} = \frac{Y_4}{x^2}\right|_{x=\kappa R}$$

(From A.4b and A.10b)

so that

$$G_{m+1} = G_m - \frac{\left.\frac{Y_2}{x^2}\right|_{x=\kappa R} + S}{\left.\frac{Y_4}{x^2}\right|_{x=\kappa R}} \qquad (A.12)$$

Finally, equations (A.11a) and (A.11b) can be rearranged to the following forms

$$F(3) = d^2Y_{1(G)}/dG\,dx = Y_4/x^2 \qquad \text{(A.13a)}$$

$$F(4) = d^2Y_2/dx\,dG = \frac{d}{dx}\left(\frac{dY_2}{dG}\right) = \frac{d}{dx}\left[\frac{d}{dG}\left(x^2\,\frac{dY_1}{dx}\right)\right] = \frac{d}{dx}\left[x^2\,\frac{d^2Y_1}{dGdx}\right]$$

$$= 2x\,d^2Y_1/dGdx + x^2\,d^3Y_1/dGdx^2 = \frac{d}{dG}\left[2x\,\frac{dY}{dx} + x^2\,\frac{d^2Y_1}{dx^2}\right]$$

$$= \frac{d}{dG}\left[x^2 \sinh Y_1\right] = \frac{d}{dG}\left[\frac{x^2}{2}\left(e^{Y_1} - e^{-Y_1}\right)\right]$$

$$= \frac{x^2}{2}\left[e^{Y_1}\,\frac{dY_1}{dG} + e^{-Y_1}\,\frac{dY_1}{dg}\right] = x^2\,\frac{dY_1}{dG}\cosh Y_1$$

$$= x^2\,Y_3 \cosh Y_1 \qquad \text{(A.13b)}$$

The set of four first order differential equations is then (Equations A.6a, A.6b, A.13a and A.13b)

$$dY_1/dx = F(1) = Y_2/x^2$$

$$dY_2/dx = F(2) = x^2 \sinh Y_1$$

$$dY_3/dx = F(3) = Y_4/x^2$$

$$dY_4/dx = F(4) = x^2\,Y_3 \cosh Y_1$$

The four initial conditions are

$$Y_1 = G_m \qquad \text{at} \quad x = a * \kappa R$$

$$Y_2 = \kappa^2 \left.\frac{dY_1}{dx}\right]_{x=a*\kappa R} = 0$$

$$Y_3 = dY_1/dG_m = 1$$

$$Y_4 = dY_2/dG = 0$$

These ordinary differential equations were solved by the numerical method of Runge-Kutta (Hornbeck, 1975) which is easy to program and has good stability characteristics. A hard copy of the algorithm is attached to this appendix

Algorithm for the Numerical Solution of the Poisson-Boltzmann Equation

```
implicit real*8(a-h,o-z)
integer i,ier,iero,ierl,iopt,m,ma,n,k,kl
double precision runge,f
double precision dexp,dabs
dumension yi(4),y(4,200),f1(4),f2(4),f3(4),f4(4),yl(4),p(4,200),yn(200)
common /st/p,l
common /da/so,al,arg
call setfil(7,"data")
call setfil(9,"out")
zp=1.d0
zm=-1.d0 ·
k=0
gelktt=0.d+00
geltbl=0.d+00
geltb2=0.d+00
read(7,701) diel,agg,temp,dbl
701 format (3(f6.2,lx),f8.5)
write(6,702) diel,agg,temp,dbl
702 format (3(f6.2,lx),f8.5)
c   Use this correlation for initial guess
c   g = - exp (3.1362 + 0.8546(a*ak))
650 read(7,700) so,ak,g,eps,m,a
700 format (2(f10.4),f12.4,lx,f10.4,i3,lx,f3.1)
write (9,651) g
651 format (7x,d17.8)
so=so-dble(float(k))*so*2.d-01
sol=so
kl=1
gel=0.d+00
600 yi(2)=0.d+00
yi(3)=1.d+00
yi(4)=0.d+00
it=0
222 yi(1)=g
 gold=g
223 h=dble(float(a-1))*ak/dble(float(m))
if (h .lt. 1.0d-01) goto 224
m=2*m
goto 223
224 n=m+1
itemax=100
it=it+1
al=ak
if (g .gt. 0.d+00) g=0.d+00
call runge(yi,y,h,zp,zm,al,m)
goto 999
101 alfa=al
goto 102
```

```
c   Note that we will use the dimension x=r=0 at ∞ and x=r=(a-1)*kR at
the charged surface and x=r=a*kR at the center of the sphere
999 g=gold-(y(2,n)-so*(dble(float(a-1))**2)*(ak**2))/y(4,n)
if (g .gt. 0.d+00) g=-(gold**2)
delg=dabs((g-gold)/g)
if ((delg .lt. eps) .or. (it .gt. itemax)) goto 101
goto 222
102 if (it .lt. itemax) goto 103
103 do 43 ja=1,n
ra=dble(float(ja-1))*h
43 yn(ja)=y(2,ja)/(dble(float(a-1))**2*(ak**2))
write(9,601) y(1,n),yn(n)
601 format(7x,d17.8,7x,d17.8)
if (kl .eq. 1) goto 661
if (kl .eq. 2) goto 662
if (kl .eq. 3) goto 663
if (kl .eq. 4) goto 664
if (kl .eq. 5) goto 665
if (kl .eq. 6) goto 666
if (kl .eq. 7) goto 667
if (kl .eq. 8) goto 668
if (kl .eq. 9) goto 669
if (kl .eq. 10) goto 670
661 gel=gel+y(1,n)
goto 671
662 gel=gel+4.d+00*y(1,n)
goto 671
663 gel=gel+2.d+00*y(1,n)
goto 671
664 gel=gel+4.d+00*y(1,n)
goto 671
665 gel=gel+2.d+00*y(1,n)
goto 671
666 gel=gel+4.d+00*y(1,n)
goto 671
667 gel=gel+2.d+00*y(1,n)
goto 671
668 gel=gel+4.d+00*y(1,n)
goto 671
669 gel=gel+2.d+00*y(1,n)
goto 671
670 gel=gel+4.d+00*y(1,n)
gel=gel*sol/30.d+00
write (9,672) gel
672 format (7x,d16.8)
gelkt=1.142d-04*temp*diel*dbl*gel/(agg**(1.0/3.0))
write(9,673) gelkt
673 format(7x,d16.8)
671 kl=kl+1
so=so-sol/10.d+00
if (so .gt. -1.d-04) goto 114
goto 600
114 gelktt=gelktt+gelkt
```

```
geltbl=geltbl+k*0.2d+00*gelkt
geltb2=geltb2+((k*0.2d+00)**2)*gelkt
k=k+1
if (k .gt. 4) goto 115
goto 650
115 write(9,674) gelktt,geltbl,geltb2
674 format (1(d16.8,1x))
stop
end

subroutine runge(yi,y,h,zp,zm,al,m)
implicit real*8(a-h,o-z)
dimension y(4,200),yi(4),rk(4,4),p(4,200)
double precision f,rk,ra,h,y,yi,zp,zm,p,al
integer m,i,j
common /et/p,l
do 20 j=1,4
20 y(j,1)=yi(j)
mm=m+2
do 21 i=2,mm
l=i-1
r=dble(float(i-2))*h
do 22 j=1,4
22 p(j,1)=y(j,1)
do 23 j=1,4
23 rk(j,1)=h*f(r,j,zp,zm,al)
do 24 j=1,4
24 p(j,1)=y(j,1)+rk(j,1)/2.d+00
do 25 j=1,4
ra=r+h/2.d+00
25 rk(j,2)=h*f(ra,j,zp,zm,al)
do 26 j=1,4
26 p(j,1)=y(j,1)+rk(j,2)/2.d+00
do 27 j=1,4
ra=r+h/2.d+00
27 rk(j,3)=h*f(ra,j,zp,zm,al)
do 28 j=1,4
28 p(j,1)=y(j,1)+rk(j,3)
do 29 j=1,4
ra=r+h
29 rk(j,4)=h*f(ra,j,zp,zm,al)
do 30 j=1,4
30 y(j,1)=y(j,1)+(1.d+00/6.d+00)*(rk(j,1)+2.d+00*rk(j,2)+
$2.d+00*rk(j,3)+rk(j,4))
21 continue
return
end

double precision function f(r,j,zp,zm,al)
implicit real*8(a-h,o-z)
dimension p(4,200)
double precision p,zp,zm,am,ap,ep,em,r
integer j,l
```

```
double precision dexp
common /st/p,l
ap=(-1.d+00)*zp*p(1,l)
ep=dexp(ap)
am=(-1.d+00)*zm*p(1,l)
em=dexp(am)
if (r .lt. 1.d-04) goto 30
5 if (j .eq. 1) goto 9
if (j .eq. 2) goto 10
if (j .eq. 3) goto 11
if (j .eq. 4) goto 12
f=j
9 f=p(2,l)/(r**2)
goto 20
10 f=(r**2)*(em-ep)/2.d+00
goto 20
11 f=p(4,l)/(r**2)
goto 20
12 f=(r**2)*p(3,l)*(em+ep)/2.d+00
goto 20
30 if (j .eq. 1 .or. j .eq. 3) goto 31
goto 5
31 f=0.d+00
20 return
end
```

APPENDIX B
PROPERTIES OF DISTRIBUTED SURFACTANTS IN MIXED MICELLES

The same thermodynamic process presented in chapter III can be used to describe the thermodynamic properties of mixed micelles as it was discussed in chapter VI. In this appendix, however, a different approach is presented and it is based on the phase-separation concept (Chapter II) instead of the mass-action law. This approach allows us to determine the surfactant distributions in the monomer-bulk solution and in the mixed micelles. One of the disadvantages of using this model is that the aggregate size distribution cannot be predicted.

B.1 Discrete Distribution of Surfactants

Rubingh (1979) applied the phase-separation model to describe the properties of two surfactants in aqueous solution. In this analysis, the model is extended for n-surfactants which are discretely distributed in the solution.

The phase equilibrium approach regards micelles as a distinct phase in equilibrium with the surfactant monomer/solvent solution. The chemical potential of the surfactant in both phases are then equal

$$\mu_{i,1} = \mu_{i,M} \qquad (B.1)$$

where i is a species index and it ranges from 1 to m

l represents the monomer phase

M represents the micelle phase

In terms of standard state properties, equation (B.1) becomes

$$\mu^{o}_{i,l} + RT \ln a_{i,l} = \mu^{o}_{i,M} + RT \ln a_{i,M} \qquad (B.2)$$

For the concentrations of interest, the solution is dilute in both surfactant monomers and micelles so an ideal solution with a Henry s law reference state is assumed. The same argument cannot be applied, however, to the micelle interior where a mixture of surfactants are located with a high density. Equation (B 2) reduces then to

$$\mu^{o}_{i,l} + RT \ln X_{i,l} = \mu^{o}_{i,M} + RT \ln \gamma_{i,M} X_{i,M} \qquad (B.3)$$

where x is the mole fraction

γ is the activity coefficient

The standard state chemical potential, $\mu^{o}_{i,M}$, is the potential of species i in pure or single surfactant micelle. It can be substituted by

$$\mu^{o}_{i,M} = \mu^{o}_{i,l} + RT \ln X^{pure}_{i,l} \qquad (B.4)$$

Equation (B.3) becomes

$$\mu^{o}_{i,M} + RT \ln X_{i,l} = \mu^{o}_{i,l} + RT \ln X^{pure}_{i,l} + RT \ln \gamma_{i,M} X_{i,M}$$

or

$$X_{i,l} = X^{pure}_{i,l} \gamma_{i,M} X_{i,M} \qquad (B.5)$$

Solving for $X_{i,M}$ and using the relation $\sum_{i=1}^{m} X_{i,m}=1$ leads to

$$\sum_{i=1}^{m} \frac{X_{i,1}}{X_{i,1}^{pure}\,\gamma_{i,M}} = 1 \qquad (B.6)$$

From the Hall and Pethica definition of the ratio between monomer concentration and total surfactant concentration at the CMC (Equation 2.1), the ratio $\frac{X_{i,1}}{X_{i,1}^{pure}}$ can be replaced by the ratio of the CMC:

$$\frac{X_{i,1}}{X_{i,1}^{pure}} = \frac{X_{i,CMC}}{X_{i,CMC}^{pure}} = \frac{C_{i,CMC}}{C_{i,CMC}^{pure}} = \frac{\alpha_i\, C_{CMC}}{C_{i,CMC}^{pure}} \qquad (B.7)$$

where C_{CMC} is the mixture critical micelle concentration

$C_{i,CMC}^{pure}$ is the CMC of pure component i

α_i is the fraction of i in the total mixed surfactant

Substituting (B.7) in (B.6), we can solve for C_{CMC}

$$C_{CMC} = \frac{1}{\sum_{i=1}^{m} \frac{\alpha_i}{C_{i,CMC}^{pure}\,\gamma_{i,M}}} \qquad (B.8)$$

Equation (B.8) relates the mixture CMC to the pure component CMC, the distribution of surfactants in that mixture and the nonideality in the micelle interior. The surfactant distribution in the micelle, $X_{i,M}$, can be also related to these variables by substituting equations (B.7) and (B.8) in equation (B.5):

$$X_{i,M} = \frac{\alpha_i\, C_{CMC}}{C_{i,CMC}^{pure}\,\gamma_{i,M}}$$

$$= \frac{\alpha_i}{C_{i,CMC}^{pure}\,\gamma_{i,M}} \cdot \frac{1}{\sum_{i=1}^{m} \frac{\alpha_i}{C_{i,CMC}^{pure}\,\gamma_{i,M}}}$$

so that

$$X_{i,M} = \frac{1}{1 + \sum_{\substack{j=1 \\ j \neq i}}^{m} \frac{\alpha_j}{\alpha_i} \frac{C^{pure}_{j,CMC}}{C^{pure}_{i,CMC}} Y_{j,M}} \qquad (B.9)$$

Equation (B.9) can be written in a matrix form:

$$\underset{\sim}{X} = (\underset{\sim}{I} - \underset{\sim}{A})^{-1} \underset{\sim}{B} \qquad (B.10)$$

where

$$\underset{\sim}{X} = \begin{bmatrix} X_{1,M} \\ X_{2,M} \\ \vdots \\ X_{m,M} \end{bmatrix} ; \quad \underset{\sim}{I} = \begin{bmatrix} 1 & 0 & 0 & \cdots \\ 0 & 1 & 0 & \cdots \\ \vdots & & & \\ 0 & 0 & \cdots & 1 \end{bmatrix} ; \quad \underset{\sim}{B} = \begin{bmatrix} 0 \\ 0 \\ \vdots \\ 1 \end{bmatrix}$$

$$\underset{\sim}{A} = \begin{bmatrix} 0 & \frac{\alpha_1}{\alpha_2} \frac{C^{pure}_{2,CMC}}{C^{pure}_{1,CMC}} Y_{2,M} & 0 & \cdots & 0 & \cdots \\ 0 & 0 & \frac{\alpha_2}{\alpha_3} \frac{C^{pure}_{3,CMC}}{C^{pure}_{2,CMC}} Y_{3,M} & 0 & & \cdots \\ \vdots & \vdots & \vdots & & & \\ 0 & 0 & 0 & & \frac{\alpha_{m-1}}{\alpha_m} \frac{C^{pure}_{m,CMC}}{C^{pure}_{m-1,CMC}} Y_{m,M} & \\ -1 & -1 & -1 & -1 & 0 & \end{bmatrix}$$

At a concentration that is higher or lower than the CMC, equation (B.7) is not applicable and a new formalism is required. The derivation begins by writing a material balance for each component i:

$$X_{i,M} = \frac{\alpha_i C_t - C_{i,1}}{C_t - \sum_{i=1}^{m} C_{i,1}} \qquad (B.11)$$

where C_t is the total mixed surfactant concentration.

Solving for $\mu^{pure}_{i,1}$ from equation (B.5) and substituting it in (B.11) we get:

$$X_{i,M} = \frac{\alpha_i C_t - C^{pure}_{i,1}\ \gamma_{i,M}\ X_{i,M}}{C_t - \sum_{i=1}^{m} C^{pure}_{i,1}\ \gamma_{i,M}\ X_{i,M}} \qquad (B.12)$$

The standard state chemical potential, $\mu^{o}_{i,M}$, in equation (B.4) can be chosen at a reference state such that

$$C^{pure}_{i,1} = C^{pure}_{i,CMC} \qquad (B.13)$$

This reference state allows us to determine the surfactant distribution in the mixed micelle, $X_{i,M}$, as a function of pure component CMC at any mixed surfactant concentration, C_t.

$$X_{i,M} = \frac{\alpha_i C_t - C^{pure}_{i,CMC}\ \gamma_{i,M}\ X_{i,M}}{C_t - \sum_{i=1}^{m} C^{pure}_{i,CMC}\ \gamma_{i,M}\ X_{i,M}} \qquad (B.14)$$

Equation (B.14) can be rearranged to the following form:

$$X^2_{i,M} + \left\{ \sum_{\substack{j=1 \\ j\neq i}}^{m} X_{i,M}\ X_{j,M}\ \frac{C^{pure}_{j,CMC}\ \gamma_{j,M}}{C^{pure}_{i,CMC}\ \gamma_{i,M}} \right\} - \left(\frac{C_t}{C^{pure}_{i,CMC}\ \gamma_{i,M}} + 1 \right) X_{i,M}$$

$$+ \frac{\alpha_i C_t}{C^{pure}_{i,CMC}\ \gamma_{i,M}} = 0 \qquad (B.15)$$

In a matrix form, equation (B.15) becomes

$$\underset{\sim}{X}\ \underset{\sim}{D}\ \underset{\sim}{X} - \underset{\sim}{E}\ \underset{\sim}{X} + \underset{\sim}{F} = \underset{\sim}{0} \qquad (B.16)$$

where

$$\underline{X} = \begin{bmatrix} X_{1,m} \\ X_{2,M} \\ \vdots \\ X_{m,M} \end{bmatrix} \quad ; \quad \underline{F} = \begin{bmatrix} \dfrac{\alpha_1 C_t}{C^{pure}_{1,CMC}\gamma_{1,M}} \\ \vdots \\ \dfrac{\alpha_m C_t}{C^{pure}_{m,CMC}\gamma_{m,M}} \end{bmatrix} \quad ; \quad \underline{0} = \begin{bmatrix} 0 \\ \vdots \\ 0 \end{bmatrix}$$

$$\underline{\underline{X}} = \begin{bmatrix} X_{1,M} & 0 & 0 & \cdots & 0 \\ 0 & X_{2,M} & 0 & \cdots & 0 \\ 0 & 0 & X_{3,M} & \cdots & 0 \\ 0 & 0 & 0 & \cdots & X_{m,M} \end{bmatrix} \quad ;$$

$$\underline{\underline{W}} = \begin{bmatrix} \dfrac{C_t}{C^{pure}_{1,CMC}\gamma_{1,M}} + 1 & 0 & \cdots & 0 \\ 0 & \dfrac{C_t}{C^{pure}_{2,CMC}\gamma_{2,M}} + 1 & \cdots & 0 \\ \vdots & & & \\ 0 & 0 & \cdots & \dfrac{C_t}{C^{pure}_{m,CMC}\gamma_{m,M}} + 1 \end{bmatrix}$$

$$\underline{\underline{D}} = \begin{bmatrix} 1 & \dfrac{C^{pure}_{2,CMC}\gamma_{2,M}}{C^{pure}_{1,CMC}\gamma_{1,M}} & \cdots\cdots & \dfrac{C^{pure}_{m,CMC}\gamma_{m,M}}{C^{pure}_{1,CMC}\gamma_{1,M}} \\ \dfrac{C^{pure}_{1,CMC}f_{1,M}}{C^{pure}_{2,CMC}\gamma_{2,M}} & 1 & \cdots\cdots & \dfrac{C^{pure}_{m,CMC}f_{m,M}}{C^{pure}_{2,CMC}\gamma_{2,M}} \\ \vdots & & & \\ \dfrac{C^{pure}_{1,CMC}\gamma_{1,M}}{C^{pure}_{m,CMC}\gamma_{m,M}} & \dfrac{C^{pure}_{2,CMC}\gamma_{2,M}}{C^{pure}_{m,CMC}\gamma_{m,M}} & \cdots\cdots & 1 \end{bmatrix}$$

After solving for $X_{i,M}$ from equation (B 16), the surfactant distribution in the monomer solution can be obtained from equation (B 5)

$$X_{i,1} = X^{pure}_{1,CMC}\ \gamma_{i,M}\ X_{1,M} \tag{B.17}$$

or

$$\underline{C} = \underline{X}\ \underline{G}$$

where

$$\underline{C} = \begin{bmatrix} C_{1,1} \\ \vdots \\ C_{m,1} \end{bmatrix}\ ; \qquad \underline{G} = \begin{bmatrix} C^{pure}_{1,CMC}\ \gamma_{1,M} \\ \vdots \\ C^{pure}_{m,CMC}\ \gamma_{m,M} \end{bmatrix}$$

We have so far described the properties of mixed micelles but they all are functions of the activity coefficient, $\gamma_{i,M}$ which needs to be modeled. The regular solution theory is one method that can be used. The excess free energy expression is assumed to be

$$\frac{g^E}{RT} = \sum_{i=1}^{m-1} \sum_{j=i+1}^{m} X_{i,M}\ X_{j,M}\ \beta_{ij} \tag{B.18}$$

where β_{ij} is a binary interaction parameter

The activity coefficient relation to g^E is

$$\ln \gamma_{i,M} = \left. \frac{\partial N_{t,M}\ g^E/RT}{\partial N_{i,M}} \right|_{T,P,N_{j\neq i}} \tag{B.19}$$

where $N_{t,M}$ is the total number of moles in the micelle

$N_{i,M}$ is the number of moles of species i in the micelle

Substituting equation (B.18) in (B.19) and differentiating, we get:

$$\ln \gamma_{i,M} = \left[\sum_{\substack{j=1 \\ j \neq i}}^{n} \beta_{ij} \sum_{\substack{k=1 \\ k \neq i}}^{m} X_j X_k - \sum_{j=1}^{m-1} \sum_{k=j+1}^{m} \beta_{jk} X_j X_k \right] \qquad (B.20)$$

Equations (B.8), (B.9) and (B.20) are used to determine the CMC, $X_{i,M}$ and $\gamma_{i,M}$ for mixed surfactant systems. Also equations (B.15), (B.17) and (B.20) will determine $X_{i,M}$, $X_{i,1}$ and $\gamma_{i,M}$ for higher or lower concentrations than the CMC. The computation starts by assuming a unit activity coefficient for all components. The mole fractions, $X_{i,M}$, can then be calculated from equation (B.9) and (B.15) which allows to recalculate $\gamma_{i,M}$ from (B.20) and the procedure is repeated until a satisfactory convergence. The data needed for this model are:

1. Pure component CMC
2. Binary parameters

B 2 Continuous Distribution of Surfactants

For a continuous distribution, the summation in equation (B.8) can be replaced by an integral so that

$$C_{CMC} = \frac{1}{\int_0^{\infty} \frac{\alpha_{(y)} dy}{C_{CMC}^{pure}(y) \; \gamma_M(y)}} \qquad (B.21)$$

where y is a variable that represents a characteristic property of the components, it may be molecular weight or chain length, for example. The surfactant distribution in the micelle, $X_M(y)$, at the CMC and any other concentration becomes

$$X_M(y) = \text{[illegible]}_{(y)}\ C_{CMC}/C^{pure}_{CMC}(y)\ \gamma_M(y) \qquad \text{at the CMC} \qquad \text{(B.22)}$$

$$= \frac{{}^{+}(y)\ C_t - C^{pure}_{CMC}(y)\ \gamma_M(y)\ X_M(y)}{C_t - \int_0^{\infty} C^{pure}_{CMC}(y)\ \gamma_M(y)\ X_M(y)} \qquad \text{other conc.} \qquad \text{(B.23)}$$

The surfactant distribution in the monomer solution, $X_1(y)$, is given by equation (B.5)

$$X_1(y) = X^{pure}_{CMC}(y)\ \gamma_M(y)\ X_M(y) \qquad \text{(B.24)}$$

The activity coefficient, $\gamma_M(y)$, is modeled according to the regular solution theory written in terms of the solubility parameter, $\delta(y)$:

$$RT\ \ln\ \gamma_M(y) = \underline{V}(y)(\delta(y) - \overline{\delta})^2 \qquad \text{(B.25)}$$

where $\underline{V}(y)$ is the molar volume

$\delta(y)$ is the solubility parameter

$\overline{\delta}$ is the average solubility parameter

The solubility parameter is averaged by a volume fraction $\phi(y)$ defined as

$$\phi(y) = \frac{\alpha_{(y)}\ \underline{V}(y)}{\int_0^{\infty} \alpha_{(y)}\ \underline{V}(y)\ dy} \qquad \text{(B.26)}$$

so that

$$\overline{\delta} = \int_0^{\infty} \phi(y)\ \delta(y)\ dy \qquad \text{(B.27)}$$

Choosing the variable y to represent the chain length of the components, we need to describe the distribution of the fraction $\alpha_{(y)}$, the CMC, $C_{CMC}^{pure}(y)$, the molar volume, $\underline{V}(y)$, and the solubility parameter, $\delta(y)$.

Two distributions were chosen for $\alpha_{(y)}$ as an illustration; logarithmic normal and normal distributions. Other distributions such as κ^2 distribution can also be used depending on the system in hand. The logarithm of the CMC varies linearly with chain length and it is fitted to the form

$$\ln C_{CMC}^{pure}(y) = A_1 + B_1 y$$

The solubility parameter and the molar volume vary linearly with chain length and the fitted forms are

$$\delta(y) = A_2 + B_2 y \quad \text{and} \quad \underline{V}(y) = A_3 + B_3 y$$

These functions were used to determine the CMC (Equation B.21) and the surfactant distribution (Equation B.22 and B.23) for the two distributions mentioned above.

Logarithmic Normal Distribution

This distribution is given by the following equation:

$$\alpha_{(y)} = \frac{1}{\sqrt{2\pi}\,\bar{\sigma}} \exp - \frac{(\ln y - \ln \varepsilon)^2}{2\bar{\sigma}^2} \frac{1}{y} \qquad (B.28)$$

where $\bar{\sigma}$ is related to the standard deviation σ by $\bar{\sigma} = \sigma/\log e$

ε is the mean of the distribution

$$\varepsilon = \int_0^y y\alpha_{(y)}\, dy \; ; \quad \sigma^2 = \int_0^\infty (y-\varepsilon)^2\, \alpha_{(y)}\, dy \qquad (B.29)$$

The derivation starts by determining the average solubility parameter, $\bar{\delta}$ (Equations B.26 and B.27)

$$\int_0^\infty \alpha_{(y)}\, \underline{V}(y)\, dy = \int_0^\infty \frac{A_3 + B_3 y}{\sqrt{2\pi}\,\bar{\sigma}} e^{-\frac{(\ln y - \ln\varepsilon)^2}{2\bar{\sigma}^2}} \frac{dy}{y} \qquad (B.30)$$

Expanding the term $(\ln y - \ln\varepsilon)^2$ and integrating by parts, equation (B.30) becomes

$$a_o \equiv \int_0^\infty \alpha_{(y)}\, \underline{V}(y)\, dy = A\sqrt{\pi/D}\, \exp\{(C+1)^2/4D\} + B\sqrt{\pi/D}\, \exp\{(C+2)^2/4D\} \qquad (B.31a)$$

where

$$A = \frac{A_3}{\sqrt{2\pi}\,\bar{\sigma}} \exp\left\{-\frac{(\ln\varepsilon)^2}{2\bar{\sigma}^2}\right\} \qquad (B.31b)$$

$$B = \frac{B_3}{\sqrt{2\pi}\,\bar{\sigma}} \exp\left\{-\frac{(\ln\varepsilon)^2}{2\bar{\sigma}^2}\right\} \qquad (B.31c)$$

$$C = \frac{\ln\varepsilon}{\bar{\sigma}^2} - 1 \qquad (B.31d)$$

$$D = \frac{1}{2\bar{\sigma}^2} \qquad (B.31e)$$

Simularly,

$$\int_0^\infty \alpha_{(y)} \underline{V}(y)\, \delta(y)\, dy = \int_0^\infty \frac{(A_3+B_3 y)(A_2+B_2 y)}{\sqrt{2\pi}\,\bar{\sigma}} \exp -\frac{(\ln y - \ln\varepsilon)^2}{2\bar{\sigma}^2} \frac{dy}{y} \qquad (B.32)$$

Again, expanding $(\ln y - \ln\varepsilon)^2$ and integrating by parts leads to

$$a_o \equiv \int_0^\infty \alpha_{(y)} \underline{V}(y)\, \delta(y) dy = A A_2 \sqrt{\pi/D}\, \exp\left\{\frac{(C+1)^2}{4D}\right\} + (AB_2 + A_2 B)\sqrt{\pi/D}\, \exp\left\{\frac{(C+2)^2}{4D}\right\} + B B_2 \sqrt{\pi/D}\, \exp\left\{\frac{(C+3)^2}{4D}\right\} \qquad (B.33)$$

Substituting equations (B.25), (B.28), (B.31) and (B.33) in (B.21), the CMC of a continuous surfactant distribution is obtained

$$\frac{1}{C_{CMC}} = \int_0^{\infty} \frac{1/\sqrt{2\pi}\sigma \exp^{-(\ln y - \ln \varepsilon)^2/2\sigma^2} \, dy/y}{\exp(A_1+B_1 y) \exp\left\{\left(\frac{A_3+B_3 y}{RT}\right)\left(A_2+B_2 y - \frac{b_o}{a_o}\right)^2\right\}} \qquad (B.34a)$$

$$= \frac{1}{C_o} \int_0^{\infty} (\exp - (d_o y + e_o y^2 + f_o y^3)) \, y^{(C-D\ln y)} \, dy \qquad (B.34b)$$

where $$\frac{1}{C_o} = \sqrt{2\pi}\,\sigma \exp\left\{\frac{(\ln \varepsilon)^2}{2\sigma^2} + A_1 + \frac{A_3}{RT}\left(A_2 - \frac{b_o}{a_o}\right)^2\right\} \qquad (B.34c)$$

$$d_o = B_1 + 2\frac{A_3}{RT}\left(A_2 - \frac{b_o}{a_o}\right) + \frac{B_3}{RT}\left(A_2 - \frac{b_o}{a_o}\right)^2 \qquad (B.34d)$$

$$e_o = \frac{A_3}{RT} B_2^2 + 2\frac{B_3}{RT} B_2 \left(A_2 - \frac{b_o}{a_o}\right) \qquad (B.34e)$$

$$f_o = \frac{B_3}{RT} B_2^2 \qquad (B.34f)$$

An analytical solution to equation (B.34b) can be found by expanding the term $\exp(d_o y + e_o y^2 + f_o y^3)$ to

$$\exp -(d_o y + e_o y^2 + f_o y^3) = \sum_{i=0}^{\infty} \frac{(-1)^i (d_o y + e_o y^2 + f_o y^3)^i}{i!}$$

but the solution is long and complex. Its numerical solution is much more simpler and faster.

Finally, the surfactant distribution in the micelle is determined by substituting equation (B.34b) in (B.22)

$$X_M(y) = \frac{\frac{1}{\sqrt{2\pi}\,\sigma}\exp^{-\frac{(\ell ny-\ell n\varepsilon)^2}{2\sigma^2}}\frac{C_o}{y}}{\left[\int_0^\infty \{\exp-(d_o y+e_o y^2+f_o y^3)\}\gamma^{(C-D\ell ny)}dy\right]\exp(A_1+B_1 y)\gamma_M(y)} \tag{B.35}$$

where

$$\gamma_M(y) = \exp\left\{\left(\frac{A_3+B_3 y}{RT}\right)\left[A_2+B_2 y-\frac{b_o}{a_o}\right)^2\right\}$$

Normal Distribution

This distribution is defined by the following equation:

$$\alpha(x) = \frac{1}{\sqrt{2\pi}\,\sigma}\exp^{-\frac{(x-\varepsilon)^2}{2\sigma^2}} \tag{B.36}$$

If the variable x is taking to be equal to zero at the mean, its range will be : $-\infty<x<\infty$ and $x=\varepsilon=0$ at the mean of this normal distribution. Following the same derivation performed on the log-normal distribution we get:

$$a_o = \int_{-\infty}^{+\infty}\alpha(x)\,\underline{V}(x)dx = \int_{-\infty}^{+\infty}\frac{1}{\sigma\sqrt{2\pi}}e^{-\frac{x^2}{2\sigma^2}}(A_3+B_3x)dx = A_3 \tag{B.37}$$

$$b_o \equiv \int_{-\infty}^{+\infty}\alpha(x)\,\underline{V}(x)\,\delta(x)dx = \int_{-\infty}^{+\infty}\frac{e^{-\frac{x^2}{2\sigma^2}}}{\sigma\sqrt{2\pi}}(A_3+B_3x)(A_2+B_3x)dx$$

$$= \frac{1}{\sigma\sqrt{2\pi}}\left[A_2\,A_3\sqrt{2\pi\sigma^2}+B_2\,B_3\frac{\sqrt{\pi}}{2\left(\frac{1}{2\sigma^2}\right)^{3/2}}\right] \tag{B.38}$$

Substituting equations (B.25), (B.36), (B.37) and (B.38) in (B.21), the CMC of the mixture is

$$\frac{1}{C_{CMC}} = \frac{\int_{-\infty}^{+\infty} \frac{1}{\sqrt{2\pi}\,\sigma} \exp^{-\frac{x^2}{2\sigma^2}}\, dx}{\exp(A_1+B_1x)\ \exp\left\{\left(\frac{A_3+B_3x}{RT}\right)\left(A_2+B_2x-\frac{b_o}{a_o}\right)^2\right\}} \qquad \text{(B.39a)}$$

$$= \frac{1}{C_o}\int_{-\infty}^{+\infty} \exp(d_o x + e_o x^2 + f_o x^3)dy \qquad \text{(B.39b)}$$

where $$\frac{1}{C_o} = \sqrt{2\pi}\ \sigma\ \exp\left\{A_1 + \frac{A_3}{RT}\left(A_2 - \frac{b_o}{a_o}\right)^2\right\} \qquad \text{(B.39c)}$$

$$d_o = -B_1 - 2\frac{A_3}{RT}B_2\left(A_2-\frac{b_o}{a_o}\right) - \frac{B_3}{RT}\left(A_2-\frac{b_o}{a_o}\right)^2 \qquad \text{(B.39d)}$$

$$e_o = -\frac{1}{2\sigma^2} - \frac{A_3}{RT}B_2^2 - 2\frac{B_3}{RT}B_2\left(A_2-\frac{b_o}{a_o}\right) \qquad \text{(B.39e)}$$

$$f_o = -\frac{B_3}{RT}B_2^2 \qquad \text{(B.39f)}$$

Again, equation (B.39b) can be solved either analytically or numerically. The surfactant distribution, $X_M(x)$, becomes

$$X_M(x) = \frac{\left\{\frac{C_o}{\sqrt{2\pi}\ \sigma}\exp^{-x^2/2\sigma^2}\right\}}{\left\{\int_{-\infty}^{+\infty}\exp(d_o x+a_o x^2+f_o x^3)dy\right\}\ \exp(A_1+B_1x)\ Y_M(x)} \qquad \text{(B.40)}$$

where

$$Y_M(x) = \exp\left\{\left(\frac{A_3+B_3x}{RT}\right)\left(A_2+B_2y-\frac{b_o}{a_o}\right)^2\right\}$$

REFERENCES

Backlund, S., and Rundt, K., "Electromotive Force Studies in the System Sodium Dodecylsulfate-Water-n-Alcohol," Acta Chem. Scand. A, 34, 433 (1980).

Backlund, S., and Rundt, K., "Counterion Association and Gibbs Energy of Micellization in Aqueous Solutions with and without Alcohol," in Surfactant Chemistry, Ed. Birdi, K.S., Lyngby, Denmark (1981).

Backlund, S., Rundt, K., Birdi, K.S., and Dalsager, S., "Aggregation of Sodium Dodecyl Sulfate in Aqueous Sodium Chloride Solutions," Coll. Polym. Sci., 259, 1105 (1981).

Balmbra, R.R., Clunie, J.S., Corkill, J.M., and Goodman, J.F., "Effect of Temperature on the Micelle Size of a Homogeneous Nonionic Detergent," Trans. Faraday Soc., 58, 1661 (1962).

Balmbra, R.R., Clunie, J.S., Corkill, J.M., and Goodman, J.F., "Variations in the Micelle Size of Nonionic Detergents," Trans. Faraday Soc., 60, 979 (1964)

Becher, P., 'Micelle Formation in Aqueous and Nonaqueous Solutions," in Nonionic Surfactants, Ed., Schick, M.J., Marcel Dekker, New York, N.Y. (1970).

Bendedouch, D., Chen, S.H., and Koehler, W.C., "Structure of Ionic Micelles from Small Angle Neutron Scattering," J. Phys. Chem., 87, 153 (1983).

Ben-Naim, A., Water and Aqueous Solutions. Introduction to a Molecular Theory, Plenum Press, New York, N.Y (1974).

Ben-Naim, A., and Stillinger, F.H., "Critical Micelle Concentration and the Size Distribution of Surfactant Aggregates," J. Phys. Chem., 84, 2872 (1980)

Beret, S., and Prausnitz, J.M., "Perturbed Hard-Chain Theory : An equation of State for Fluids Containing Small or Large Molecules," AICHE J., 21, 1123 (1975).

Birdi, K.S., "Aggregation of Bile Salt," Finn. Chem. Lett., 142 (1982).

Birdi, K.S., "Calorimetric Determination of the Enthalpy of Micelle Formation in Aqueous Media," Col. and Polym. Sci., 261, 45 (1983).

Birdi, K.S., Dalsager, S.U., and Backlund, S., "Aggregation Behaviour of Sodium Dodecyl Sulphate Micelles in Aqueous Solutions Studied by Membrane Osmometry," J. Chem. Soc. Faraday I, 76, 2035 (1980).

Boublik, T., "Hard Convex Body Equation of State," J. Chem. Phys., 63, 4084 (1975).

Brugman, R.J., "A Molecular Thermodynamic Model for Aqueous Solutions of Nonpolar Compounds and Micelle Formation," A dissertation presented at the University of Florida (1979).

Brun, T.S., Hoiland, H., and Vikingstad, E., "Partial Molal Volumes and Isentropic Partial Molal Compressibilities of Surface-Active Agents in Aqueous Solutions," J. Coll. Int. Sci., 63, 89 (1978).

Buff, F.P., "The Spherical Interface. I. Thermodynamics," J. Chem. Phys., 75, 463 (1981).

Cabane, B., "Structure of the Water/Surfactant Interface in Micelles - an NMR Study of SDS Micelles Labeled with Paramagnetic Ions," J. Physique, 42, 847 (1981).

Carnahan, N.F., and Starling, N.E., "Equation of State for Nonattracting Rigid Spheres," J. Chem. Phys., 51, 635 (1969).

Carnie, S.L., and Chan, D.Y.C., "The Structure of Electrolytes at Charged Surfaces : Ion-Dipole Mixtures," J. Chem. Phys., 73, 2949 (1980).

Chan, D.Y.C., Mitchell, D.J., Ninham, B.W., and Pailthorpe, B.A., "Towards a Microscopic Theory of Hydrophobic Solutions," J. Chem. Phys., 69, 691 (1978).

Chang, E.T., Gokcen, N.A., and Foston, T.M., "Thermodynamic Properties of Gases in Propellants II. Solubilities of Helium, Nitrogen, and Argon Gas in Hydrazine, Methylhydrazine, and Unsymmetrical Dimethylhydrazine," J. Phys. Chem., 72, 638 (1968).

Corkill, J.M., Goodman, J.F., and Harrold, S.P., "Thermodynamics of Micellization of Nonionic Detergents," Trans. Faraday Soc., 60, 202 (1964).

Corkill, J.M., Goodman, J.F., and Ottewill, R.H., "Micellization of Homogeneous Nonionic Detergents," Trans. Faraday Soc., 57, 1627 (1961).

Corti, M., Claudio, M., and Degiorgio, V., "Cloud Point Transition in Nonionic Micellar Solutions," J. Phys. Chem., 88, 309 (1984).

Crovetto, R., Fernandez-Prini, R., and Japas, M.L., "Contribution of the Cavity-Formation or Hard-Sphere Term to the Solubility of Simple Gases in Water," J. Phys. Chem., 86, 4094 (1982).

Cutler, S.G., Meares, P., and Hall, D.G., "Ionic Activities in Sodium Dodecyl Sulfate Solutions from Electromotive Force Measurements," J. Chem. Soc. Faraday Trans. 1, 74, 1758 (1978).

Desnoyers, J.E., Caron, G., Delisi, R., Roux, A., and Perron, G., "Thermodynamic Properties of Alkyldimethylamine Oxides in Water-Application of a Mass-Action Model for Micellization," J. Phys. Chem., 87, 1397 (1983).

Dill, K.A., and Flory, P.J., "Molecular Organization in Micelles and Vesicles," Proc. Natl. Acad. Sci., 78, 676 (1981).

Donbrow, M., and Jan, Z.A., "Refractometric Determination of the Critical Micelle Concentration of Nonionic Surface Active Agents," J. Pharm. Pharmacol., 15, 825 (1963).

Doughty, D.A., "Effect of Co-Ion on the Preferential Interaction Parameter and Micelle Aggregation Number. Sodium Dodecyl Sulfate in Aqueous Sodium Halide," J. Phys. Chem., 87, 5286 (1983).

Elworthy, P.H., and Macfarlane, C.B., "Chemistry of Nonionic Detergents. Part V. Micellar Structures of a Series of Synthetic Nonionic Detergents," J. Chem. Soc., 907 (1963).

Evans, D.F., and Chen, S.H., "Thermodynamics of Solution of Nonpolar Gases in a Fused Salt," J. Am. Chem. Soc., 103, 481 (1981).

Evans, D.F, and Wightman, P.J., "Micelle Formation above 100 °C," J. Coll. Int. Sci., 86, 515 (1982).

Evans, D.F, Yamauchi, A., Roman, R., and Casassa, E.Z., "Micelle Formation in Ethylammonium Nitrate, a Low-Melting Fused Salt," J. Coll. Int. Sci., 88, 89 (1982).

Evans, D.F, Lumry, R., and Ramadan, M.S., "Why Micelles Form in Water and Hydrazine. A reexamination of the Origins of Hydrophobicity," J. Phys. Chem., 87, 4038 (1983a).

Evans, D.F, Yamauchi, A., Wei, G.J., and Bloomfield, V.A., "Micelle Size in Ethylammonium Nitrate as Determined by Classical and Quasi-Elastic Light Scattering," J. Phys. Chem., 87, 3539 (1983b).

Evans, D F, Allen, M., Ninham, B.W., and Fouda, A., "Critical Micelle Concentrations for Alkyltrimethylammonium Bromides in Water from 25 to 160 °C," J. Sol. Chem., 13, 1 (1984).

Franks, F., "Solute-Water Interactions and the Solubility Behaviour of Long-Chain Paraffin Hydrocarbons," Nature, 210, 87 (1966).

Fujimatsu, H., Takagi, K., Matsuda, H., and Muroiwa, S., "Temperature Dependences of Micellar Molecular Weight and Radius of Nonionic Surface Active Agent in the Aqueous Solution," J. Coll. Int. Sci., 94, 237 (1983).

Gibbons, R.M., "The Scaled Particle Theory for Particles of Arbitrary Shape," Mol. Phys., 17, 81 (1969).

Gibbons, R.M., "The Scaled Particle Theory for Mixtures of Hard Convex Particles," Mol. Phys., 18, 809 (1970).

Gill, S.J., Nichols, N.F., and Wadso, I., "Calorimetric Determination of Enthalpies of Solution of Slightly Soluble Liquids," J. Chem. Therm., 8, 445 (1976).

Hall, D.G., and Pethica, B.A., "Thermodynamics of Micelle Formation," in Nonionic Surfactants, Ed., Schick, M.J., Marcel Dekker, New York, N.Y. (1970).

Hamann, S.D., "The State of Ionic Micelles at High Pressures," Rev. of Phys. Chem. of Japan, 48, 60 (1978).

Hayashi, S., and Ikeda, S., "Micelle Size and Shape of Sodium Dodecyl Sulfate in Concentrated NaCl Solutions," J. Phys. Chem., 84, 744 (1980).

Hayter, J.B., and Penfold, J., "Self-Consistent Structural and Dynamic Study of Concentrated Micelle Solutions," J. Chem. Soc. Faraday Trans. 1, 77, 1851 (1981).

Hayter, J.B., and Zemb, T., "Concentration-Dependent Structure of Sodium Octanoate Micelles," Chem. Phys. Let., 93, 91 (1982).

Hill, T.L., Thermodynamics of Small Systems, Vol. 1 and 2, Benjamin, New York (1963-64).

Hornbeck, R.W., Numerical Methods, Quantum Publishers, New York, N.Y. (1975).

Houseniopp, I.A., and Scott, D.W., "Vapor Heat Capacities and Enthalpies of Vaporization of Five Alkane Hydrocarbons," J. Chem. Therm., 13, 415 (1981).

Israelachvili, J.N., Mitchell, D.J., and Ninham, B.W., "Theory of Self-Assembly of Hydrocarbon Amphiphiles into Micelles and Bilayers," J. Chem. Soc. Faraday II, 72, 1525 (1976).

Jonsson, B., "Monte Carlo Simulations of Liquid Water between Two Rigid Walls," Chem. Phys. Let., 82, 520 (1981).

Jonsson, B., Wennerstrom H., and Halle, B., "Ion Distributions in Lamellar Liquid Crystals: A Comparison between Results from Monte Carlo Simulations and Solutions to the Poisson-Boltzmann Equation," J. Phys. Chem., 84, 2179 (1980).

Kale, K.M., Crusseler, E.L., and Evans, D.F., "Characterization of Micellar Solutions Using Surfactant Ion Electrodes," J. Phys. Chem., 84, 593 (1980).

Kalyanasundaram, K., and Thomas, J.K., "On the Conformational State of Surfactants in the Solid State and in Micellar Form. A Laser-Excited Raman Scattering Study," J. Phys. Chem., 80, 1462 (1976).

Lianos, P., and Zana, R., "Use of Pyrene Excimer Formation to Study the Effect of NaCl on the Structure of Sodium Dodecyl Sulfate Micelles," J. Phys. Chem., 84, 3339 (1980).

Lianos, P., and Zana, R., "Fluorescence Probe Studies of the Effect of Concentration on the State of Aggregation of Surfactants in Aqueous Solution," J. Coll. Int. Sci., 84, 100 (1981).

Lianos, P., and Zana, R., "Micelles of Tetradecyltrialkylammonium Bromides with Fluorescent Probes," J. Coll. Int. Sci., 88, 594 (1982).

Lianos, P., and Zana, R., "Micellar Properties of Alkyltrimethylammonium Hydroxides in Aqueous Solution," J. Phys. Chem., 87, 1289 (1983).

Linse, P., Gunnarsson, G., and Jonsson, B., "Electrostatic Interactions in Micellar Solutions. A Comparison between Monte Carlo Simulations and Solutions to the Poisson-Boltzmann Equation," J. Phys. Chem., 86, 413 (1982).

Loeb, A.L., Overbeek, J. Th. G., and Wiersema, P.H., The Electrical Double Layer around a Spherical Colloidal Particle, MIT Press, Cambridge, Mass. (1961).

Lucas, M., and Bury, R., "The Influence of Solute Size on the Thermodynamic Parameter of Transfer of a Nonpolar Hydrophobic Solute from Gas to Water or from Light to Heavy Water," J. Phys. Chem., 80, 999 (1976).

Marchesi, M., "Molecular Dynamics Simulation of Liquid Water between Two Walls," Chem. Phys. Let., 97, 224 (1983).

Mazer, N.A., and Olofsson, G., "Calorimetric Studies of Micelle Formation and Micellar Growth in Sodium Dodecyl Sulfate Solutions," J. Phys. Chem., 86, 4584 (1982).

McAuliffe, C., "Solubility in Water of Paraffin, Cycloparaffin, Olefin, Acetylene, Cycloolefin and Aromatic Hydrocarbons," J. Phys. Chem., 70, 1267 (1966).

Menger, F.M., and Boyer, S.J., "Water Penetration into Micelles as Determined by Optical Rotary Dispersion," J. Am. Chem. Soc., 102, 5936 (1980).

Missel, P.J., Mazer, N.A., Benedek, G.B., and Carey, M.C., "Influence of Chain Length on the Sphere-to-Rod Transition in Alkyl Sulfate Micelles," J. Phys. Chem., 87, 1264 (1983).

Missel, P.J., Mazer, N.A., Benedek, G.B., Young, C.Y., and Carey, M.C., "Thermodynamic Analysis of the Growth of Sodium Dodecyl Sulfate Micelles," J. Phys. Chem., 84, 1044 (1980).

Mitchell, D.J., and Ninham, B.W., "Electrostatic Curvature Contribution to Interfacial Tension of Micellar and Microemulsion Phases," J. Phys. Chem., 87, 2996 (1983).

Miura, M., and Kodama, M., "The Second CMC of the Aqueous Solution of Sodium Dodecyl Sulfate. I. Conductivity," Bulletin of the Chem. Soc. of Japan, 45, 428 (1972).

Mukerjee, P., "Hydrophobic and Electrostatic Interactions in Ionic Micelles. Problems in Calculating Monomer Contributions to the Free Energy," J. Phys. Chem., 73, 2054 (1969).

Mukerjee, P., and Mysels, K.J., "Critical Micelle Concentrations of Aqueous Surfactant Systems," Nat. Stand. Ref. Data Ser., Nat. Bur. Stand., No. 36 (1971).

Neff, N.O., and McQuarrie, D.A, "A Statistical Mechanical Theory of Solubility," J. Phys. Chem., 77, 413 (1973).

Nilsson, P.G., Wennerstrom, H., and Lindman, B., "Structure of Micellar Solutions of Nonionic Surfactants Nuclear Magnetic Resonance Self-Diffusion and Proton Relaxation Studies of Polyethylene Oxide Alkyl Ethers," J. Phys. Chem., 87, 1377 (1983).

Osugi, J., Sato, M., and Ifuku, N., "The Effect of Pressure and Temperature on the Micelle Formation of Dodecylbenzyldimethylammonium Chloride Solution," Rev. of Phys. Chem. of Japan, 38, 58 (1968).

Perry, R.L., Teiotte, J.C., and O'Connell, J.P., "Solutions Thermodynamics for Reactive Components," Fluid Phase Equilibria, 5, 245 (1981).

Phillips, J.N., "The Energetics of Micelle Formation," Trans Faraday Soc., 51, 561 (1955).

Pierotti, R.A., "The Solubility of Gases in Liquids," J. Phys. Chem., 67, 1840 (1963).

Pierotti, R.A, "Aqueous Solutions of Nonpolar Gases," J. Phys. Chem., 69, 281 (1965).

Polak, J., and Lu, B.C.Y., "Mutual Solubilities of Hydrocarbons and Water at 0 and 25 °C," Can. J. Chem., 51, 4018 (1973).

Porte, G., and Poggi, Y., "Behavior of Micellar Aqueous Solutions in High Magnetic Field," Physical Review Letters, 41, 1481 (1978).

Pratt, L.R., and Chandler, D., "Theory of the Hydrophobic Effect," J. Chem. Phys., 67, 3683 (1977).

Pratt, L.R., and Chandler, D., "Hydrophobic Solvation of Nonspherical Solutes," J. Chem. Phys., 73, 3430 (1980)

Pratt, L.R., Rosenberg, R.O., Berne, B.J., and Chandler, D., "Comment on the Structure of a Simple Liquid Solvent near a n-Butane Solute Molecule," J. Chem. Phys., 73, 1002 (1980).

Ray, A., and Nemethy, G., "Micelle Formation by Nonionic Detergents in Water-Ethylene Glycol Mixtures," J. Phys. Chem., 75, 809 (1971).

Reed, M.T., and Gubbins, K.E., "Applied Statistical Mechanics," McGraw-Hill Chemical Engineering Series, New York, N.Y. (1973).

Reiss, H., "Scaled Particle Theory of Hard Sphere Fluids to 1976," in Statistical Mechanics and Statistical Methods in Theory and Application, Ed., U. Landman, Plenum Press, New York, N.Y. (1977).

Reiss, H., Frisch, H.L., and Lebowitz, J.L., "Statistical Mechanics of Rigid Spheres," J. Chem. Phys., 31, 369 (1959).

Rosen, M.J., Cohen, A.W., Dahanayake, M., and Hua, X.Y., "Relationship of Structure to Properties in Surfactants. 10. Surface and Thermodynamic Properties of 2-Dodecyloxypoly(ethenoxyethanol)s, $C_{12}H_{25}(OC_2H_4)_6OH$, in Aqueous Solution," J. Phys. Chem., 86, 541 (1982)

Rubingh, D.N., "Mixed Micelle Solutions," in Solution Chemistry of Surfactants, Ed., Mittal, K.L., Vol. I, 337, Plenum Press, New York, N.Y. (1979).

Ruckenstein, E., and Nagarajan, R., "Critical Micelle Concentration. A Transition Point for Micellar Size Distribution," J. Phys. Chem., 79, 2622 (1975).

Ryu, K., Lowery, J.M., Evans, D.F., and Cussler, E.L., "Studies of Model Bile Solutions Using Surfactant Ion Electrodes," J. Phys. Chem., 87, 5015 (1983).

Sinanoglu, O., "The Solvophobic Theory for the Prediction of Molecular Conformations and Biopolymer Bindings in Solutions with recent Direct Experimental Tests," Int. J. of Quantum Chem., 18, 381 (1980).

Sinanoglu, O., "Microscopic Surface Tension down to Molecular Dimensions and Microthermodynamic Surface Areas of Molecules or Clusters," J. Chem. Phys., 75, 463 (1981).

Singh, H.N., Saleem, S.M., Singh, R.P , and Birdi, K.S., "Micelle Formation of Ionic Surfactants in Polar Nonaqueous Solvents," J. Phys. Chem., 84, 2191 (1980).

Sokolov, S.N., Sokolov, N.S., and Trushkin, A.O., "Equation for Calculating the Heat of Evaporation of Liquid Methane Series Hydrocarbons over a Wide Temperature Range," Deposited Doc., Viniti 816, 6 pp. (Russ. 1981).

Stigter, D., "On the Adsorption of Counterions at the Surface of Detergent Micelles," J. Phys. Chem., 68, 3603 (1964).

Stigter, D., 'Micelle Formation by Ionic Surfactants," J. Coll. Int Sci., 47, 473 (1974a).

Stigter, D., "Micelle Formation by Ionic Surfactants. II. Specificity of Head Groups, Micelle Structure," J. Phys. Chem., 78, 2480 (1974b).

Stigter, D., "Micelle Formation by Ionic Surfactants III. Model of Stern Layer, Ion Distribution and Potential Fluctuations," J. Phys. Chem., 79, 1008 (1975a).

Stigter, D., "Micelle Formation by Ionic Surfactants IV. Electrostatic and Hydrophobic Free Energy from Stern-Gouy Ionic Double Layer," J. Phys. Chem., 79, 1015 (1975b).

Stillinger, F.H., "Structure in Aqueous Solutions of Nonpolar Solutes from the Standpoint of Scaled-Particle Theory," J. Sol. Chem., 2, 141 (1973).

Sugihara, G., and Mukerjee, P., "High-Pressure Study of Micelle Formation in Aqueous Solutions of Sodium Perfluorooctanoate," J. phys. Chem., 85, 1612 (1981).

Sutton, C., and Calder, J.A., "Solubility of Higher-Molecular-Weight n-Paraffins in Distilled Water and Sea Water," Env. Sci. and Tech., 8, 654 (1974).

Tanaka, M., Kaneshina, S., Shin-No, K., Okajima, T., and Tomida, T., "Partial Molal Volumes of Surfactant and its Homologous Salts Under High Pressure," J. Coll. Int. Sci., 46, 132 (1974).

Tanford, C., "Micelle Shape and Size," J. Phys. Chem., 76, 3020 (1972).

Tanford, C., "The Hydrophobic Effect," John Wiley and Sons, New York (1973).

Tanford, C., "Thermodynamics of Micelle Formation : Prediction of Micelle Size and Size Distribution," Proc. Nat. Acad. Sci., 71, 1811 (1974).

Tully-Smith, D.M., and Reiss, H., "Further Development of Scaled Particle Theory of Rigid Sphere Fluids," J. Chem. Phys., 53, 4015 (1970).

Ueno, M., Nakahara, M., and Osugi, J., "The Effect of Pressure on Micelle Formation and Solubility of Hexadecyltrimethylammonium Bromide in Water," Rev. of Phys. Chem. of Japan, 47, 25 (1977).

Wilhelm, E., Battino, R., and Wilcock, R J., "Low -Pressure Solubility of Gases in Liquid Water," J. Chem. Reviews, 77, 219 (1977).

Zana, R., "Ionization of Cationic Micelles : Effect of the Detergent Structure," J. Coll. Int. Sci., 78, 330 (1980).

Zemb, T., Drifford, M., Mayoun, M., and Jehanno, A., "Light Scattering Study of Solutions of Sodium Octanoate Micelles," J. Phys. Chem., 87, 4524 (1983).

BIOGRAPHICAL SKETCH

Michel Hourani was born on November 8, 1958, in Tripoli, Lebanon. He graduated from Pere Carme High School in 1976 and received his Bachelor of Science in chemical engineering from the University of Southwestern Louisiana in May 1980. He commenced graduate studies in the Department of Chemical Engineering, University of Florida, in August of 1980, and received the Master of Science degree in December, 1981.

I certify that I have read this study and that in my opinion it conforms to acceptable standards of scholarly presentation and is fully adequate, in scope and quality, as a dissertation for the degree of Doctor of Philosophy.

John P. O'Connell, Chairman
Professor of Chemical Engineering

I certify that I have read this study and that in my opinion it conforms to acceptable standards of scholarly presentation and is fully adequate, in scope and quality, as a dissertation for the degree of Doctor of Philosophy

Dinesh O. Shah
Professor of Chemical Engineering

I certify that I have read this study and that in my opinion it conforms to acceptable standards of scholarly presentation and is fully adequate, in scope and quality, as a dissertation for the degree of Doctor of Philosophy.

Raymond W. Fahien
Professor of Chemical Engineering

I certify that I have read this study and that in my opinion it conforms to acceptable standards of scholarly presentation and is fully adequate, in scope and quality, as a dissertation for the degree of Doctor of Philosophy.

Theo E. Hogen Esch
Professor of Chemistry

I certify that I have read this study and that in my opinion it conforms to acceptable standards of scholarly presentation and is fully adequate, in scope and quality, as a dissertation for the degree of Doctor of Philosophy.

Federico A. Vilallonga
Professor of Pharmacy

This dissertation was submitted to the Graduate Faculty of the College of Engineering and to the Graduate School, and was accepted as partial fulfillment of the requirements for the degree of Doctor of Philosophy.

June, 1984

Dean, College of Engineering

Dean for Graduate Studies and Research